Principles and applications of CVD powder technology

Constantin Vahlas, Brigitte Caussat, Philippe Serp and George N. Angelopoulos

Centre Interuniversitaire de Recherche et d'Ingénierie des Matériaux, CIRIMAT-UMR CNRS 5085, ENSIACET-INPT, 118 Route de Narbonne, 31077 Toulouse cedex 4, France
Laboratoire de Génie Chimique, LGC-UMR CNRS 5503, ENSIACET-INPT, 5 rue Paulin Talabot, BP1301, 31106 Toulouse cedex 1, France
Laboratoire de Catalyse, Chimie Fine et Polymères, LCCFP-INPT, ENSIACET, 118 Route de Narbonne, 31077 Toulouse cedex 4, France
Department of Chemical Engineering, University of Patras, University Campus, 26500 Patras, Greece

Abstract

Chemical vapor deposition (CVD) is an important technique for surface modification of powders through either grafting or deposition of films and coatings. The efficiency of this complex process primarily depends on appropriate contact between the reactive gas phase and the solid particles to be treated. Based on this requirement, the first part of this review focuses on the ways to ensure such contact and particularly on the formation of fluidized beds. Combination of constraints due to both fluidization and chemical vapor deposition leads to the definition of different types of reactors as an alternative to classical fluidized beds, such as spouted beds, circulating beds operating in turbulent and fast-transport regimes or vibro-fluidized beds. They operate under thermal but also plasma activation of the reactive gas and their design mainly depends on the type of powders to be treated. Modeling of both reactors and operating conditions is a valuable tool for understanding and optimizing these complex processes and materials. In the second part of the review, the state of the art on materials produced by fluidized bed chemical vapor deposition is presented. Beyond pioneering applications in the nuclear power industry, application domains, such as heterogeneous catalysis, microelectronics, photovoltaics and protection against wear, oxidation and heat are

potentially concerned by processes involving chemical vapor deposition on powders. Moreover, simple and reduced cost FBCVD processes where the material to coat is immersed in the FB, allow the production of coatings for metals with different wear, oxidation and corrosion resistance. Finally, large-scale production of advanced nanomaterials is a promising area for the future extension and development of this technique.

Keywords: Powders; Chemical vapor deposition; Fluidization; Coatings; Films

1. Introduction

Modification of surface properties of powders that are used as solid process materials in industrial applications, through either grafting or deposition of films or coatings, is an area of science and technology which interests numerous fields: fabrication of monolithic or composite parts, mechanics, transport (vehicle structure and motors), catalysis, energy production, microelectronics, optoelectronics, leisure industry, etc. The properties required for engineering structures are protection against corrosion, oxidation or wear, biocompatibility, wetting, adhesion, durability, catalytic activity, toughness, etc. Surface treatments of particles are applied through various techniques, either wet, such as sol–gel and impregnation, or dry, such as pyrolysis and chemical vapor deposition (CVD). Choosing the most appropriate depends on the requirements of the surface treatment and on the characteristics of the particles to be coated, such as shape, density, porosity, size and size distribution. Dry techniques involving surface modification of powders imply the use of a reactive gas phase. In this case, a complex process prevails, composed of two elemental processes taking place simultaneously: (i) mixing of powders in such a way that their entire surface is presented to the reactive gas phase and (ii) either homogeneous or heterogeneous gas–solid chemical reactions. Fluidization is a well-known particle treatment process among all those used to meet the requirement of gas–solid contact [1]. It has been traditionally used for several decades in very large units of petroleum and mineral industries. On the other hand, gas–solid reactions are often used in the context of various CVD processes: those involving either halogen or organometallic chemistry ensuring robust or flexible, low temperature operation, respectively, or even those involving plasma activation, taking thus advantage of non-equilibrium plasmas providing active species at low temperatures compatible with a wide range of substrate materials. Therefore, the association of such mature techniques, namely

fluidized bed chemical vapor deposition (FBCVD) is expected to lead to innovative, flexible and cost-effective particle treatment processes [2].

Fig. 1 presents the evolution of published papers dealing with CVD on—mainly fluidized powders as a function of the year of publication. The histogram and the curve illustrate the percentage (left) and the cumulated percentage (right), respectively, for a sample of 150 papers. Although this amount is not exhaustive, it can be considered as representative of the scientific and technical production in this field in the open literature and in patents. The period covered in this diagram concerns the years 1981–2004. Only a limited number of publications are available for period 1960–1980, and they essentially deal with particle coatings for nuclear applications as discussed later. This indicates that CVD on powders is a relatively new technique. During its childhood (1980–1990), its extension was relatively slow since yearly published documents up to 1994 were merely the double of those published in 1981, with an exception in 1991 when, interestingly, numerous reports were published which aimed at applications other than nuclear.

Fig. 1. Numbers of papers dealing with CVD on powders as a function of the year of publication. The histogram illustrates the percentage (left) and the curve the cumulated percentage (right) for a sample of 150 papers.

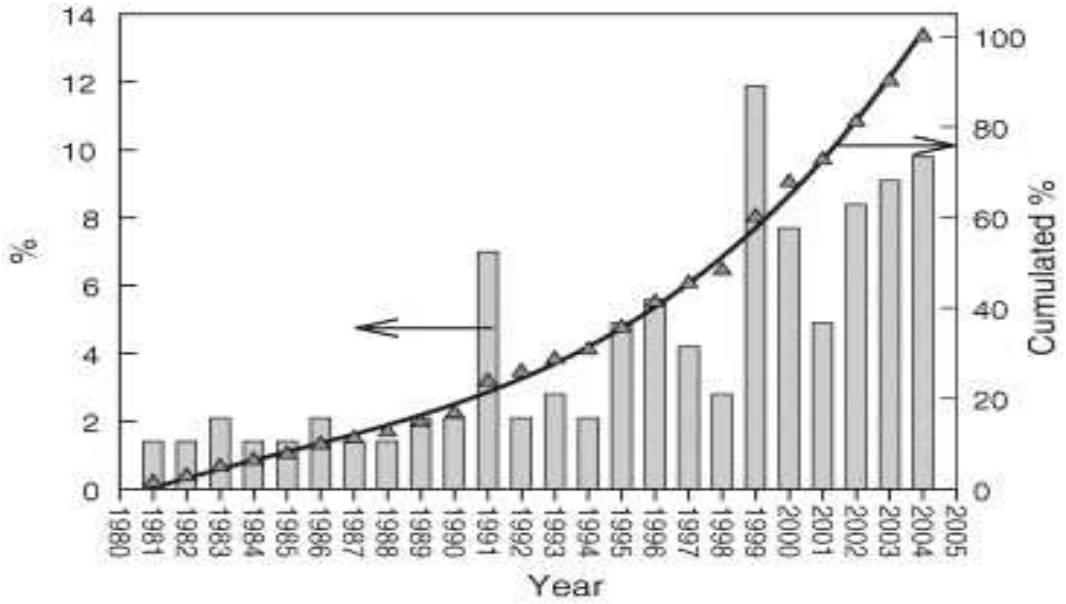

Since 1994 and especially since 2000, the slope has become steeper. Trends in the first months of 2005 (not reported) are compatible with those observed in this figure. Indeed, process and material investigations on the previously mentioned application domains, also including the use of CVD for the production of powders, for example, ultrapure silicon, and for the surface treatment of bulk pieces immersed in a FB, are far from being exhaustive. They concern rather thick and continuous deposits on dense (non-porous) powders. The numerous experimental and theoretical studies performed on this topic improved the understanding of various undesirable phenomena occurring during deposition, such as bed clogging and formation of parasitic fines. However, the recent strong rise in the volume of the scientific and technical literature in this field is mainly attributed to new classes of materials for which large-scale production through a reliable, reproducible and robust process is a necessary condition of development. In general, such new trends in powder processing by CVD concern deposition of nanometric films on powders consisting of particles which present one or more of the following characteristics: meso- or micro-porosity, submicron size, wide size distribution or shape factor much less than one. Production of supported catalysts on particles is a domain where CVD on powders can potentially replace more traditional, wet methods like liquid impregnation, which prevails nowadays for the production of such materials. This field of application is of great interest to industry and can hardly be overestimated: in the USA, the “catalysis industry” is the largest single economic activity, with an annual turnover in solid catalysts as such of around US$ 7 billion [3]. The importance of nanomaterials for society and economy is foreseen to become extremely strong in the future. Among them, carbon nanotubes (CNTs), is a unique material, whose wide application development is critically dependent on the availability of methods for low-cost, large-scale production. It will be shown below that FBCVD is a promising response to this limitation, which also restricts fundamental research on CNTs and nano-objects in general.

However, the extension of the application of CVD on powders to these and other new domains of nanotechnology requires additional hard points of the process to be overcome. These can be summed up as individual particle treatment, efficient gas–solid mixing and confinement of submicron powders, while for instance, operating at sub-atmospheric pressure, in continuous mode, with a bed whose characteristics are continuously modified during the operation. Such constraints require appropriate reactor design and finely tuned operating conditions.

The present review aims to provide information to assist the chemical engineer and the materials scientist to meet these constraints. The manuscript is organized as follows: first, the different ways to induce an efficient contact between a gas and particles will be presented and discussed, followed by the basic principles of fluidization and the classification of powders as a function of their behavior in a FBCVD reactor. Then, the constraints on FBs brought about by the simultaneous operation of CVD will be developed. This will lead to the presentation of the different types of CVD reactors for deposition on powders, and for their surface treatment. This first part, essentially dealing with chemical engineering aspects, will be completed with a detailed presentation of modeling of FBCVD reactors and processes. The second and third parts will develop the state of the art on materials produced by FBCVD. The organization of the second part will be based on the different application domains, namely surface treatment of powders for the preparation of supported catalysts, of wear, oxidation and heat resistant materials, of materials for microelectronics and photovoltaics, of nuclear fuel and finally for new materials. The fourth part mainly focuses on the use of FBCVD reactors for the coating of bulk parts, mainly for the formation of wear and corrosion resistant protective coatings on metals. Finally, the fabrication of powders (including nano-objects; e.g. nanotubes) by CVD is discussed, before providing concluding remarks.

2. Gas-powder contactors and CVD processes: chemical engineering aspects

2.1. Ways to ensure gas–solid contact in CVD on particles

Ensuring efficient contact between the gas phase and the growing surface in CVD processes is rarely a problem for deposition on flat substrates. A different situation prevails when deposition is attempted on the entire available surface of a piece lying on a support. CVD on powders corresponds to this latter case. The technical solutions developed to face this situation are shown schematically in Fig. 2, adapted from ref. [4]. The simplest ones are fixed bed and flat hearth, where gas flows, respectively, through and over powders whose particles do not move relative to each other. In this case, if the gas flow rate is sufficiently low, the gas merely percolates through the void species between the stationary particles. This mode of gas solid contact has often been used for CVD processes devoted mainly to catalyst preparation

and CNT synthesis (see refs. [5] and [6] and references therein) and recently to grafting metalorganic species in mesoporous silica [7]. However, there are numerous drawbacks related to these simple solutions: (i) as in the case of chemical vapor infiltration, diffusion limitations may affect the efficient contact between the gas reactants and the inner particles; (ii) it is impossible to perform deposition on the entire surface of each particle due to contact points among them and with the reactor walls; (iii) when high growth rates and/or high thickness is aimed, clogging phenomena can occur; (iv) finally, due to the previous drawbacks, the scale-up of these processes is problematic. An improvement of this situation is to impose a movement to the particles of the powder relative to each other. Fig. 2 depicts technical solutions that have been used to induce relative particles movement. These are rotary cylinders, pneumatic conveying, vertical moving beds and fluidized beds. In such cases, it is expected that each particle will present its entire surface to the gaseous reactants during the process. The use of rotary cylindrical reactors has been reported for the deposition of tungsten carbide (WC) on fine titanium nitride (TiN) powders [8]. However, strong thermal gradients detrimental to the control of the process and to deposit quality often occur in such reactors.

Fig. 2. Contacting modes for CVD on powders in gas–solid reactors. Adapted from ref. [4].

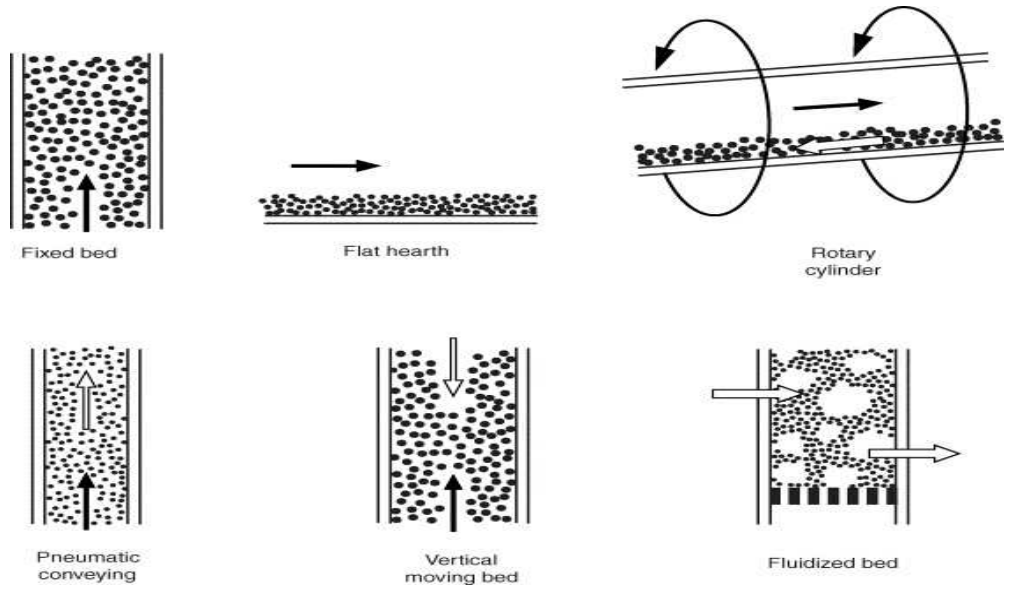

The most frequently employed method to treat powders by CVD is by maintaining them in a FB regime. Through this technique, a bed of solid particles over a gas-distributing plate (often called the grid), is made to behave like a liquid by passing gas through it at a flow rate above

a certain critical value [1]. Compared with deposition on flat surfaces (wafers), FBCVD presents considerable differences. Indeed, in order to ensure satisfactory uniformity of deposits on each wafer and from wafer to wafer, most classical industrial CVD processes, especially those running under low pressure, are organized in terms of temperature, pressure and gas flow rates so as to be limited by surface kinetics. In fluidized bed deposition, the situation is drastically different. Substrates are powders and often (micro-)porous, resulting in extremely high available growth surface to heated volume ratios (S/V) in the deposition area. Fig. 3 illustrates this trend [9]. The histogram reports typical S/V values for atmospheric pressure single wafer and low pressure multi-wafer industrial reactors, for laboratory scale fluidised-bed reactors operating with non-porous and with porous powders (specific surface area of 1 and 160 m^2/g, respectively), and for industrial reactors for the chemical vapor infiltration of pyrolytic carbon. It can be noticed that the S/V ratios for these processes extend over 6 orders of magnitude. CVD on flat surfaces does not exceed 10^2 m^{-1}, to be compared with FBCVD for which this ratio is between 10^4 and 3×10^7 m^{-1}. As expected, S/V for chemical vapor infiltration (CVI) is very high, but it is still more than 100 times lower than FBCVD on porous particles.

Fig. 3. Typical values of growth area per heated volume in the deposition region for different CVD processes [9].

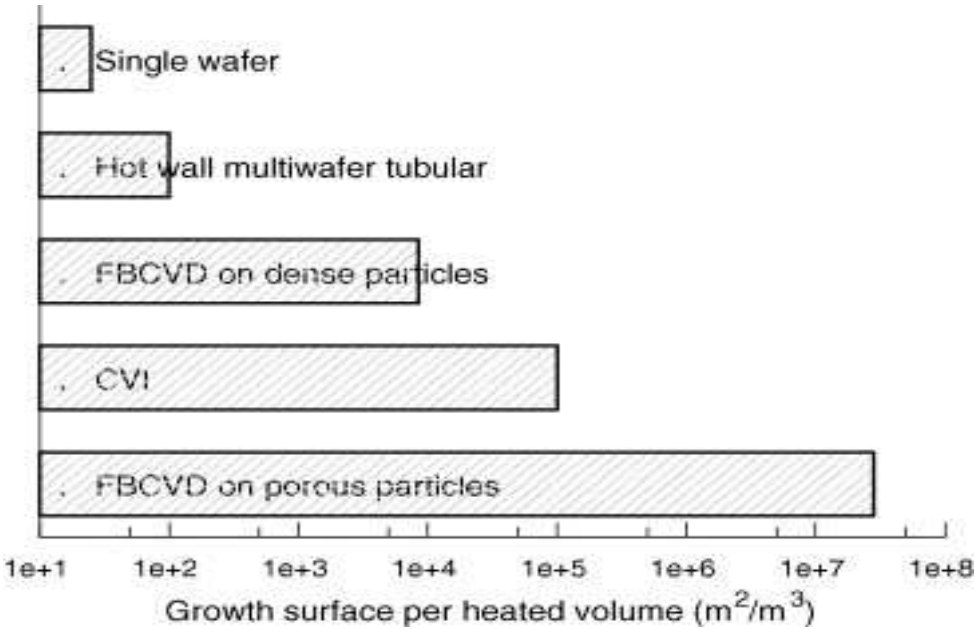

Although Fig. 3 provides trends rather than precise values, it does illustrate why surface reactions are so extended that gaseous precursors are very often totally consumed a few centimeters after their entrance into the fluidised-bed reactor in a laboratory scale contactor. Fortunately, the vigorous mixing of the particles always compensates for this potential source of error, and ensures uniform deposition. Due to the high degree of gas–solid mixing, diffusive phenomena only occur near the boundaries of bubbles, which may be formed by the fluidizing gas, and mass transfer rates are mainly convective, ensuring homogeneous deposition. A further consequence of the high degree of contact between gases, powders and reactor walls in FBCVD, in contrast with classical CVD processes, is that fluidized contactors intrinsically lead to high heat transfer rates, thus ensuring isothermal conditions both radially and axially in the bed [10].

Due to these intrinsic advantages, FBCVD has been extensively used for deposition on particles [9]. However, the evolution of technological requirements in terms of: (i) types of powders to be treated, (ii) properties of use and (iii) environmental constraints means new techniques have been proposed in the open literature or in patents to ensure deposition on powders. Based on this situation, the basic principles of classical fluidised-bed CVD reactors will be first presented in this part. Then, the constraints imposed either by the CVD process or by the powders to be treated will be developed and technical solutions to face these new situations will be reviewed. Finally, modeling of CVD fluidised-bed reactors as a tool to understand and optimize processes and materials will be briefly discussed.

2.2. Basic principles of fluidization and of powder classification

The behavior of a fluidised-bed reactor is so complex that, according to Geldart … *it is more difficult to predict it than to calculate the arrival time of a space probe traveling to Saturn* … ([10], p. 11)! This difficulty is systematically pointed out in the numerous books dedicated to fluidization [1], [4], [10], [11] and [12]. In essence, the behavior of the bed depends on the particle characteristics and on gas velocity. Low flow rates correspond to a fixed bed. At higher velocity, fluidization takes place and generally gives rise to heterogeneous systems, characterized by gas bubbles which form at the bottom of the bed, just above the distributor, travel through the bed, grow, coalesce and then burst at the upper surface. These two regimes are separated by a third one, characterized by a homogeneous situation for which practically no influence of bubbles has to be taken into account. Bed expansion is initiated in this latter regime, which corresponds to the minimum fluidization velocity, U_{mf}. For gas velocities

higher than U_{mf}, the drag force on an individual particle exceeds the force exerted by gravity, thus leading to fluidization. The morphology of the particle bed, which is representative of the different fluidization regimes, is schematically illustrated in the upper part of Fig. 4(a). Crossing of the bed by the gas flow results in a pressure drop (ΔP) through the bed. ΔP variations with gas velocity provide essential information on the characteristics of the bed. For this reason, the hydrodynamic behavior of the latter is investigated by ΔP measurements between the bottom and the top of the bed. Such variations are schematically reported in the lower part of Fig. 4(b). In zone (a), corresponding to low gas velocity, the bed is fixed and ΔP is proportional to gas velocity. U_{mf} is the gas velocity at the intersection point between this straight line and the plateau observed during fluidization (zone c), for which ΔP equals the weight of particles per unit area. Measurements performed at increasing and decreasing flow rates lead to the hysteresis observed in zone (b), due to lower interparticle forces for defluidization conditions. For this reason, measurements of U_{mf} performed in practice at decreasing flow rates. For velocities higher than the terminal velocity of particles, ΔP decreases due to powder entrainment. Optimum operation conditions for laboratory scale contactors generally correspond to three or four times the U_{mf} and to a quantity of powders yielding a ratio between the height of the static bed and the diameter of the reactor of between 2 and 4.

Fig. 4. Pressure drop–gas velocity relationship, characteristic of fluidized-bed reactors (lower part) and schematics of the contacting form of the powder by the gas, representative of the different domains in this relationship (upper part).

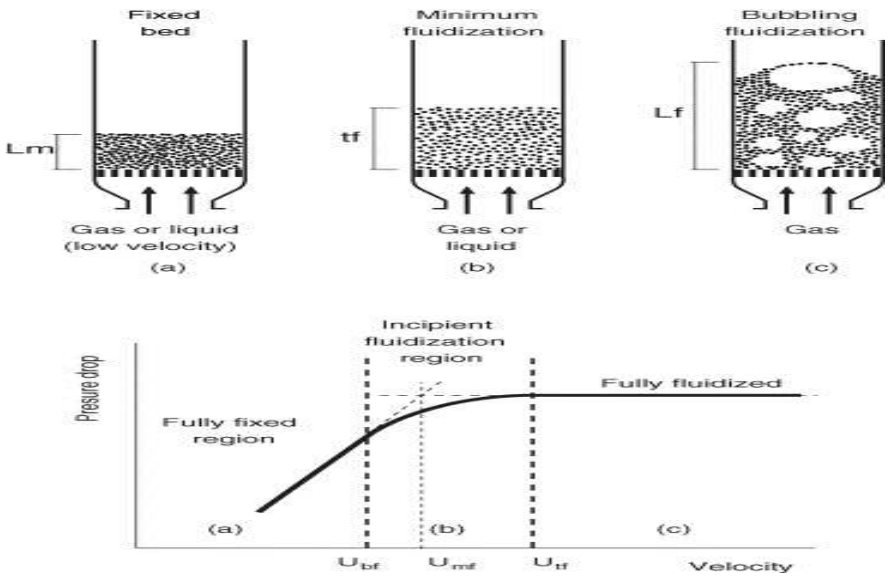

The situation described above holds for ideally fluidizable particles. However, the behavior of a fluidization system is closely dependent on the properties of the solid particles, such as size, density, cohesiveness or the amount of very fine particles (fines) they often contain. Consequently, data obtained for one powder cannot be used for others with different properties. To limit the need for systematic experimental investigations, Geldart classified powders into four different groups characterized by their density and mean diameters [13]. This classification is schematically presented in Fig. 5, focused on conditions prevailing for fluidization with a gas rather than with a liquid.

Fig. 5. Powder classification diagram as a function of the mean particle size of the powder and of the difference between the density of the powder and that of the fluidizing gas. Adapted from ref. [13].

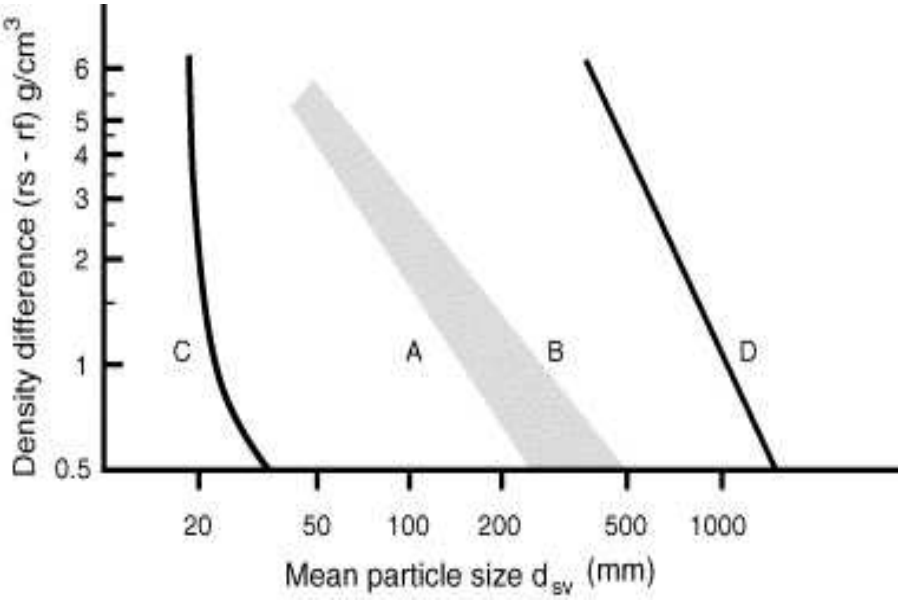

The powders easiest to fluidize belong to groups A and B. Group A gathers particles with small mean size (20–150 μm) and/or low particle volumic mass (less than about 2 g/cm^3). Group B contains most powders composed of particles whose mean size and density range between 40 and 500 μm, and 1–4 g/cm^3, respectively, sand being the most typical material of this group. Group D corresponds to particles which are large; i.e. whose diameter exceeds 800 μm, and/or very dense. Finally, group C contains powders which are in anyway cohesive, due (i) to very small particles size (typically less than 20 μm, but this limit is rapidly shifted to larger particles size with decreasing density difference between the particles and the fluidizing gas), (ii) to strong electrostatic charges and (iii) to the presence in the bed of very wet or sticky materials. It is worth noting that, in Geldart's classification, groups C and A, and groups A and B are separated by transitional regions rather than by sharp boundaries. The presence of such transitional zones, especially between groups C and A, implies it is a priori difficult to classify such particles and, as different rules govern fluidization of the two groups, to control their fluidizability. Hence, it is often necessary to experimentally determine the fluidization behavior for each of these particular cases.

2.3. Behavior of powders in FBCVD reactors, advanced classifications

A typical example of FBCVD process involving group A (aerable) powders concerns the preparation of supported catalysts on porous particles [6]. In this case, as the powder is generally easy to fluidize and the deposit consists of dispersed aggregates, FBCVD can be conveniently performed with respect to the constraints imposed by CVD itself as discussed in

Section 2.4. Powders of this group are only slightly cohesive and, consequently, their beds expand considerably at velocities between U_{mf} and the velocity at which bubbling begins. One of the best studied FBCVD processes in group B (sand-like) particles is ultrapure silicon synthesis on 100 μm silicon particles, as a new way to produce electronic grade silicon for the microelectronic industry [14]. Bed expansion is low and the bed collapses rapidly when the gas supplied is cut off.

In fact, there are few differences in a fluidized bed with regard to CVD processes between powders belonging to groups A and B. The main one is formation of smaller bubbles at higher U/U_{mf} values for fluidized beds composed of group A powders in comparison with those of group B. Consequently, gas–solid contact is better in the former case, which favors homogeneous deposits on powders and reduces by-passing of gaseous reactants. This advantage of group A over group B powders is further enhanced by the fact that, in most cases, bed expansion is higher for group A, which results in an increase of residence time of gas in the bed, and consequently of the gas reactants conversion into deposit. Nevertheless, for small diameter group A powders; i.e. for those which are close to group C, risks of channeling exist for low U/U_{mf} ratios, which can lead to the drawbacks characteristic of fixed beds, in particular plugging of the bed during CVD operations.

A typical FBCVD process on group D (spoutable) particles concerns the coating of radioactive particles by pyrolytic carbon and silicon carbide in order to obtain spherical fuel elements with high qualification yield, i.e. uniform, defect-free coating on each particle [15]. Beds composed of group D powders generally present no or low expansion and poor gas–solid contact. Consequently, in this case, particular fluidization techniques, such as spouted beds are often used. As shown below, for this technology, the gas distributor grid is replaced by a cone, generating a spout of gas through the particles.

In some cases, including commercial powders, the size distribution of the particles is not narrow enough for them to be classified in a single Geldart group. Hence, if fluidization conditions correspond to the main population of particles, larger ones may remain at the bottom part of the bed, and at the same time fines may be elutriated.[1] This situation will lead to heterogeneous deposits; i.e. thicker deposits on larger particles, and to loss of a fraction of the smallest particles. To overcome these drawbacks: (i) sieving is often performed prior to deposition if modification of the characteristics of the starting material is allowed and (ii) technical solutions are applied at the exit of the reactor, such as the addition of cyclones

allowing part of the fines to return to the bed, and/or the addition of filters preventing the fines from contaminating the upstream setup or the environment.

The flourishing of nanotechnologies has led to an increasing demand for processes involving CVD on group C (cohesive) powders [16], [17], [18], [19], [20], [21], [22] and [23]. For these powders, the interparticle forces including electrostatic and Van der Waals attraction are often greater than the forces exerted by the fluid. Consequently, either powders do not fluidize at all or particle agglomeration can occur, with agglomerates reaching sizes of several millimeters. Even if a kind of fluidization can be achieved in the latter case, formation of such agglomerates reduces the contact surface between particles and gas, limits mass transfer of reactants and prevents uniform deposition on each individual particle. Moreover, the agglomerates are consolidated by deposition both on their external part and into the open pores. To face these problems, fluidization can be assisted, for example, by mechanical stirring or vibration. Alternatively, powders can be treated in dilute phase contactors, such as circulating fluidized beds, as detailed in Section 2.5.

More precise criteria to classify particles have been introduced by Molerus [24]. By also taking into account the nature of powders, i.e. soft or hard, and the adhesive or cohesive forces between the particles, the author derived limiting conditions which result in a classification of powders that is equivalent to the definition given by Geldart [13]. With this new classification, the separation between powders of groups A and C is attributed solely to the fact that free particle motion is suppressed by the dominance of cohesive forces in group C.

More recently, Goossens investigated the ability of powders to fluidize depending on the gas flow around each particle by considering the Reynolds and Archimedes adimensional numbers [25]. Such ability is controlled by the competition between laminar and turbulent flows around each particle. For flow around small particles, typically those of Geldart's group C, laminar flow effects are largely predominant over turbulent ones. Such effects are unable to break the local cohesion between neighboring particles and consequently fluidization of each isolated particle is not possible. For flow around bigger particles, typically those of Geldart's group A, some strong turbulent effects are present allowing the dissociation of clusters of particles temporarily formed by local interparticle forces within the fluidized mass, thus leading to gentle fluidization. Moreover, Goossens considered more precisely the transition regime between groups C and A: in analogy with Dry et al. [26], he added a domain

between those of these two groups, named AC. Following his classification, for AC powders, the turbulent flow effects around each particle are small but sufficiently strong to generate a loose structure of partially contacting particles within the fluidized mass. He finally pointed that interparticle forces can be larger than standard for soft particles, irregular ones and particles with specific adsorption properties for the fluidizing gas. This is a valuable remark in view of FBCVD for the processing of nanomaterials, such as filaments or nanotubes (see Section 3.5).

In conclusion, optimum conditions for FBCVD processes can be achieved more easily for Geldart A and B powders. CVD treatments on group D powders can a priori be performed in spouted-bed reactors. Difficulties arise when particles of groups AC and especially C have to be treated.

2.4. Constraints on fluidized bed due to the CVD process

Besides limitations due to the handling of powders themselves, additional constraints appear due to simultaneous CVD operation. These constraints arise from: (i) imposed CVD operating conditions and especially pressure and temperature, (ii) side deposition on the reactor walls and on or in the gas distributor, (iii) clogging of the bed due to high deposition rates and/or to low-quality fluidization, (iv) homogeneous nucleation and (v) handling of the CVD precursors.

Conventional CVD processes on massive substrates often operate at reduced pressure to allow the diffusion coefficient in the gas phase to be significantly enhanced, hence leading to the control of the process by heterogeneous chemical reactions. Consequently, uniform growth rates are expected at every point on the surface of flat substrates as well as efficient diffusion into submicronic trenches or infiltration into porous preforms. In contrast to this situation, most fluidised-bed contactors operate at atmospheric pressure. This is not a drawback for FBCVD processes since the motion of the gas around each particle is enhanced by the vigorous movements of particles in the bed. However, applications exist for which deposition is also required to occur inside porous particles. In that case, diffusion through the pores depends more on the operating pressure than on the relative movement of the particles, and deposition at reduced pressure is necessary. This is typically the case of supported catalyst preparations; i.e. catalytic metallic nanoparticles deposited on and inside porous supports [6]. Few studies deal with fluidization under reduced pressure ([27] and [28] and references

therein) and, as a result, the behavior of fluidized beds under these conditions is not well-known. A practical low limit for the operation of fluidized beds is 7.3 kPa; below this value fluidization quality is degraded due to heterogeneous behavior between the top and bottom parts of the bed. Finally, for low-pressure operation, contamination of the vacuum system by elutriated particles must be prevented by adding appropriate filters. The filtering equipment most commonly used are centrifugal separators (cyclones), inertial filters or separators by sedimentation for particle diameters higher than 10 μm and, for particle diameters lower than 10 μm, electrofilters and bag filters [29]. It is worth noting that, on the laboratory scale, cyclones have a poor efficiency and electrofilters are difficult to tune.

Another important parameter is the operating temperature. Numerous conventional fluidized beds operate above ambient temperature. For these contactors, the vigorous mixing of the particles by the gas flow ensures isothermal conditions. This situation is hardly influenced by chemical reactions occurring in the bed, since thermal inertia and vigorous mixing often compensate any endo- or exothermicity of reactions. But, for spouted beds and dilute-phase contactors, such as circulating or vertical moving fluidized beds, radial heterogeneities in temperature may occur, particularly for large-diameter reactors. Moreover, the calorific capacity of powders in large-diameter reactors does not compensate for the cooling induced by the inlet gas flow and it is often necessary to preheat the carrier gas.

The design and positioning of the grid is critical in FBCVD owing to the risk of plugging up. This question was recently dealt with in [9] and is schematically illustrated by the flow chart of Fig. 6. This figure resumes information from literature research and personal experience. It shows that plugging of the grid is subjected to constraints which are more severe when either one or both of the following situations occur: (i) the powders to be fluidized either belong to group C or present a wide particle size distribution with large amounts of fines, or are fluidized in the form of agglomerates and (ii) metalorganic (MO) precursors are used in the CVD process. The first point involves the use of distributors or frits with reduced apertures (holes or porosity, respectively). The second one usually involves moderate or low operating temperatures and, consequently smooth temperature gradients. Considering the isothermal conditions, which prevail in fluidized beds, the distributor in such a case must be placed at a position where: (i) temperature is both lower than that of deposition or decomposition of the precursor and higher than that of condensation or sublimation of the precursor and (ii) the fluidized bed is in the deposition zone. In some cases, these constraints cannot be satisfied and

it is necessary to inject the precursor directly in the bed just above the distributor [30], or to use appropriate reactor design not containing any grid or other support to maintain the particles in the deposition zone [31].

Fig. 6. Flow chart illustrating the factors leading to the plugging of the distributor in FBCVD reactors, and the possible solutions to this problem. T_{dep} and T_{cond}: deposition and precursor condensation temperature, respectively [32].

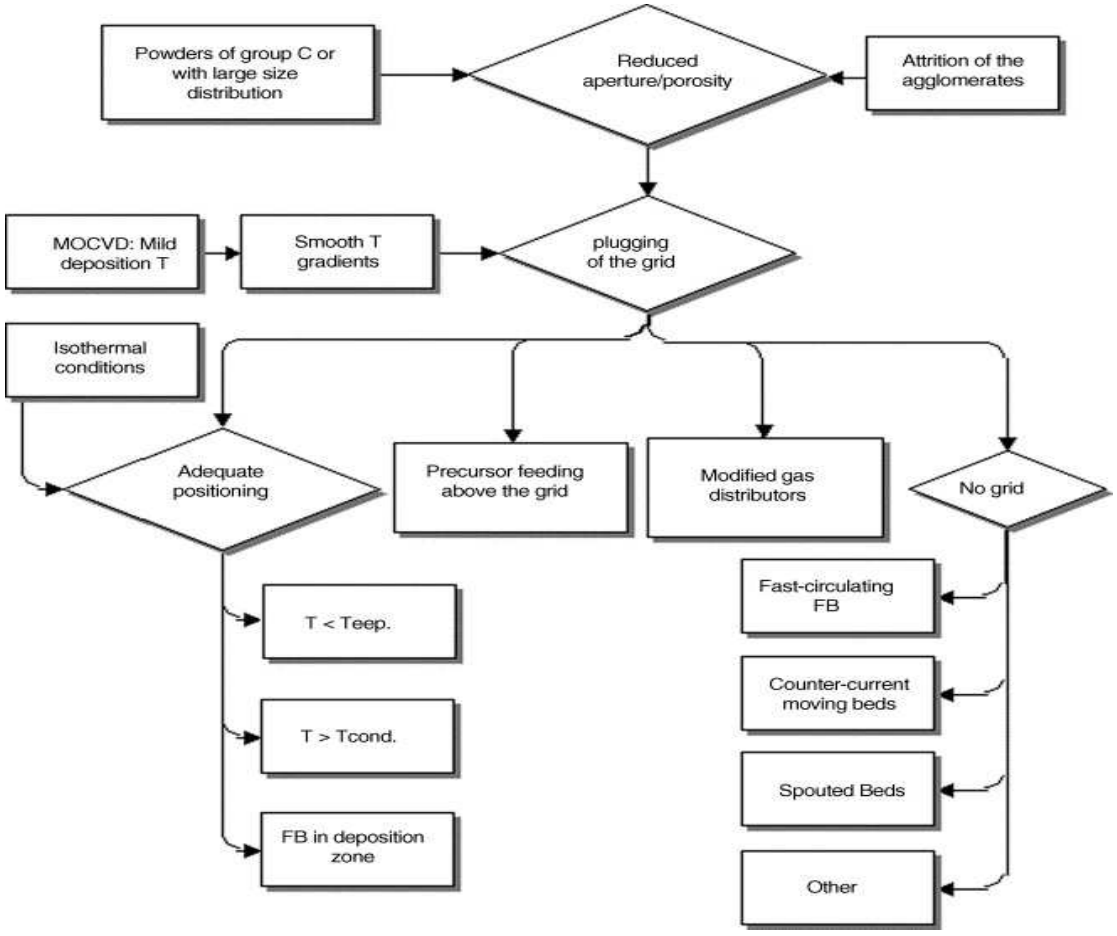

Another specificity of some FBCVD processes is related to the possibility of bed agglomeration during deposition. This unwanted phenomenon occurs when deposition rates are high and/or when the fluidization quality, i.e. the intensity of particle mixing due to gas flow, is poor. Indeed, continuous deposits may produce an increase in surface cohesiveness of particles, which could be due to deposited chemisorbed species making the particles sticky [33]. This increase in particle cohesiveness can be observed by using thermal and pressure

drop measurements through the bed [14] and [33]. When the interparticles cohesive forces become higher than the disintegration force, depending on the intensity of particles movements, clogging speeds up and aggregates tend to solidify. When such problems occur, the critical operating range must be determined in terms of initial molar fraction of reactants, temperature and flow rate, to optimize the fluidization hydrodynamics. An efficient way to follow and try to prevent clogging is to monitor on-line both the differential pressure drop of the bed and the temperature profile along the reactive zone. Moreover, in the particular case of silicon deposition from silane SiH_4 or disilane Si_2H_6, undesirable fine particles form above the fluidized bed in the colder upstream zones of the equipment [33] and [34]. These parasitic fines are composed of oily brown hydrogenated silicon. Their amount was found to be proportional to the percentage of reactive gas remaining unconverted in the fluidized bed. The mechanisms recognized most often involve homogeneous polymerization due to the existence of thermal gradients in the upper regions of the FBCVD reactor [14]. The main drawback of such powdering is the risk of contamination of the bed.

Particular characteristics of the CVD precursor should also be taken into account for the design of a FBCVD reactor. Generally speaking, a chemical precursor must meet a number of requirements to be successful [35] and [36], such as: (i) good volatility, (ii) adequate thermal stability, especially during the gas-phase transport, (iii) high purity, (iv) clean decomposition, avoiding the contamination of the resulting material, (v) absence of, or reduced toxicity: this also applies to the decomposition products, (vi) convenient and high yield preparation protocol and (vii) sufficient stability during storage. Toxicity and/or stability of the precursor can involve some severe constraints for running the process safely, among which careful checking of apparatus sealing or use of a glove box for deposition, use of integrated systems for in situ generation of the precursor and/or of specific sensors. Concerning precursor volatility, it will impose the choice of specific delivery systems [37]. Generally speaking, delivery of gases via mass flow controllers and of liquid precursors via the use of mass flow controllers and bubblers is commonly used in CVD processes. Delivery of solid precursors through specially designed sublimators is less common due to the often high sublimation temperatures and to unstable and unreliable precursor flow rates to the CVD reactor. In that case, isothermicity should be ensured from the sublimator to the distributor grid to avoid any precursor condensation. As for deposition on flat substrates, methods combining the principles of both liquid and solid state delivery have been developed for liquid or hard-to-sublime compounds, whereby droplets or spray of, respectively, pure precursor and precursor-

containing solutions are injected directly in the FBCVD reactor [38]. Careful tuning of the solution flow is needed to allow quick solvent vaporization and production of homogeneous deposits. Additional constraints may arise from high carrier gas flow rates, sometimes necessary for fluidization, that will cool down the precursor and thereby affect the deposition quality. Pre-heating of the gases before the precursor delivery system should then be performed. Finally, if reactive gases are used to assist precursor decomposition, special care should be taken in the design of the reactant inlet in order to avoid precursor decomposition before the bed or on the distributor grid. Solutions previously mentioned about grid positioning and precursor injection in the vicinity of the grid also apply here.

2.5. Types of reactor for performing CVD on powders

The choice of the FBCVD reactor is mainly related to the type of powder to be treated. In some particular cases, the CVD operating conditions may also influence the technical solutions selected.

2.5.1. Classical FBCVD reactors

A typical FBCVD reactor is schematically presented in Fig. 7 [33]. It is used to deposit silicon from SiH_4, either to protect powders against corrosion or oxidation [39] and [40], or to produce ultrapure silicon for microelectronic or photovoltaic uses [34]. The 5.3 cm diameter stainless steel reactor contains an expanded freeboard section to allow particles entrained by the gas flow to drop back into the bed, a gas distributor and water-cooled distributor flanges to prevent any premature decomposition of the precursor. The thermal profile along the apparatus is measured by several thermocouples fixed to a thin rod as illustrated in Fig. 7 and connected to a computer. A fast response differential pressure transducer monitors the pressure drop between the top and the bottom parts of the reactor. The fluidization quality can thus be followed all along experiments. Outlet effluents are treated using a cyclone and a bag filter, to collect elutriated particles or fines formed during experiments; the hydrogen content of the gas phase is measured by a catharometer connected to a computer. A vacuum pump associated with an absolute pressure gauge allows operation under reduced pressure, down to 1.3 kPa.

Fig. 7. Typical FBCVD setup used for the deposition of silicon from SiH_4. Adapted from ref. [33].

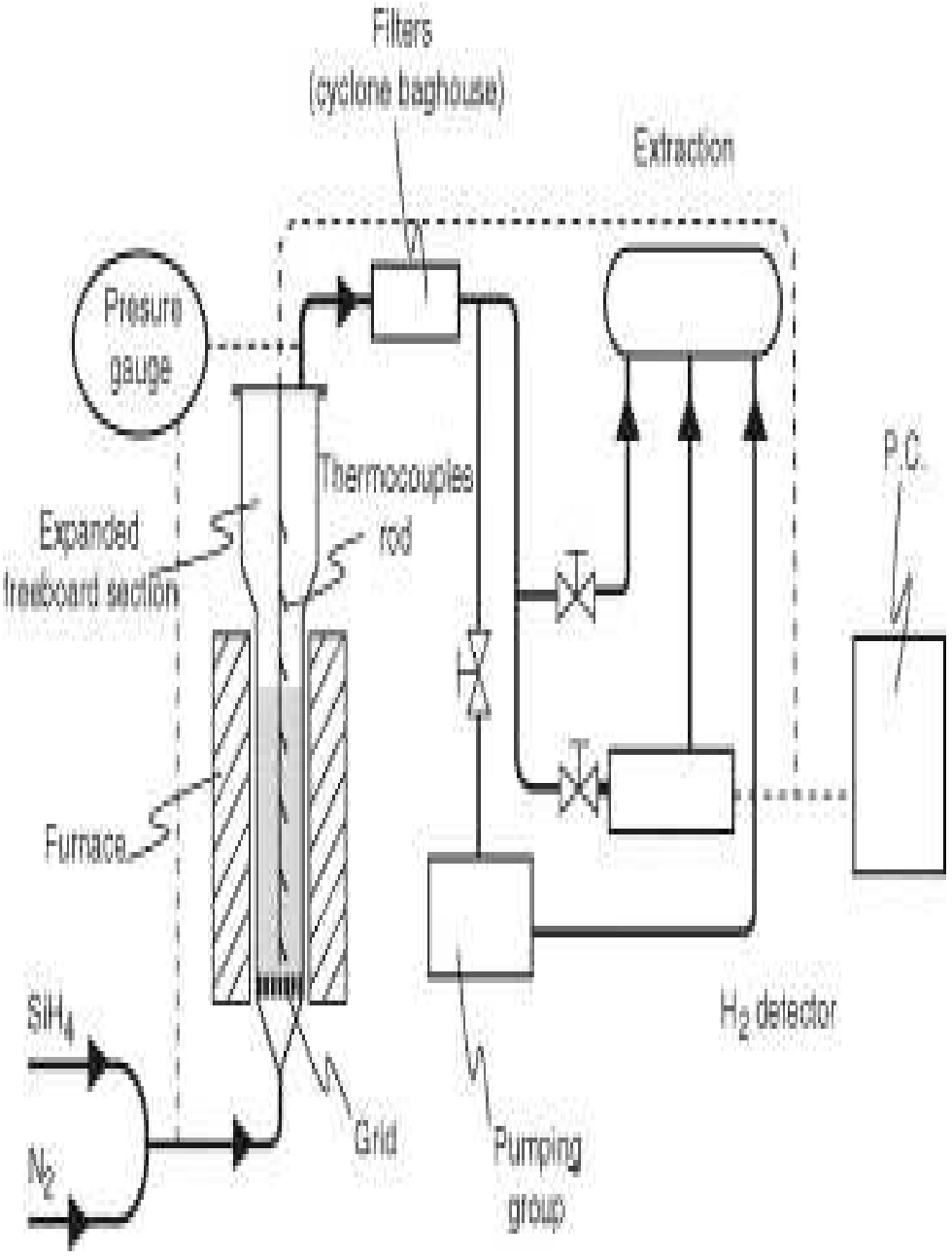

2.5.2. Spouted-bed reactors

Beyond the different solutions to the problem of deposition on the grid and its subsequent plugging that have been mentioned in the previous section, a radical approach would be to design a reactor which does not contain any grid or other support to maintain the particles in the deposition zone. In the mid fifties, Mathur and Gishler were the first to propose such a setup, characterized as “Canadian fluidization”, or actually better known as spouted-bed (SB)

reactor [41]. Fig. 8 illustrates the principle of operation of a SB and the SB reactor that has been used by Juarez for doping NiCoCrAlYTa powders with rhenium and ruthenium [42].

Fig. 8. Left: schematic representation of the spouted bed. Right: SBCVD reactor used by Juarez for the deposition of Re and Ru on the surface of NiCoCrAlYTa powders [42].

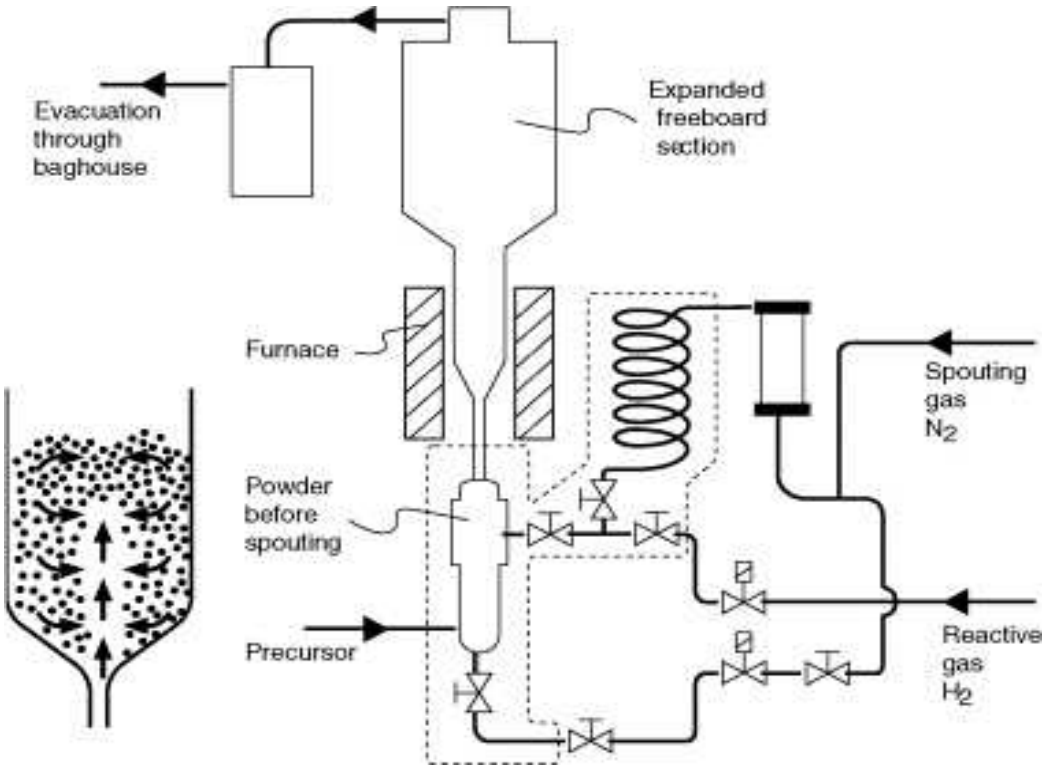

Spouting consists in forcing a jet of gas vertically upwards through the mass of solid particles. The high-velocity jet causes a stream of solids to rise rapidly upwards in a hollowed central core or spout within the bed. The particles, having reached somewhat above the bed level, fall back onto the annular space between the spout and the container wall and travel downwards as a packed bed. The gas flares out into the annulus as it travels upwards. Thus, a systematic cyclic pattern of solids movement is established with effective contact between the gas and the solids [43]. Most SB reactors are cylindrical with a conical base. However, entirely conical reactors have also been proposed for physical and chemical operations where vigorous contact is needed to avoid dead zones in the bed, for example, when the solid is sticky and tends to fuse [44]. Particle flow in a SB has been visualized (e.g. [32], [42], [45] and [46]) and has recently been simulated by Kawaguchi et al. [47].

SB reactors were originally developed as a method for achieving contact between Geldart group D solid particles and gas. They are used to perform either physical operations ([43] and references therein) including coating and granulation ([48] and references therein) and chemical operations, such as pyrolysis ([49] and references therein), oxidation [50], combustion [51] or polymerization [52]. They present several advantages over the fluidized bed, concerning both physical and chemical (including CVD) operations:

i. Easy construction, such as the non-requirement of a distributor grid or any other sophisticated gas distributor.

ii. A lower pressure drop than in a fluidized bed. This point concerns industrial scale reactors for which the pressure loss of the gas crossing the distributor may be considerable. In such cases, input pressure of the gas has to be relatively high, leading to increased technical problems.

Iii. Possibility to process powders which are difficult to handle, e.g. sticky, with a wide particle size distribution, thermally sensitive or those that must be vigorously mixed with the gas phase [44].

iv. Shorter residence time of the gaseous by-products than in fluidized-bed reactors leading to decreased side-reactions.

Like fluidised-bed reactors [53], [54], [55] and [56], spouted beds are compatible with other-than-thermal activation sources. For example, plasma heating of the particles in a SB was reported by Horio et al. [57]. Finally, like fluidized beds, SBs can be used in recycling mode [48]. However, SBs also present severe drawbacks, such as bypassing of gas, attrition or less isothermal operation than FBs. Moreover, while serving as a well-established gas–solid contacting technique for coarse group D particles, SBs operating with fine particles have received little attention, although spouting of particle sizes as small as 90–100 μm has been reported in some cases [31], [45], [58] and [59].

2.5.3. Specific technologies

Fine and ultrafine powders are difficult to fluidize in conventional FB and SB CVD reactors. This is due to the formation of agglomerates, of channels and of defluidization zones. Performing CVD in such configurations often leads to the stabilization of agglomerates and to

partial or total agglomeration of the bed, instead of deposition on the entire surface of each individual particle. Solutions, such as the addition of coarse particles that are used to improve the behavior of the powders in simpler FB reactors cannot necessarily be applied to CVD processes. Consequently, alternative reactor configurations have been proposed in the literature for the deposition on such ultrafine powders. These configurations will be presented later. However, it should be pointed out here that for particle sizes lower than 5 μm, fluidization of and a fortiori deposition on the entire surface of individual particles remains an unsolved problem essentially due to elutriation and to the low fluidizability of powders.

A first approach to the problem of fluidization of fine particles is to use vibro-fluidised-bed reactors, as schematically presented in Fig. 9 [60], [61], [62], [63], [64] and [65]. By breaking channels and cracks, vibration improves the fluidity of beds. Moreover, for group C powders, U_{mf} decreases as the vibration strength is increased. In practice, an assembly with one or two eccentric motors is fixed to the reactor. The motors are connected to a vibrator, which ensures vertical, horizontal or twisting vibrations with frequencies between 15 and 60 Hz and amplitudes of several millimeters. In some cases, these two parameters control the size of the agglomerates. Vibro-fluidized bed technology implies costly equipment and heavy industrial infrastructures. Moreover, uniform vibrations along the reactor are difficult to achieve.

Fig. 9. Scheme of the vibro-fluidized-bed reactor used for the preparation of oxide superconductive composite particles. Adapted from ref. [65].

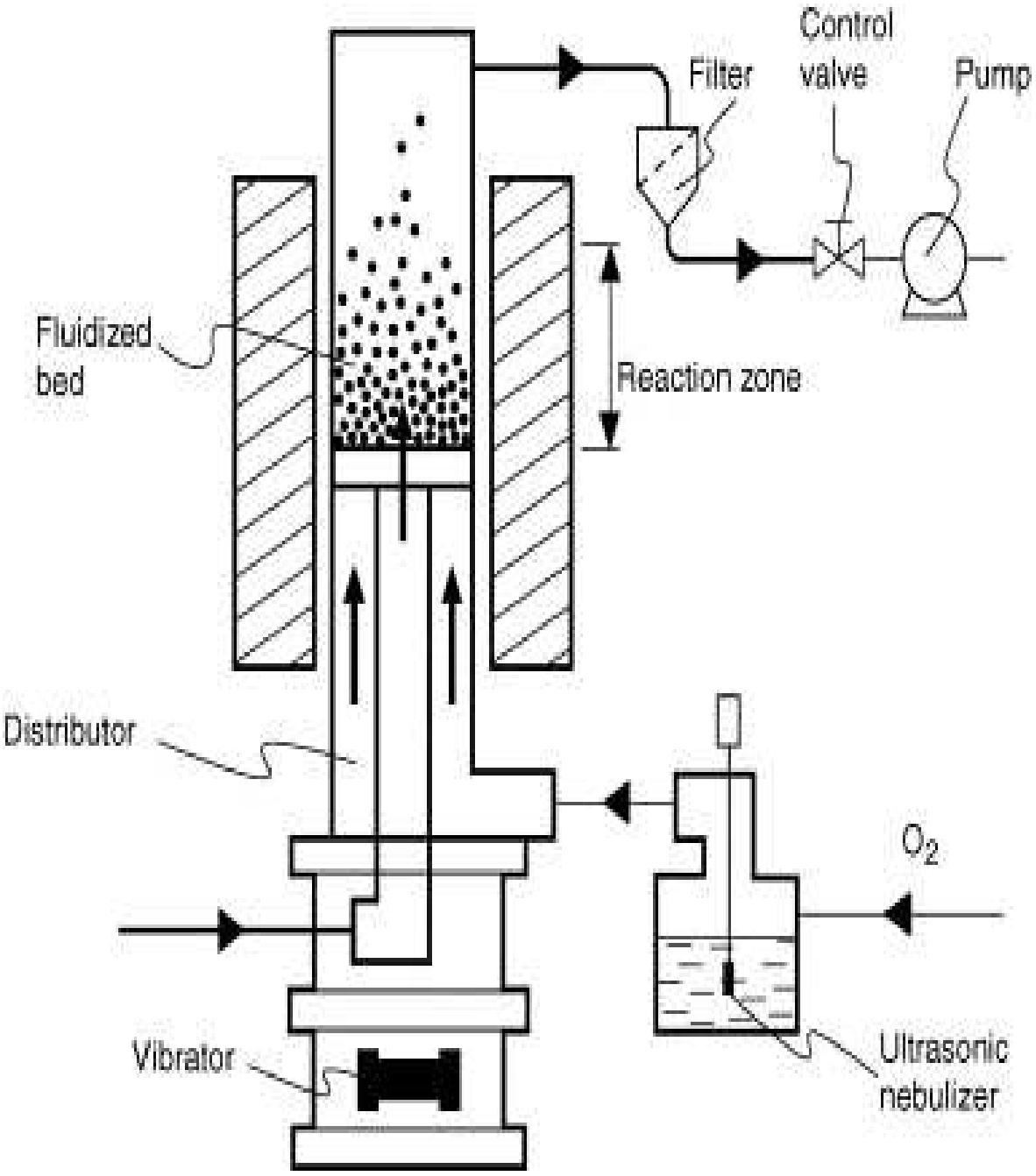

A simpler method to activate fluidization during CVD operations is to use mechanical stirrers inside the bed instead of vibrators that are located outside the reactors, as presented in Fig. 10 [61], [66] and [67]. Various geometries of stirrers are possible, such as scraper or cage stirrers [68], and helical or comb-like paddles [61]. In this case, technical difficulties must be overcome, such as the establishment of a leak-free connection between the rotating axis of the stirrer and the reactor. Another problem is linked to side deposition on the rotating parts and the subsequent potential contamination of the bed due to the risk of delamination of these undesirable deposits. This drawback has been met in particular by Kimura et al. [69]. For this reason, the authors replaced this technology by a floating type FBCVD system [70]. Their setup is schematically illustrated in Fig. 11. In this scheme, the authors divided the behavior of the particles into three different zones in the reactor, namely I, II and III. CVD was performed in zone III, where powders were dilute and collisions among the particles seldom appeared to occur. Although the authors performed deposition on very small agglomerates in this configuration, it was still not possible to ensure deposition on each individual particle. Moreover, since this zone of the reactor does not correspond to the fluidized bed, it can hardly be in isothermal conditions both in radial and axial directions. Also, due to the reduced quantity of powders in the floating zone: (i) conversion of reactants is low and (ii) the yield of the process in terms of treated powders per unit time is also poor.

Fig. 10. SBCVD reactor used to deposit SiC on carbon coated ceramic beads. Adapted from ref. [71].

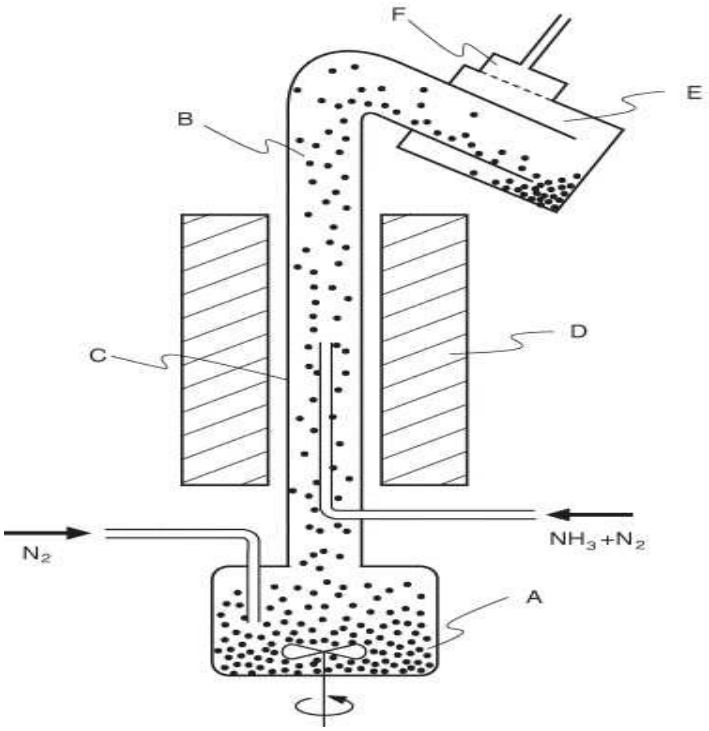

Fig. 11. Schematic illustration of the experimental setup used for the synthesis of AlN/SiC composite powders by floating-type fluidized CVD. Adapted from ref. [70].

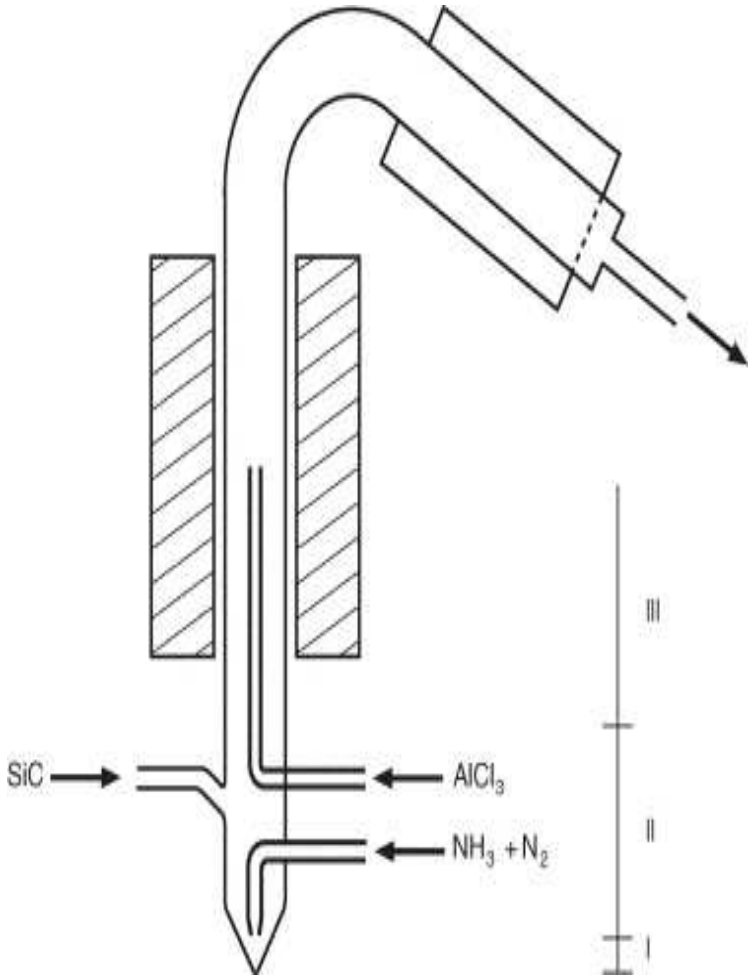

An alternative way to perform CVD on fine powders with increased productivity is the use of moving bed contactors. Golman and Shinohara applied this solution both in counter-current and in co-current configurations; i.e. by feeding the gas from the bottom and from the top, respectively, while feeding the powder from the top [72] and [73]. Fig. 12 presents the two setups that have been used by these authors. The main advantage of this configuration is the increase of the productivity in terms of treated powders. However, it also involves some

drawbacks. As in the case of floating type FBCVD reactors, since the contactor works in a dilute regime, operation cannot be isothermal and conversion of reactants is incomplete. In addition, the residence time of the particles in the deposition zone is intrinsically short, implying only small amounts of deposited material and consequently limiting this configuration to specific applications. To avoid elutriation of fines and to control residence time better, Golman and Shinohara pre-agglomerated their submicronic particles intograins of several hundred microns. Finally, a technological problem concerns the control of the powder feeding rate from the source tank: vibration of the tank can help.

Fig. 12. Schemes of counter current moving bed CVD reactors. Adapted from refs. [72] (a) and [73] (b).

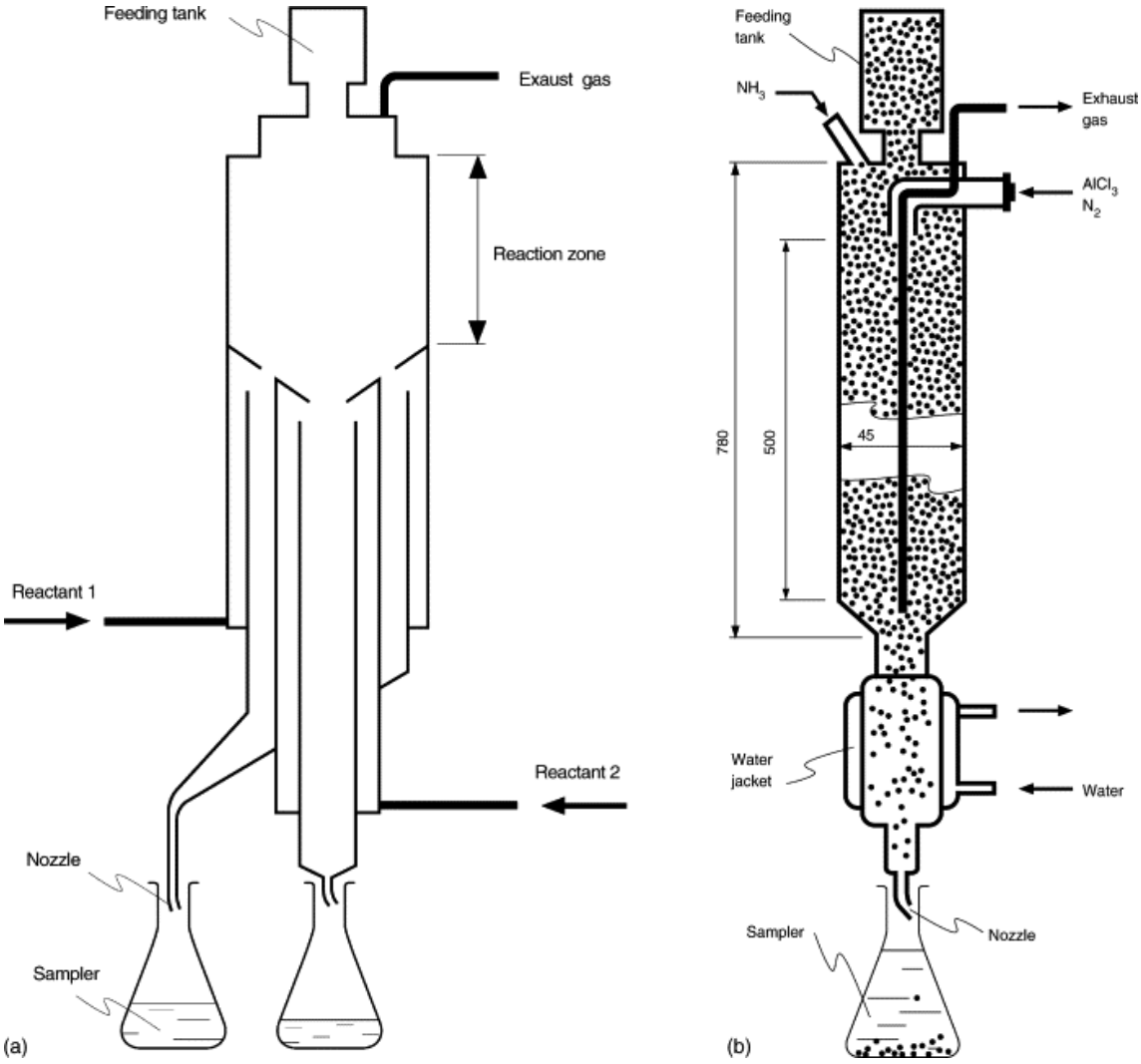

Residence time in the deposition zone can be increased if particles are re-circulated in a closed system. This can be achieved in a so-called circulating fluidised-bed reactor, as represented in Fig. 13. Typically, this kind of reactor consists of a vertical tube in which the powder is in a fast fluidization regime. The tube is associated with an oversized cyclone, which ensures the capture and recycling of particles, which are re-introduced in the bottom of the reactor by a dip leg, while gases are evacuated through the upper part of the cyclone. The fast fluidization regime is generally characterized by a much diluted upward solid flow in the tube center and a fluctuating downward flow of particles at the tube walls. This intense longitudinal back mixing allows a flat vertical temperature profile, but radial temperature gradients can exist due to the high degree of dilution and the coexistence of opposite gas flows. Additionally, this fluidization regime ensures some steady agglomerates of relatively uniform size. The design and tuning of such processes are far from trivial. The main

technological difficulties concern the filtering of the finest particles at the top of the reactor and the re-introduction of particles at the bottom of the bed, where agglomeration may occur, particularly for cohesive ultrafine powders.

Fig. 13. Circulating bed CVD reactor (right, adapted from ref. [53]), and suggested flow structure for fast fluidization conditions (left, adapted from ref. [74]).

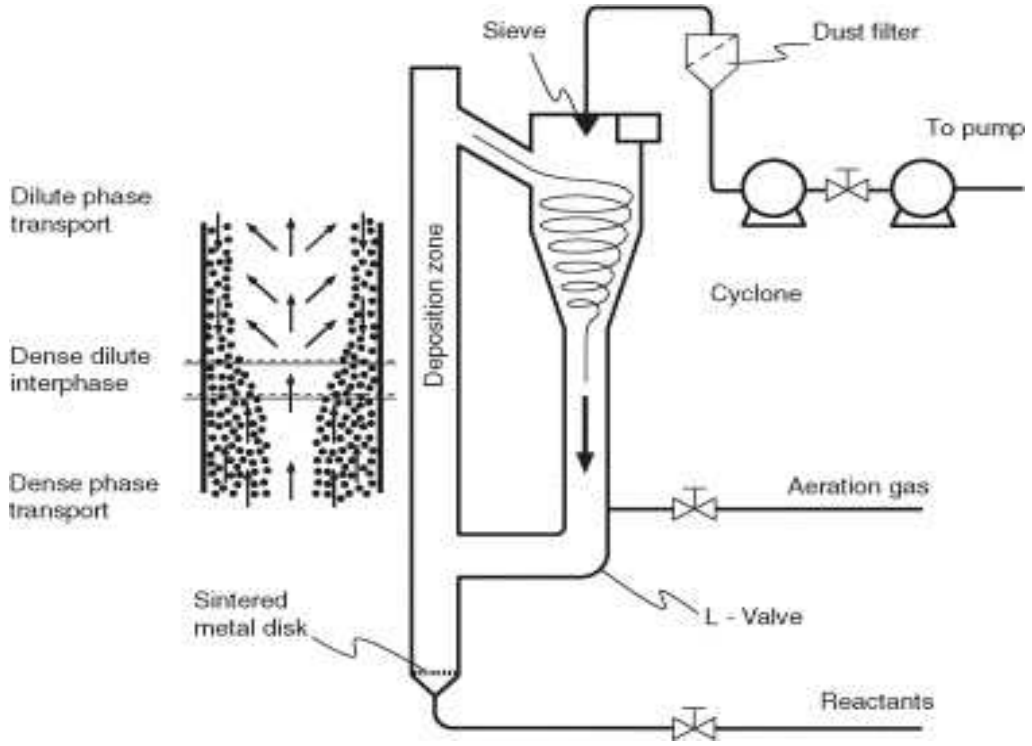

A final technological solution to perform CVD on the entire surface of fine (~5 μm) particles involves the use of a rotating drum CVD reactor equipped with a specially designed comb-like guide [8]. Although properly speaking fluidization does not occur in this setup, gas–solid contact can be reached fairly efficiently through the simultaneous consideration of particle density and diameter and rotation velocity of the reactor. To temporarily limit particle agglomeration and particle sticking to the reactor walls, the authors claim that the use of a fixed comb-like guide can recirculate and homogenize the batch and de-agglomerate the powders by exerting sufficient shear on them. However, both operation in continuous mode and trapping of particles at the exit appear a priori difficult.

2.5.4. PECVD and other activated technologies

Most of the technologies mentioned above use thermal activation of chemical deposition reactions. However, if coatings of particular microstructure or composition are needed, or when deposition on temperature-sensitive substrates is required, plasma-enhanced (PE) decomposition of the precursors is often used. However, the combination of FB and plasma is a recent field of research [2]. As for thermal CVD, several families of FB-PECVD processes exist, classified as a function of the operating pressure (atmospheric or under vacuum), the operating temperature (ambient or high temperature) and the type of gas-particle contactors (conventional FB, circulating FB, spouted bed, rotary drum, etc.). A review of PECVD on powders has been performed by Karches [38] and additional information can be found in refs. [1] and [2]. Such operations are most often performed under reduced pressure of typically 0.1–2 kPa. A specific problem of FB-PECVD processes is that plasmas hardly penetrate a dense (fixed or even fluidized) bed. It can be achieved in some cases by increasing power density typically to 10 W/cm^3 in the case of pure argon. The risk is the creation of hot spots and the local melting of particles. For this reason, the plasma is usually generated in a position in the reactor where a dilute phase exists: freeboard in a classical fluidized bed [75] or riser in a circulating fluidized bed [53]. From this point of view, the use of a rotating drum may appear interesting, and has already been tested ([23] and references therein).

A recent application dealing with this technology is the encapsulation of 150 μm SiC particles by 1 μm thick alumina film in a circulating PECVD reactor operating at low temperature and low pressure (0.4–0.9 kPa) with the aim to improve the hardness and the chemical stability of the powders used as abrasive materials [76]. The deposition of nitride films (TiN and Si_3N_4) on group D inert particles (silica and corundum) in an arc PECVD spouted-bed reactor operating under atmospheric pressure and relative high temperature (600–900 K) has also been reported, as illustrated in Fig. 14 [2]. The plasma generator is located at the conical bottom part of the reactor and the plasma jet is used as the spouted gas. This plasma discharge combines the effects of thermal plasma (excitation of heavy species) and of out-of-equilibrium plasma (generation of electrons, excited species and radicals and ions at low temperature).

Fig. 14. Arc PECVD spouted-bed reactor used by Sanchez et al. for the deposition of nitride films on group D particles. Adapted from ref. [2].

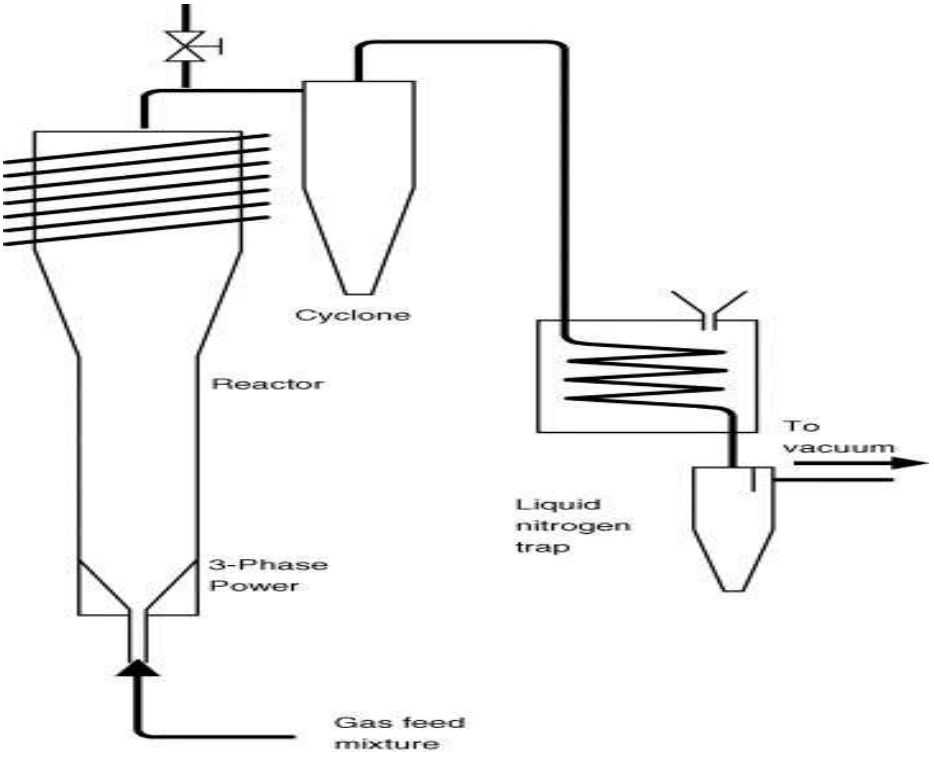

Finally, Bretagnol et al. reported a cold plasma fluidized bed process used to modify the surface properties of polymeric powders [77]. Likewise, Guo et al. developed a technique for depositing polymer coatings on powders of various sizes [78]. Such cold plasma processes find applications in biotechnology. Also, to prepare materials for use as deuterium–tritium containing targets in inertial confinement fusion experiments, Theobald et al. coated a limited number of 1 mm polyalphamethylstyrene microshells by amorphous hydrogenated carbon films [79] and [80]. In their study, they used a reactor composed of two parts: the upper one where active species are generated by remote plasma created in a helical resonator coil and the lower one where such microshells are placed in a pan under agitation that is either piezoelectric or with a solenoid. Precursors used were trans-2-butene and plasma-activated hydrogen. Dense, 60 μm thick coatings were thus obtained, with low surface roughness, at a deposition rate of 1.8 μm/h [81].

2.6. Modeling of FBCVD reactors

The most direct route to analyse and even to predict the influence of operating conditions on the behavior and efficiency of chemical processes is modeling. Such numerical tools are particularly valuable during scale-up phases.

Models of FB contactors have existed since the sixties. The first generation of models, named bubbling bed models, was based on the two-phase theory: the bed is generally assumed to contain a bubble phase corresponding to gas bubbles in which particles are present in small amounts and an emulsion phase representing the rest of the bed [82], [83] and [84]. Either plug flow or perfectly mixed conditions are postulated in each region, and interphase gas transfers are most often evaluated from overall mass balance, involving empirically determined mass transfer coefficients [85]. For instance, the main assumptions of Kato and Wen's model [82] are the following: (i) the FB is isothermal, (ii) bubbles are growing as they ascend through the bed and their diameter is calculated from an empirical correlation (iii) the FB is represented by a series of compartments, the height of which being equal to the mean diameter of the bubbles at the corresponding level, as illustrated in Fig. 15, (iv) each compartment is composed of two phases, the bubble phase corresponding to the bubbles and their surrounding cloud of particles, and the emulsion phase, corresponding to the rest of the bed, (v) the gas is taken to be perfectly mixed in each phase and (vi) mass transfer exists between these two phases in each compartment; it is quantified through an empirical mass transfer coefficient.

Fig. 15. The FB as represented by the Kato and Wen model. Adapted from ref. [82].

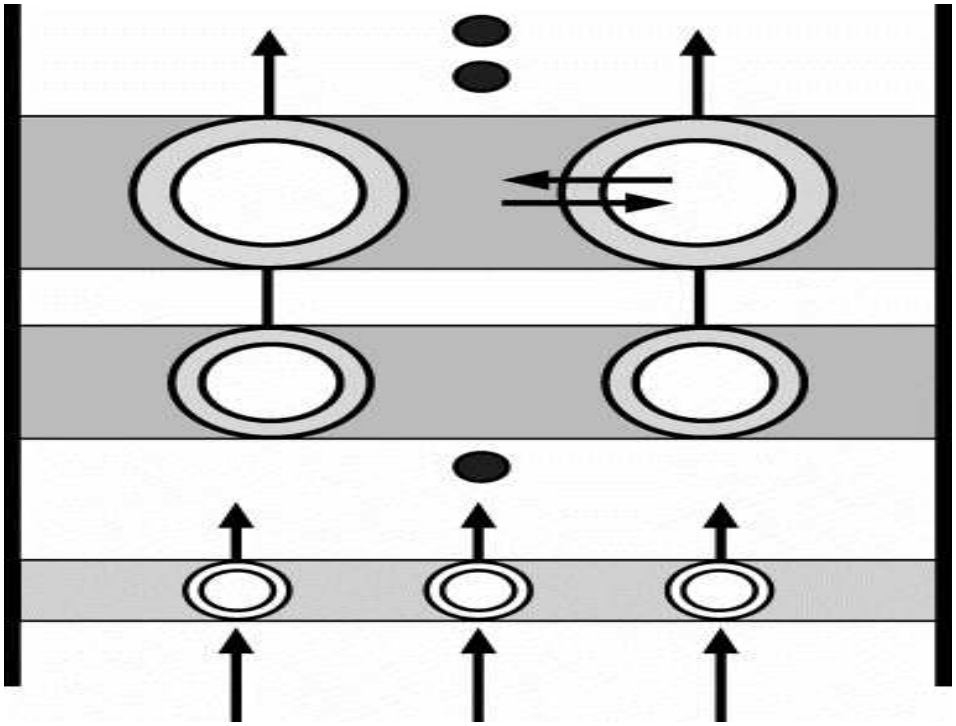

Several groups of authors theoretically analysed the influence of gas flow rate variations induced by non-equimolar chemical reactions occurring in a FB. Indeed, chemical reactions will affect the general gas flow and local mass transfers in the FB. Consequently, the equations of the classical bubbling bed models must be modified to take these phenomena into consideration. In the case of FBCVD, Caussat et al. assumed that an increase in the total number of gaseous molecules due to CVD reactions produces additional mass transfer from the emulsion (where heterogeneous reactions mostly occur) towards bubbles, leading to an increase of bubble diameters [86].

The application of such models to FBCVD processes has only been achieved for silicon deposition from SiH_4 and Si_2H_6 [85]. The reason for such exclusivity is that, as for classical CVD processes, modeling requires access to the homogeneous and heterogeneous chemical mechanisms involved and to the corresponding kinetics laws. SiH_4 pyrolysis is certainly the most mastered of all CVD chemical systems. This is particularly true when organized in a FB, since two groups of authors have established specific kinetic laws for SiH_4 homogeneous and heterogeneous decomposition in a FB [87] and [88].

Lai et al. [89], Furusawa et al. [87] and Li et al. [90] were the first to adapt a classical FB model to account for SiH_4 decomposition, considering, as appropriate, nucleation, coagulation and catching of fines in the bed [90]. Their aim was to understand how the fines are formed and to predict the influence of operating conditions on the percentage of fines formed during deposition so as to decrease this unwanted parasitic production. The authors concluded that fines proceed from homogeneous reactions inside the bubbles in the bed and that their formation increases with the inlet silane concentration and with the bed voidage.

Caussat et al. modified four classical FB models, in order to progress in understanding the phenomena of clogging and fines formation [91]. It is worth noting that in this work, a complete homogeneous kinetic scheme was considered, allowing the prediction of local concentrations of SiH_4, disilane Si_2H_6, silylene SiH_2, tri-Si_3H_8 and tetra-silane Si_4H_{10} and their contribution to the deposits formed along the bed height, in good agreement with experiments. For instance, the evolution of the silicon deposition rate along the bed height calculated from the Kato and Wen model is given in Fig. 16. These curves show that only the first half of the bed is efficient for deposition, due to the high specific surface area offered by the bed particles. From this original result, it was deduced that an increase in the deposition rate of the process could be obtained without exceeding the critical value of agglomeration, by using

distributed injection of silane. However, this group of authors showed that such classical FB models are unable to correctly represent highly reactive chemical processes involving intense contributions of unsaturated species, such as for CVD, silicon deposition from Si_2H_6 [85]. In that case, the strong assumptions and the numerous inadequate empirical coefficients governing these models lead to imprecise results.

Fig. 16. Silicon deposition rate along the bed height calculated from the Kato and Wen model. Adapted from ref. [91].

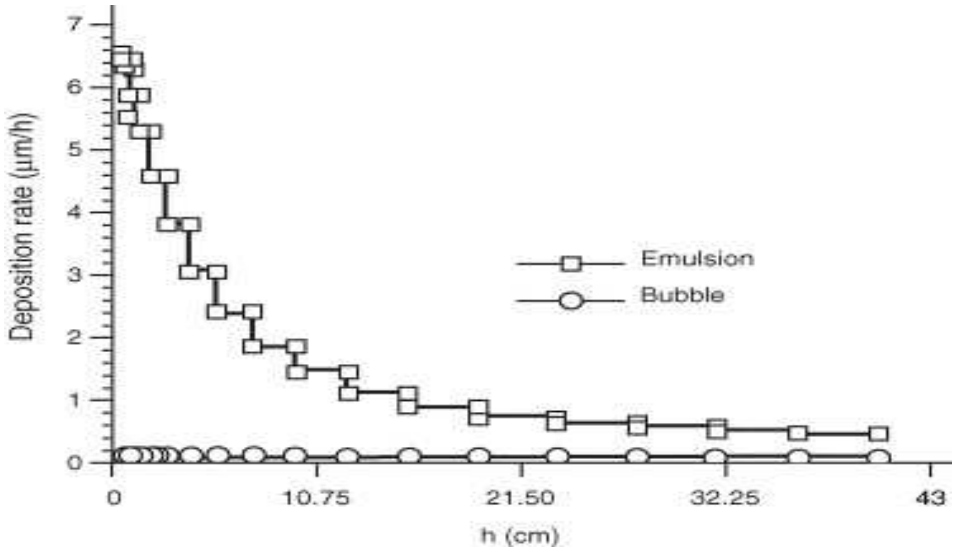

Due to these intrinsic limitations, new generations of FB models have been under development for several years, often based on a Eulerian–Eulerian representation, leading to the so-called two fluid hydrodynamics models. This family of models treats the gas and solid phases of the FB as two continuous and fully interpenetrating media. Such models solve mass, momentum and energy balance equations for both the gas and solid phases in a given number of cells standing for the bed [92]. Today, several commercial multiphase computational fluid dynamics (CFD) codes, such as CFX, Fluent, MFIX, are available to represent FB contactors [93]. As illustrated in Fig. 17, such models today provide very complete and impressive results concerning the hydrodynamic behavior of FB. Indeed the local gas and solid velocities and the transient bubbling phenomenon can be predicted by such approaches. These CFD codes undoubtedly hold the greatest potential for future FB modeling.

Fig. 17. Gas velocity field in a FB calculated by the CFD code Fluent. Adapted from ref. [94].

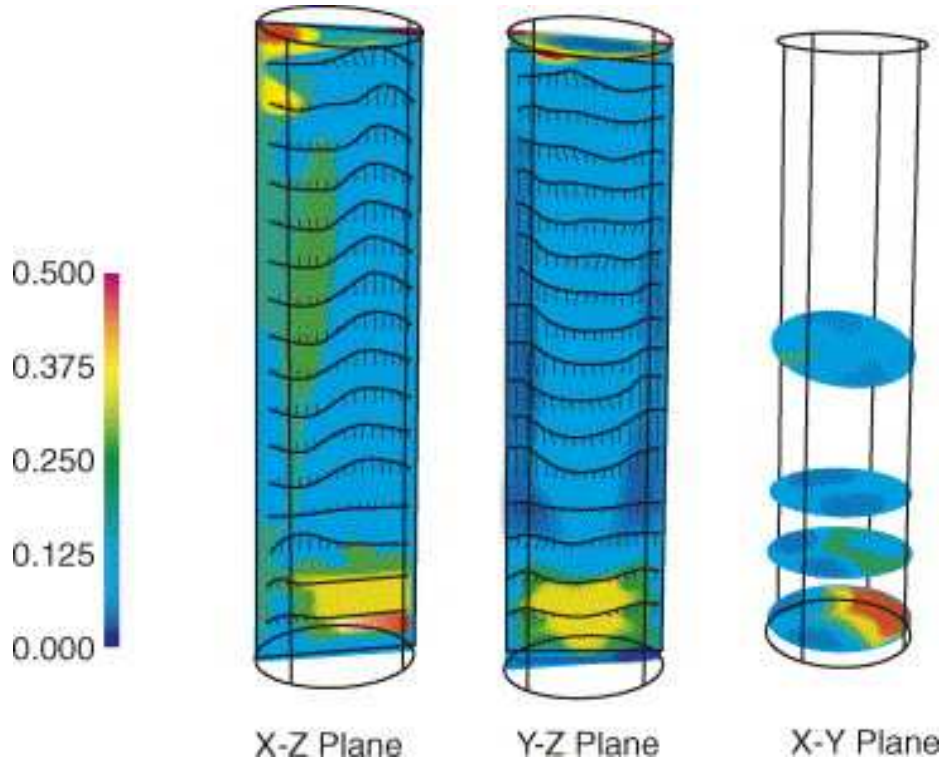

However, the computational costs involved in such approaches remain currently high, especially for 3D simulations, and numerous intrinsic aspects of FB (particle interactions, relative motion between phases, etc.) are not accurately represented, due to the complexity of the phenomena involved. For these reasons, today CFD simulations mostly deal with pure hydrodynamic studies and rarely treat thermal gradients or reactive mass transfers inside FB. Despite these limitations, Guenther et al. [92] succeeded in adapting the kinetic scheme of Caussat et al. [91], again for the case of silicon deposition from SiH_4, in the two-fluid hydrodynamic model MFIX. They thus calculated local gas velocities, bed voidage and mass fraction profiles everywhere in the FB in transient conditions. A good agreement was obtained with the corresponding experimental results. Finally, volumetric optical properties (spectral absorption, scattering and extinction coefficients) of differently expanded narrow-path fluidized beds of a photocatalyst obtained by plasma-deposition of titania onto quartz sand, relevant for photoreactor design purposes, were determined by using a unidirectional and unidimensional (1DD) model for the solution of the radiative transfer equation [95].

3. Materials produced by fluidized bed CVD

3.1. Supported catalysts

The preparation of a supported catalyst consists in depositing an active phase (metal, oxide, etc.) on an “inert”, preferably high surface area, solid porous support that is often a powder. The dispersion of the active phase; i.e. the ratio between surface atoms and bulk atoms of the deposited material, is a key parameter to obtain very active catalysts. The higher the dispersion of a given quantity of the metal, the higher its catalytic performance. It is therefore desirable to process catalysts in the form of nanoparticles or sub-monolayers deposited on a given support, also considering the fact that the metal catalyst is often expensive. Various synthetic routes can be used to produce such systems [96], the most common being liquid phase impregnation, ion exchange or deposition–precipitation. A common point characterizing these techniques is that they may use environmentally harmful liquid solvents. Moreover, corresponding processes involve several steps, such as drying, oxidation or reduction, potentially leading to reduced reproducibility of the prepared materials. Consequently, the development of flexible (a few key steps during the process) and solvent-free techniques have received increasing attention during the last decade. Those involving preparation from the gas phase and particularly CVD are becoming well established methods for catalyst preparation [6].

Generally speaking, two gas phase methods can be distinguished for the preparation of supported catalysts: batch and continuous. The former consists in gas phase adsorption of the precursor on the support followed by a thermal treatment in order to obtain the active catalyst. This method, called gas phase impregnation-decomposition (GPI-D) is well suited for the production of highly dispersed, low loading catalysts [97]. In most studies reported, several cycles are carried out to increase the amounts of deposited metal. The growth of aggregates should be the dominant phenomenon when the first GPI-D cycle is completed. Although this method does not fit with the classically accepted definition of CVD, it is worth mentioning the IUPAC recommendations defining chemical vapor deposition as *deposition taking place by adsorption or reaction from the gas phase*. GPI-D is by far the most used for catalyst preparation from a gas phase. For the continuous process (also called CVD process), the precursor vapors are simultaneously adsorbed and decomposed on the heated support. The main advantage of CVD processes lies in the possibility to control the particle size for a given metal loading by adjusting the precursor vapor pressure, which governs the nucleation rate.

While several studies deal with the fixed bed technique, the use of a fluidized bed has proved its efficiency to simultaneously achieve narrow distribution of the particle size on the surface of the grains and homogeneous dispersion on the whole surface of the porous support.

Compared with the conventional wet impregnation methods, the absence of any solvent favors the diffusion of the precursor inside the pores and precludes the drying step during which redistribution of the active phase can take place. Additionally, the use of reactive organometallic complexes as metal precursors provides an efficient way to produce often clean deposits at low temperatures, and thus to obtain high dispersion of the active phase on the support. Of course, drawbacks do exist in CVD-based processes. Among others, one can mention the difficulty to optimize the process, which can be attributed to the sheer number tunable parameters, and the possible toxicity of precursors and decomposition products. This point can be restrictive for catalyst manufacture on the industrial scale.

3.1.1. Catalytic performance of CVD-FB prepared materials

The advantages of CVD over liquid phase impregnation procedure for catalyst preparation often result in better catalytic activity [98], [99], [100], [101], [102], [103], [104] and [105]. Table 1 presents selected examples of catalytic studies using GPI-D or CVD catalysts. These catalysts have been used in several catalytic reactions of industrial interest, such as hydroformylation, carbonylation or hydrogenation [106]. Thus, a Co/SiO_2 catalyst was prepared by a sequential GPI-D technique from the organometallic $[Co(acac)_3]$ precursor. The complex was firstly adsorbed at 453 K and 6–10 kPa under nitrogen on a fixed bed of silica, preheated to 873 K and then was decomposed under hydrogen. This catalyst was found to be three times more active for ethylene hydroformylation than a classically impregnated catalyst prepared from cobalt nitrate [98]. This result was directly correlated to the smaller particle size obtained with the gas phase process: 4.3 nm for a 5% (w/w) Co/SiO_2 (GPI-D) and 11.3 nm for a 4% (w/w) Co/SiO_2 (impregnated).

Table 1.

Representative examples of catalytic studies using CVD or GPI-D catalysts

Catalytic system	Metal loading (%)	Particle size (nm)	Reaction	Catalytic activity	Ref.

Catalytic system	Metal loading (%)	Particle size (nm)	Reaction	Catalytic activity	Ref.
Co/SiO_2					[98]
GPI-D ($[Co(acac)_3]$)	5	4.3	Ethylene	GPI-D > imp.	
Impregnation ($Co(NO_3)_2 \cdot 6H_2O$)	4	11.3	Hydrofomylation	(×2)	
Mo carbide/Al_2O_3					[100]
CVD ($MoCl_5 + C_6H_6$)	1–6	1.4	CO_2 reduction	CVD > imp.	
Impregnation ($(NH_4)_2(MoO_4) + CH_4$)	–			(×20)	
Rh/AC					[99]
CVD ($[RhCl(CO)_2]_2$)	2	4–5 (Cl free)	Acetic acid	CVD > imp.	
Impregnation ($RhCl_3 \cdot 3H_2O$)	2	4–5 (remaining Cl)	Hydrocarbonylation		
Rh-Sn/SiO_2					[101], [102], [103], [104] and [105]
GPI-D ($[Sn(CH_3)_4]$)	Rh 1-Sn/Rh 0.45	2.5	NO/H_2	GPI-D > coimp.	
Co-impregnation ($RhCl_3 \cdot 3H_2O$-$SnCl_2$)	Rh 1-Sn/Rh 0.45	–		(×6)	

Molybdenum carbide catalysts were prepared on alumina by using a vapor mixture of $MoCl_5$, C_6H_6 and H_2 under low pressure. The activity of this GPI-D catalyst in the reduction of CO_2 was shown to be 20 times higher than that of a molybdenum carbide catalyst prepared by impregnation [100]. XPS measurements revealed that the oxidation state of molybdenum changes from II for the GPI-D carbide to IV for the impregnated one.

Rhodium supported CVD catalysts were prepared on activated carbon (AC) from $[RhCl(CO)_2]_2$ in a FB reactor [99]. The temperature of precursor decomposition was found to

significantly decrease upon addition of hydrogen in the gas phase. In addition, ligand hydrogenation decreased the amount of impurities in the final deposit. It is worth mentioning that, in contrast to the GPI-D process, this one-step CVD process involves reactions with fast kinetics, which do not allow the identification of the intermediate rhodium surface species. The presence of metallic rhodium in all the samples was evidenced by XRD and XPS analyses. A mean particle size of 4–5 nm was measured for 2% (w/w) Rh/AC. These CVD Rh/AC catalysts were found to be efficient for the hydrocarbonylation of acetic acid into higher acids at 20 MPa and 493 K [99].

Iwasawa and co-workers prepared Rh-Sn/SiO_2 catalysts that have proved to be very active in NO/H_2 and ketone hydrogenation reactions [101], [102], [103], [104] and [105]. The Rh/SiO_2 catalyst (mean particle size 2.5 nm) was prepared by wet impregnation from rhodium chloride, followed by a reduction step. Then, GPI-D of [$Sn(CH_3)_4$] was performed at low pressure and at 423 K. The vapors of [$Sn(CH_3)_4$] react exclusively with the rhodium aggregates and two molecules of methane per tin were evolved. By further reduction at 573 K under hydrogen, two more molecules of methane were formed, leading to surfaces free from residual carbon. The rhodium loading was kept at 14% (w/w), while the Sn/Rh ratio was varied from 0 to 1. Mean particle sizes of 2.5 and of 3 nm were measured for Sn/Rh ratios in the Rh-Sn/SiO_2 catalyst equal to 0.45 and to 0.90, respectively. The structure of these catalysts was also studied by EXAFS as a function of the Sn/Rh ratio. The Sn atoms in the bimetallic aggregates remained located at the first layer as long as the Sn/Rh ratio remains lower than 0.4; above this value Sn atoms intrude into Rh metal particles. These two different environments confer different reactivity to the catalyst. For example, in the NO/H_2 reaction optimum activity was reached for Sn/Rh = 0.4 [107], and for ketone hydrogenation [108] the best results were obtained with a Sn/Rh = 0.2. In the case of co-impregnated catalysts the particular Rh-Sn bimetallic surface structure (Sn/Rh = 0.4) is not present and these catalysts are six-fold less active than that obtained by GPI-D in the NO/H_2 reaction [107].

The higher catalytic activity or selectivity is due either to a better control of the purity of the deposited active phase or, more generally, to a better dispersion; i.e. to smaller particle sizes. It is also important to remember that the homogeneity of the deposit is a key factor for the catalytic activity of the final material. This is particularly true for CVD catalysts, or for bimetallic catalysts in the case of GPI-D. If a correct fluidization regime is not reached, the deposit will not be homogeneous and the dispersion of the active phase will be poor. The

result will be a moderately active catalyst. This was reported recently in the case of platinum deposited on activated carbon granules [109]. In this study, the catalytic activity of Pt/AC, prepared by FB-CVD or liquid impregnation, for refractory acid oxidation was reported. Due to the poor fluidization of the carbon support, the dispersion of the CVD catalyst (10 wt.%) was lower than that obtained for the impregnated samples (25 wt.%). The platinum carbon supported catalysts prepared by incipient wetness impregnation showed superior performance compared with the catalyst prepared by CVD.

3.1.2. Some important statements and phenomena linked to CVD preparation of supported catalysts

The main characteristics of the supported catalyst that have to be controlled during CVD preparation are the purity of the deposit and the dispersion of the active phase. To do so, several key parameters of the FBCVD process have to be taken into consideration. The procedure for CVD production of supported catalysts can be divided into three steps: (i) the choice of the precursor, (ii) the choice of the support and (iii) the design of the CVD reactor. Additionally, several phenomena have to be considered to ensure the controlled growth of nanoparticles or sub-monolayers. These phenomena deal with the interfacial reactivity, which will govern both the nucleation and growth steps of the deposit, as well as its chemical nature.

3.1.2.1. Selection of the precursor and of the support

The choice of the metal precursor for catalyst preparation is mainly governed by the well-known general criteria that have already been listed in Section 2.4. For this specific application metalorganic precursors are very often used and special care should be taken concerning their volatility and thermal stability under transport conditions, clean decomposition and reduced-toxicity. Preparation of a well dispersed supported catalyst by FBCVD also requires several particular substrate characteristics, such as: (i) high surface area, (ii) physical properties (density, mean particle size and size distribution) allowing convenient fluidization, (iii) inertness in the processing temperature and (iv) appropriate surface chemistry and morphology. Of particular interest is the fluidization quality since the active phase; i.e. the deposited material is present in small amounts (generally less than 5%, w/w) and consequently poor fluidization will inevitably induce strong inhomogeneities in the final material. Finally, it is worth noting that the low amounts of deposited materials associated with the high reactivity of metalorganic complexes lead, most of the time, to

complete precursor decomposition in the bed of particles also reducing the risk of bed agglomeration.

3.1.2.2. Design of the FBCVD reactor

As previously stated, the design of the FBCVD reactor is also of importance. Fig. 18 was adapted from ref. [110] and schematically illustrates a FBCVD reactor with internal diameter (i.d.) 5 cm that was built for one-step processing of metal catalyst. Due to the low volatility of many metalorganic complexes, the reactor was designed to operate under low pressure (1.3–13.3 kPa) with a sublimator. This part of the reactor is not necessary when working with liquid precursors, where a classical bubbler can be used. Information concerning the fluidization of powders under reduced pressure were reported [111], and have been discussed in Section 2.4. In this setup, reactive gases, such as O_2, H_2O or H_2, can be introduced to assist precursor decomposition. These reactants are preferably introduced in the vicinity of the distributor in order to avoid a premature decomposition of the precursor. Moreover, the sublimator and the fluidized bed are heated by two different heating glass jackets, allowing a fine tuning of both precursor and deposition temperatures. The sublimator temperature can be regulated between 263 and 423 K and the temperature of the fluidized bed between 293 and 513 K. An additional advantage of the glass setup is that it allows visual observation of the fluidized bed, and consequently a more precise control of operations during the experiments. If necessary, the catalyst obtained can be removed from the column under inert atmosphere. On-line analysis of the decomposition products is also possible by coupling the reactor with a mass spectrometer or gas chromatograph. The general procedure to prepare metal supported catalyst was reported in ref. [110].

Fig. 18. Schematic illustration of a fluidized-bed CVD reactor used for the preparation of supported metal catalysts. Adapted from ref. [110].

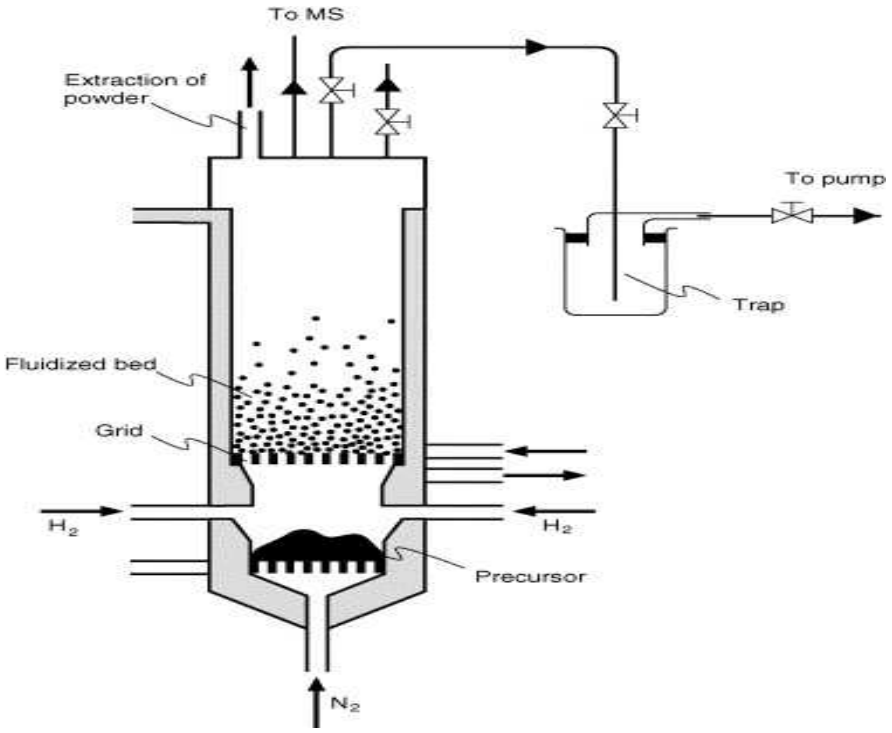

3.1.2.3. Role of the substrate surface and of the gas phase on the dispersion and the chemical nature of the active phase

Generally speaking, the deposition of sub-monolayers or dispersed nanoparticles involves two main steps: nucleation and growth. During the nucleation step, the first nuclei of the solid active phase are formed; these nuclei present high specific surfaces and high surface energies, and hence may be unstable. Below a certain critical nucleus size, due to the predominance of highly energetic surface atoms, the free energy of formation is noticeably higher than that of the corresponding macroscopic phase and the nucleus is thermodynamically unstable. Above this critical size, solid particles can grow. According to the deposition conditions, this growth step will be mainly controlled by interface and/or diffusion phenomena. Consequently, the role of surface chemistry occurring between the CVD precursor and the substrate, as well as the physical properties of the bulk gas-phase are crucial parameters that have to be taken into account to control the nucleation and growth steps of the process. The role of surface defects and of surface reactive groups, that of autocatalytic phenomena as well as the role of the supersaturation thus have to be taken into account to control both the nucleation step and the nature of the deposit.

Interfacial reactivity is governed by the reactive sites of the substrate and the coordination sphere of the precursor; i.e. the nature of the metal/ligand couple. This reactivity plays a crucial role on nanoparticle nucleation rate. Instead of discussing here the influence of the nature of the ligands on the nucleation step, we will focus on surface reactivity; i.e. the surface properties of the powder that will be used in the process. The various reactive sites that can be found on the surface of the more common substrates are: (i) the reactive surface functions, (ii) the surface defects and, in addition (iii) the anchoring sites on the deposited nanoparticles, which can induce autocatalytic effects. Finally, from a kinetic point of view, the nucleation rate and thus the final dispersion of the catalyst is also correlated to the supersaturation ratio.

In the preparation of catalysts, the substrates used are often oxides with a high surface area, such as alumina, silica, titania, magnesia and silicoaluminates. In addition, such surfaces contain hydroxyl groups whose density strongly depends on the nature of the oxide itself and on the experimental conditions in which deposition is carried out. Different kinds of –OH groups can be encountered on a M_xO_y surface, such as terminal M–OH, geminal $M(OH)_2$, bridging M(μ-OH)M or $M_3(\mu_3\text{-OH})$ functions [6]. Studies carried out on porous catalyst supports showed that, according to the material, the –OH concentration can vary from 1 to 15 –OH/nm^2. If activated carbons (ACs) are used as support, various surface oxygenated groups have been identified [112]. Additionally, for a given powder, pre-treatment can be performed and, depending on the operating conditions, namely temperature and pressure, the surface density of the oxygen-containing groups can dramatically change. For example, complete dehydroxylation of silica is possible, after treatments above 1000 K. High temperature can also significantly affect the structure of the material and in addition modify its acid–base properties. If the substrate presents crystallographic faces with no functional surface groups, potential reactive sites for precursor anchorage are defect sites on the surface. Classical theory does refer to edges, kinks or adatoms. Various mechanical, physical and chemical methods can be used to increase the amount of such sites at the surface, and hence improve the anchoring and nucleation processes.

The influence of the concentration of surface reactive groups on the dispersion of the active phase, and thus on nucleation has been unambiguously demonstrated in the case of platinum deposition on carbon [113], [114] and [115]. The surface chemistry of activated carbon substrates affects the Pt dispersion of the catalysts: Pt dispersion increases with the amount of

oxygen-bearing groups. After oxidizing treatment of the support with nitric acid, the concentration of the surface reactive groups increases significantly, as measured by CO_2 evolution from temperature-programmed decomposition experiments performed on the substrates: 1325 μmol/g for the original AC and 4616 μmol/g for the HNO_3 treated sample. Consequently, a mean particle size of 9 nm has been measured for a 2% (w/w) Pt/AC whereas it decreases to 3.5 nm for a 2% (w/w) Pt/AC-ox, reflecting more efficient nucleation; i.e. a higher nucleation rate. A similar behavior was observed for platinum deposition from $[Pt(CH_3)_2(COD)]$ on carbon nanospheres where small particle sizes were measured on nitric acid oxidized carbon nanospheres as shown in the TEM micrograph in Fig. 19.

Fig. 19. Platinum nanoparticles deposited on carbon nanospheres [116].

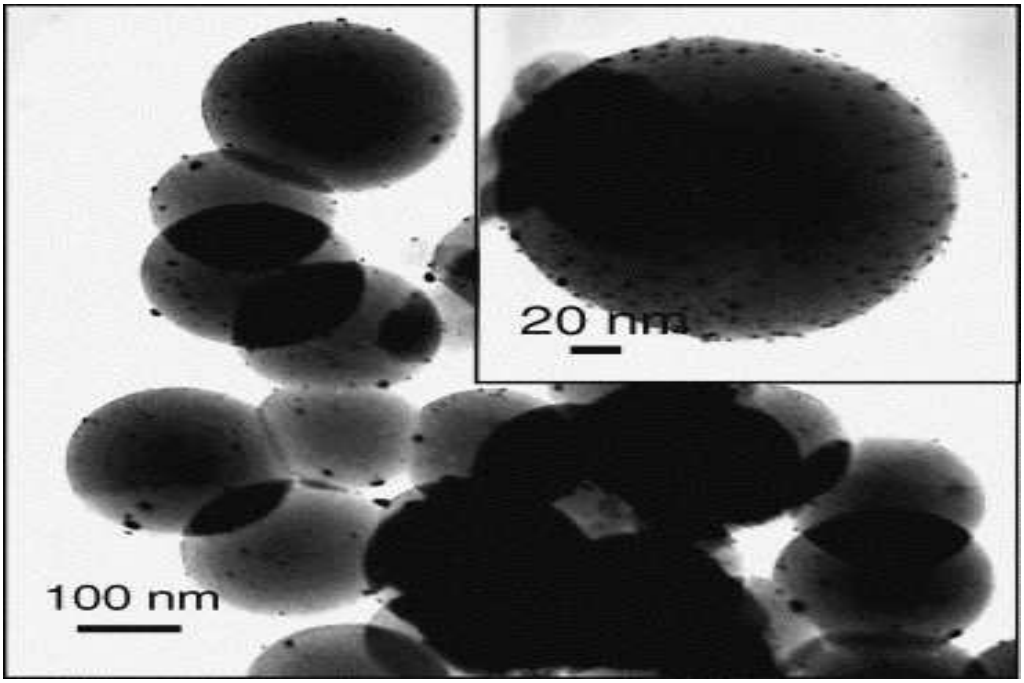

In particular cases, autocatalytic processes take place involving mainly active surface species or sites generated by the deposition procedure. When studying the deposition of rhodium on silica from $[RhCl(CO)_2]_2$ in the presence of controlled amounts of hydrogen as reactive gas, it was demonstrated by on-line mass spectrometry techniques that an autocatalytic process, which should involve hydrido-rhodium surface species, occurs and enhances the growth rate of the particles [117]. With regard to such autocatalytic phenomena, it is worth mentioning that, as in catalysis, their kinetics or their probability to occur will increase when depositing potentially reactive noble metals with respect to less reactive non-noble metals.

The supersaturation parameter also plays an important role. From a thermodynamic point of view, when the pressure of a vapor phase is increased beyond the liquid–vapor coexistence value, a state of supersaturation of the vapor phase is attained. In CVD, the supersaturation is due to the initial gas composition and supersaturation is assumed to be proportional to feed rate (Rfd) at a constant temperature. The supersaturation parameter can be define as the ratio of some particular partial pressure (around an infinite planar surface of the CVD deposit) to the corresponding equilibrium partial pressure (near the growing surface) [118], [119], [120], [121] and [122]. The CVD process for catalyst production is characterized by a weak supersaturation regime associated with the formation of critical nuclei. In the case of platinum deposition on silica, Hierso et al. have demonstrated the crucial role of a high supersaturation regime in order to obtain a high nucleation rate with regard to the growth rate [123]. Indeed, for a high supersaturation of the [$PtMe_2$(COD)] precursor obtained at a sublimation temperature of 468 K corresponding to a saturation vapor pressure of 4 Pa, a mean particle size of 2–6 nm was measured whereas for lower supersaturation obtained at a sublimation temperature of 402 K corresponding to saturation vapor pressure of 0.5 Pa, the mean particle size was measured to be around 60 nm. The combined effects of autocatalysis and supersaturation on the dispersion of the final deposit are depicted in Fig. 20. It can be concluded that very high metal dispersion will be obtained with precursors presenting high vapor pressures allowing high supersaturation and not prone to autocatalytic phenomena. In contrast, a precursor with low partial pressure and prone to autocatalysis will produce large particles.

Fig. 20. Schematic of the combined effect of autocatalytic phenomena and supersaturation on the dispersion of the final deposited material.

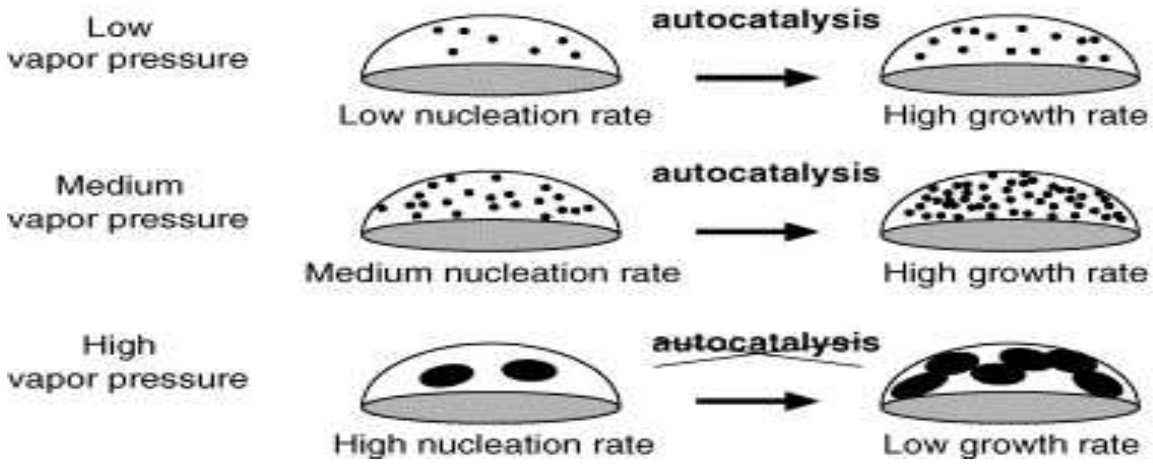

In conclusion, it appears that the control of the dispersion of the active phase on the support is a complex task and that several phenomena should be taken into account. Some general statements or rules of thumb can be noted: for nucleation: (i) the higher the supersaturation, the higher the nucleation rate, (ii) reactive surface sites lower the surface free-energy of the active phase, act as preferred nucleation sites and thus contribute to increasing the nucleation rate and (iii) in general high temperatures lower the nucleation rate by increasing the critical size of the germ. For growth: (i) the higher the supersaturation the higher the growth rate, but this can become limited by diffusion processes and (ii) autocatalytic phenomena contribute to an increase of the growth rate.

3.2. Wear, oxidation and temperature-resistant materials

CVD in fluidized beds and in the other types of contactors mentioned has been developed since the 1980s in view of either modifying surface properties of powders or producing composite raw materials for the manufacture of bulk pieces or coatings with improved mechanical or chemical performance (e.g. [124], [125], [126], [127] and [128]). The studies carried out in this context can be divided into two types: (i) micro-engineering of powders through a coating treatment in view of subsequent preparation of bulk pieces or coatings and (ii) use of the FB as a medium for the in situ coating of substrates which are either

freestanding or most often suspended in the bed volume. Characteristic examples of the process conditions and the microstructures obtained are given below for the first type, while the second one will be treated in a separate section of this paper.

Chen and Chen reported the need to improve the poor wetting between particles, such as Al_2O_3 and SiC that are most often used as reinforcement in Al-based metal matrix composites [129]. Such poor wetting between matrix and reinforcement is deleterious to the optimum crack propagation in the composite material and requires severe processing conditions to face it [130]. The authors proposed a surface treatment of the reinforcing particles (ceramic powders of mean size 250 μm) by FBCVD of Ni and Cu layers on their surface. Chloride precursors were used in this study; they were prepared in situ in a packed bed of metal particulate while the ceramic substrates were fluidized. The operating temperature was between 773 and 973 K. The deposition rate of Ni on Al_2O_3 was estimated to be 7.7 mg cm^{-2} h^{-1} which favorably compares with that of electroless Ni-plating, namely 4.2 mg cm^{-2} h^{-1}. Higher deposition rates were reported for Cu on Al_2O_3 and even on SiC, while deposition of Ni on SiC required the highest operating temperature. It is worth noting that a review of former FBCVD investigations; i.e. before 1996, is reported in this paper.

In order to increase sinterability of Si_3N_4, and therefore to take advantage of its excellent properties as a bulk material, Hanabusa et al. replaced the sintering additives that are used in the conventional sintering process for the production of commercial Si_3N_4 by Si_3N_4 ultrafine powder applied on the surface of fine Si_3N_4 particles [131]. The authors used a specially designed FBCVD reactor to accelerate homogeneous nucleation reactions and optimized CVD conditions to form the ultrafine powder on the core fine particles. They presented results of sintering tests illustrating the feasibility of their process for the preparation of other functional composite materials with convenient sinterability.

In another application, to prepare friction surfaces for automotive parts, coatings containing dispersed particles (e.g. oxides, carbides, nitrides or borides) were deposited on a substrate. Prior to their deposition on the substrate, these particles were first coated with a layer of substrate material. In this context, Miyake et al. investigated different techniques including CVD, to coat TiC-based powders by Al [125]. Then, they laid these powders on Al alloy and finally melted them with high-energy sources, such as laser, plasma or electron beams. The authors claimed that the wear-out of such a coating prepared with Al-coated particles and of

an object in contact with this coating were less than that of a coating prepared with uncoated particles.

The abrasive performance of TiC and of TiN, Si_3N_4, SiC or SiAlON (acronym for a ceramic that contains silicon, aluminium, oxygen and nitrogen) was investigated by Dierssen et al. who used FBCVD to prepare improved granular abrasive materials [124]. The inventors coated SiC particles with an integral, durable, single or multicomponent surface layer of the above materials. As in previous examples, metal chlorides were used as precursors, some of which were prepared in situ. Reactive gases, such as NH_3, H_2 or CO_2 were fed separately to minimize premature decomposition or reactions. The intended applications were coated and non-woven abrasive products and abrasive wheels.

The synthesis of AlN/SiC composite powders in view of high-temperature structural and corrosion-resistance applications was investigated by Kimura et al. using a reactive $AlCl_3$–NH_3 gas phase [70]. In this case, treatment of fine (less than a few μm) powders was required and for this reason, a floating-type FBCVD configuration was used. It was found that the mean diameter of SiC particles was increased from 0.26 μm in the as-received state to 4.7 μm after flotation. The authors concluded that, although agglomeration was promoted by floating, particles agglomerating to ~5 μm can be floated by the floating-type FB and they pointed out that this size agglomerate is less than one-tenth of that obtained with conventional FBs. Following this work, the composite ratio can be controlled by the aluminum precursor ($AlCl_3$) feed rate and by the flow rate of the gas mixture for flotation of the SiC powder, but not by the reaction temperature, as raw materials are merely wasted, being left unreacted at lower temperatures. It was claimed by the authors that such a process for the preparation of nanodispersed composite, non-oxide materials compares favorably with more traditional ones like mechanical mixing because contamination from the atmosphere and the mixing apparatus can be prevented. Formation of agglomerates through fluidization of submicron powders was also reported by Tsugeki et al. [132] and [133]. The authors presented a comparative study of sintered bodies of α-Al_2O_3–TiN composites prepared either by FBCVD of TiN on such submicron α-Al_2O_3 particles or by mechanically mixing constituent powders. They found that the electroconductivity of the material prepared by the former route is higher and consequently claimed the superior efficiency of the FBCVD process for the preparation of composite ceramic powders. Also, in a patent by Michorius and Haafkens, a process is presented for using FBCVD to apply an evenly distributed ceramic coating of TiN or SiC on

powdery particles of Al_2O_3 and/or SiC, and for producing steel objects by sintering powdery steel with approximately 10 wt.% TiN or SiC coated alumina [134]. The inventors claim that such a process allows the preparation of metallic objects with improved density. Beyond the interest per se for the presented process, this invention also reviews different patents in the field of particle processing.

Vahlas and co-workers also investigated alternatives to the mechanical mixing routes with the aim of adding a small quantity of platinum group metals, such as ruthenium and rhenium to the surface of NiCoCrAlYTa powders for the improvement of the oxidation resistance of the corresponding bond coats applied to gas turbine blades and vanes [31], [42] and [135]. In order to avoid clogging of the distributor due to the smooth temperature gradients in the reactor they used a spouted bed instead of a fluidized bed. The first problem that these authors had to face was that the raw commercial powders they treated were not prepared in view of fluidization operations: they were relatively small (average diameter 23 μm) and presented a large size distribution (extreme diameters observed 0.05 and 550 μm) as well as a high density (7.7 g/cm^3). For these reasons, it was necessary to investigate their spouting behavior prior to CVD treatments. Fig. 21 illustrates the evolution of the pressure drop ΔP across the bed as a function of gas velocity in the spouted bed. The presence of a plateau reveals convenient spouting conditions. However, the corresponding value of ΔP is approximately 1500 Pa, to be compared to the theoretical ΔP of 1800 Pa due to the apparent bed weight. This difference was attributed to the loss of part of the powders due to elutriation and electrostatic fixing on the reactor walls [32]. In this figure, it can be noted that, due to the broad particle size distribution of the powders, U_{ms} corresponds to a range of velocities, included for the investigated conditions between 0.021 and 0.029 m/s. The evolution of ΔP as a function of time for three different gas velocities, lower and higher than U_{ms} and in the range of U_{ms} is also presented in this figure. The lowest standard deviation of these fluctuations is observed for superficial velocities close to U_{ms}. This behavior corresponds to a satisfactory fluidization, the powder behaving like a homogeneous medium. For velocities higher than U_{ms}, the fluctuations of pressure drop become more significant, and they reveal a periodicity, probably due to the existence of plugging sequences. For gas velocities lower than U_{ms}, the standard deviations are the highest, indicating that the bed is unstable, because of preferential random gas channels.

Fig. 21. ΔP vs. U at decreasing gas velocity for as received (circles) and sieved (triangles) powders for H/D = 1.5. Temporary fluctuations $\Delta P(t)$, characteristic of three regimes of U: lower than, equal to and higher than U_{ms} [32]. *Insert*: Typical curve for spouted beds [136].

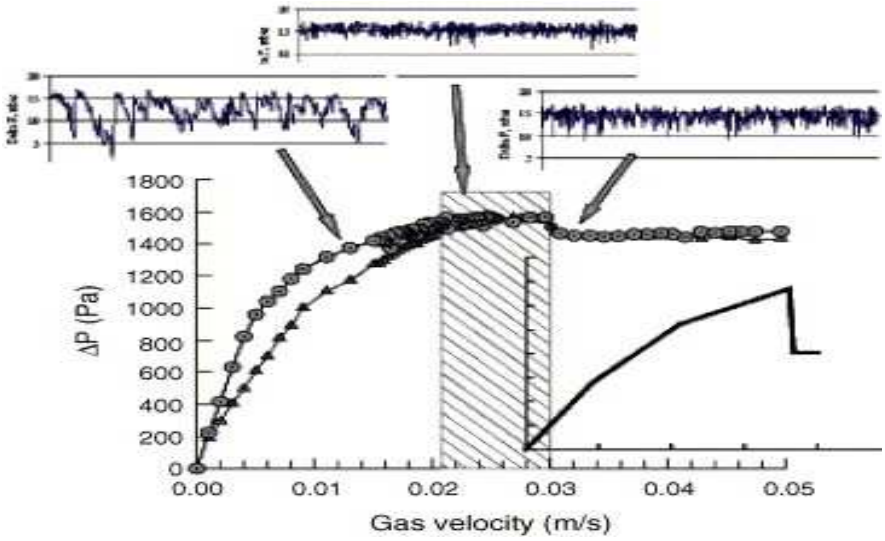

Once convenient spouting conditions were approached, the authors adapted different MOCVD processes for the deposition of Ru and Re using bis-cyclopentadienyl ruthenium and decacarbonyl di-rhenium, respectively [31] and [137]. Fig. 22 illustrates homogeneously distributed Ru (a) and Re (b) grains, deposited at atmospheric pressure on the surface of NiCoCrAlYTa particles. The Ru grains were deposited at 873 K in the presence of H_2 in the input gas, while the Re grains were deposited at 681 K.

Fig. 22. Bright field TEM micrographs of homogeneously distributed Ru (a) [31] and Re (b) [135] grains, deposited on the surface of NiCoCrAlYTa particles.

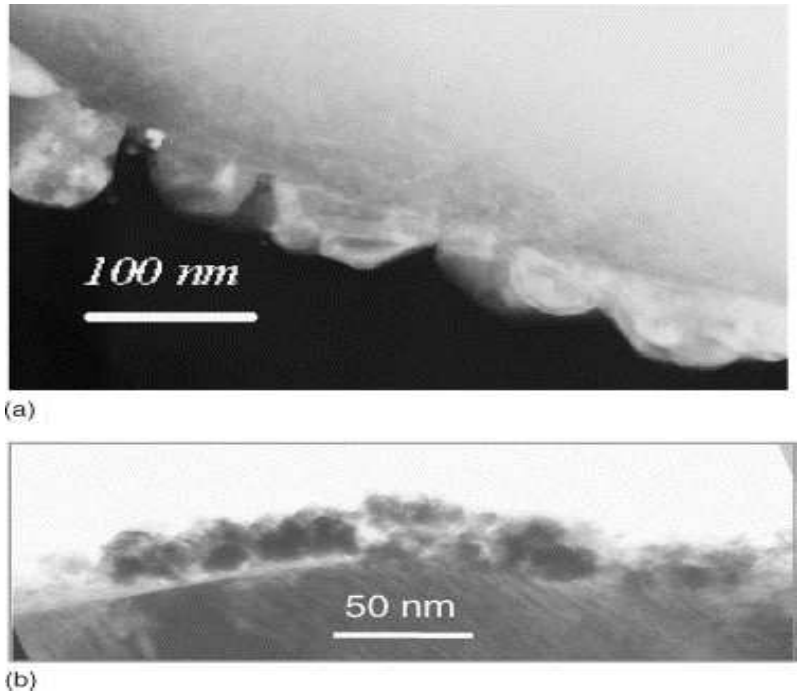

Sintering of the Ru- and Re-doped powders subjected to cyclic oxidation between ambient and 1323 K in air. Fig. 23 shows the weight gain as a function of the number of 1 h cycles for the sintered coupons prepared from the as-received and from the Ru-doped powders. It appears that the weight gain of the as-received sample is higher probably due to a more severe spallation of the superficial oxide. Indeed, this behavior is confirmed in the optical micrographs of the two samples, where partial spallation of the oxide, allowing the surface of the alloy to be further exposed to air is observed for the coupon made from as-received powders. In contrast, the entire surface of the Ru-doped sample is covered by a continuous oxide layer, confirming the improved oxidation resistance of this new material. Beyond the beneficial role of Ru on the adherence of the alumina layer, it was shown in this way that spouted bed MOCVD is an efficient method for the doping of commercial powders by different elements in view of their subsequent application as bond coats in turbine blades and vanes.

Fig. 23. Weight gain per unit surface vs. number of 1 h cycles between ambient and 1323 K in air for sintered NiCoCrAlYTA coupons prepared from as received (triangles) and Ru-doped (squares) powders. Optical micrographs of the two coupons after 900 cycles. An alumina coating has been grown on their surface. Spallation of the developed alumina coating is shown on the surface of the undoped (reference) sample, revealing poor protection function of the as-received NiCoCrAlYTa powders. In contrast, the alumina coating grown on the surface of the 1 wt.% Ru-doped sample (right) maintains its integrity [42].

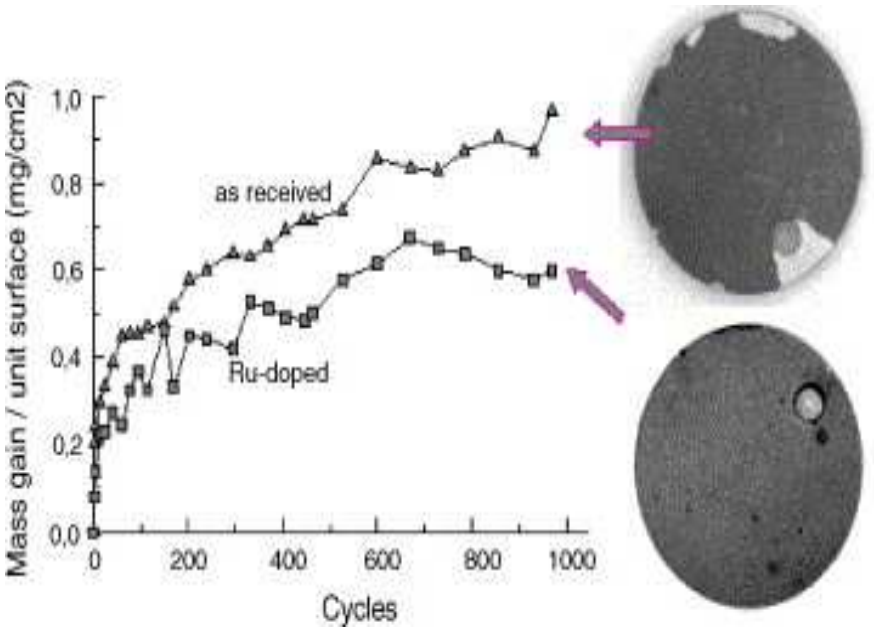

The use of FBCVD in powder metallurgy for the preparation of bulk materials with improved properties was suggested by Williams et al. [138]. The authors demonstrated the ability to coat 12 μm tungsten particles with pure and alloyed Ni, Fe and Co films starting from carbonyl precursors. Liquid-phase sintering of these composite powders provided materials with improved mechanical properties and narrower, more predictable statistical property distributions. A first application of this processing route was the replacement of the depleted uranium in kinetic energy penetrator applications. The use of sintered pieces made of composite powders prepared by FBCVD of Hf- and Ti-based coatings on micronic tungsten particles was proposed by two research groups, one in the United States [22] and one in Japan [139]. Itagaki et al. provided details on the processing of the coatings on the powders, while Stiglich et al. on the performance of the material. Interestingly, Itagaki reported that W

powders are easily fluidized at room temperature due to the existence of tungsten oxide WO_3 on the particle surface. At high temperature, this property was degraded because of the sublimation of the oxide occurring at 1100 K. In order to make a stable fluidized bed at high temperature, corresponding to the deposition conditions of the coating, the authors proposed pre-coating at 900 K and forced mixing.

More recently, Toth reported on the production of tough-coated hard powders for hard metals of novel properties [8] and [140]. In view of improving TiN-coated tungsten carbide–cobalt based cutting tools, the authors proposed a novel material consisting of an engineered homogeneous cellular structure whose interconnected tough tungsten carbide-cobalt shells each contain a wear-resistant core (e.g. TiN). They claim that the coating is found throughout the tool, combining the strength, heat resistance and toughness of cemented carbides with the chemical and abrasion wear resistance of harder materials and that, consequently such tools can be reused many times. This concept was exemplified by the deposition of WC on 37 μm porous TiN powders in a recirculating fast fluidised-bed CVD reactor, followed by mechanical mixing with Co powders before sintering [140]. Alternatively, the use of a rotating CVD reaction vessel for the deposition of such materials was also proposed by Toth [8]. In order to solve the problem of the agglomeration of the powder, the author suggested tilting the reactor and installing a fixed comb-like guide: (i) to recirculate and homogenize the batch and (ii) to apply sufficient shear to the powder to deagglomerate it.

Fig. 24 illustrates the sintered structure of CVD processed tough-coated hard powder (left) and the microstructure of the material obtained, composed of WC coated Al_2O_3 micronic particles sintered with Co as a binder. The mechanical properties of these processed materials were found to be promising, with high combinations of toughness (4000–5000 MPa), hardness/wear resistance (3000–5000 Vicker's Hv30), and light weight (5–10 g/cm^3). However, these preliminary investigations revealed a number of points that must be overcome for the process to be industrialized. They essentially meet those mentioned in the paragraph dealing with the particular technologies that can be applied for the treatment of Geldart's group C powders, i.e. the fluidization of fine powders which tend to form agglomerates and the elutriation of fines in combination with the high temperature deposition and the use of aggressive precursors, such as fluorides in the present process.

Fig. 24. Schematics of the sintered structure of CVD processed tough-coated hard powder (left) and SEM micrograph of the material obtained, composed of WC coated Al_2O_3 micronic particles sintered with Co as a binder. Adapted from http://www.allomet.net/what_tchp.html.

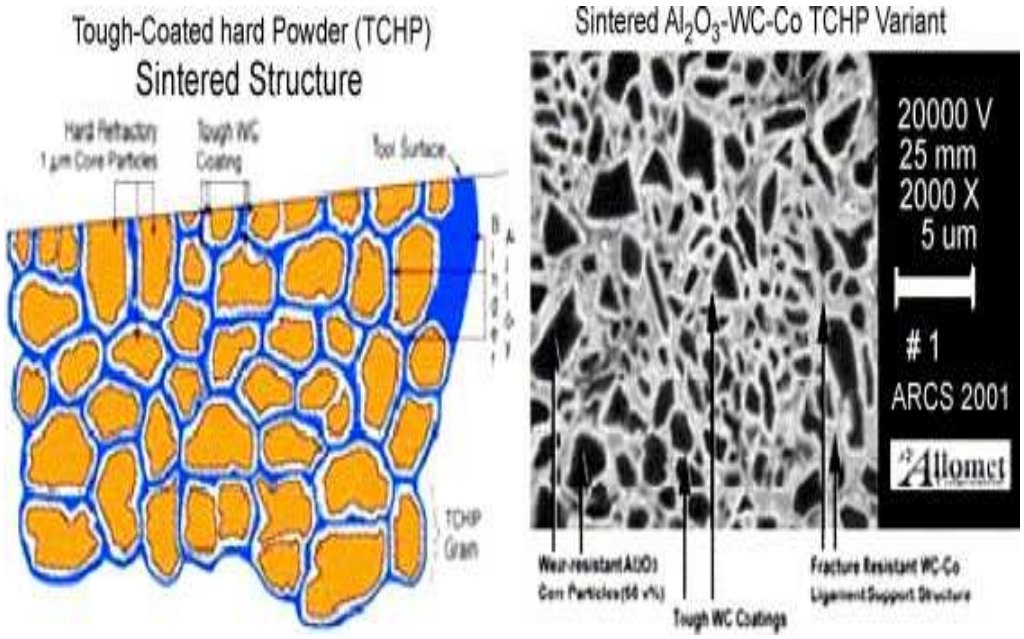

Based on a similar technology, marketed by Powdermet Inc. Sun Valley, CA, Biswas et al. investigated the use of microencapsulated micro-engineered thermal spray powders for thermal barriers and wear resistant coatings in diesel engines [141]. These coatings are composed of a plasma sprayed functionally graded system consisting of a porous $Al_2O_3/TiO_2/MgO$ insulating layer graded into a cermet wear resistant topcoat. The raw materials were prepared by coating 20 μm Al_2O_3 powders either with TiO_2/MgO by using the corresponding isopropoxides, or with a WC bond layer and a Co binder. WC was produced by first depositing metallic tungsten from decomposition of $[W(CO)_6]$ followed by carburization in the presence of CH_4. Cobalt was deposited by decomposition of $[Co_2(CO)_8]$. Raw materials were also prepared by either depositing WC and Co on 1–3 μm TiN powders or by coating WC powders of similar size with cobalt. Preliminary results revealed that the TiN/WC/Co coatings performed extremely well in wear resistance and that the coated alumina microsphere material shows promise for providing a low-cost thermal barrier coating material

through optimization of the plasma spraying process to increase alumina sphere retention in the coating and material deposition efficiency and flowability.

The works reported in this paragraph reveal that numerous possibilities are provided by microengineering of powders prior to their use as raw materials for the preparation of hard and oxidation resistant bulk pieces and coatings. Such possibilities are far from being completely explored yet. Consequently, different obstacles in the FBCVD processes involved have not been completely solved, and the link between processing conditions and materials performance is still weak. These points most often concern: (i) fluidization of powders that, due to either their density, and/or their size, and/or their size distribution belong to group C or are out of Geldart's classification, (ii) elimination – at least temporarily – of the formation of agglomerates, (iii) use of aggressive chemicals, such as fluorides, (iv) use of high operating temperatures and (v) risks of clogging either the bed or the distributor. Finally, the above mentioned works also revealed that solutions can be found to resolve these problems provided different technological aspects (for example, workers protection and environmental concerns) and scientific disciplines (such as surface science, organometallic chemistry, crystal growth, process engineering, …) are considered.

3.3. Microelectronic and photovoltaic applications

The massive synthesis of solar grade or even semiconductor grade polysilicon was one of the first applications of the FBCVD process [87]. Commercial production of polycrystalline silicon was originally conducted by hydrogen reduction of trichlorosilane $SiHCl_3$ within a Siemens bell jar reactor. In this conventional process, silicon is deposited on silicon filaments at high temperature (1423 K), forming dense polysilicon rods. Several disadvantages have been identified in this process, such as: (i) low thermal efficiency and high electrical costs because of the need to cool the bell jar, (ii) low reactor capacity due to the relatively small reaction interface and (iii) unavoidable batch operations [142]. In the eighties, the increasing demand for high purity silicon led to the development of a reaction path starting from SiH_4 instead of $SiHCl_3$. Indeed, SiH_4 is available at higher purity, it does not lead to corrosive by-products and it reacts at lower temperatures and with higher conversion rates than $SiHCl_3$ [142]. Thus, the Komatsu process employing SiH_4 in a bell jar reactor similar to the Siemens one was developed. At the same time, the idea to apply a FBCVD process emerged, due to its intrinsic advantages: high thermal efficiency, high throughput and continuous operation, low cost and easy to scale-up technology [143] and [144].

The main reactor features have already been described in Section 2.5.1. For Hsu et al., the fluidization quality and temperature distribution along the FB are determining factors for the process efficiency [144]. This technology operates at atmospheric pressure, at a mean temperature of 893 K and from monosilane SiH_4 diluted in an inert gas. The initial bed particles are most often constituted of semiconductor grade silicon seeds belonging to Geldart's group B.

However, two fundamental drawbacks have rapidly been identified concerning the FBCVD technology: particle clogging beyond a critical deposition rate and parasitic fines formation. These phenomena have motivated several experimental and theoretical studies [14], [33], [34], [85], [111] and [143]. The first [14], [34] and [143] demonstrated the feasibility of silicon deposits on initial silicon seeds, and the high throughput of this process: more than 90% of the silicon in feed is deposited on the bed particles, the other 10% corresponding to parasitic oily fines.

Hsu et al. [144] were the first to point out that the key to successful operation of this FBCVD process is to keep the distributor temperature below 623 K, in order to avoid premature SiH_4 decomposition and partial clogging of the grid. Water cooling of the distributor flanges is then mandatory for this process. By working with a 15 cm i.d. FBCVD reactor, these authors succeeded in producing 3.5 kg/h of silicon using 80% SiH_4 feed concentration without bed clogging. These are the best results in terms of silicon productivity at the lab scale published up to now.

For Kojima and Morisawa [143] as for Caussat et al. [33], clogging phenomena occurred in a 5 cm i.d. reactor whenever the SiH_4 inlet concentration exceeded 20–25% in either nitrogen or argon. Such undesirable events can be anticipated by monitoring either thermal profiles along the FB and/or pressure drop between the bottom and top parts of the bed. In Fig. 25, we report two representative examples of temperature profile evolutions with and without agglomeration phenomena in a laboratory scale reactor [33]. In this case, bed clogging was attributed to the presence of chemisorbed reactive species on particle surfaces acting as a glue and able to form irreversible agglomerates when the deposition rate is too high and/or the fluidization quality too low.

Fig. 25. Evolution of temperature profiles along the FB (a) with and (b) without clogging. Arrows indicate the beginning and the end of deposition. The corresponding time period is

characterized by hydrogen production through the overall reaction: $SiH_4 \rightarrow Si + 2H_2$. Adapted from ref. [33].

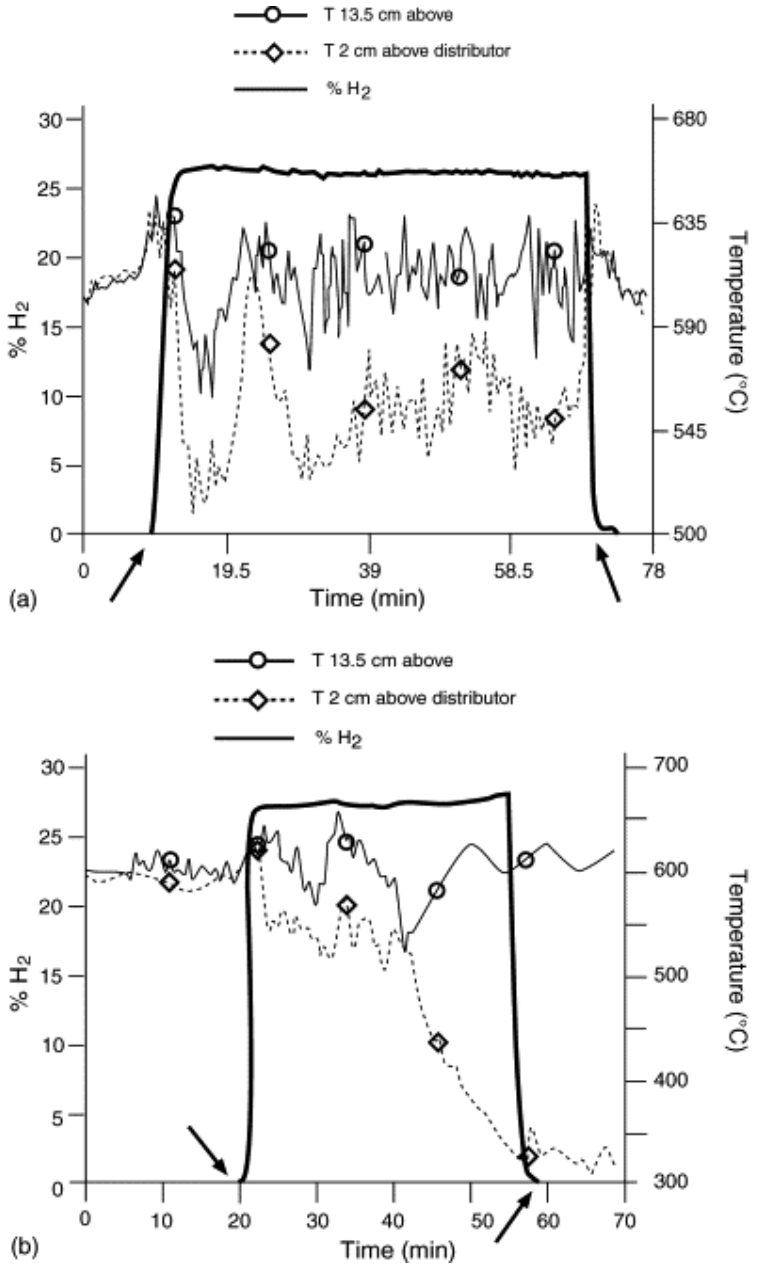

These results illustrate the major importance of the intrinsic fluidization quality, this parameter being improved with increasing bed diameter. Based on this correlation, such agglomeration phenomena would probably not occur in industrial scale reactors. In any case, multiple SiH_4 injections at various levels in the bed can be organized so as to never exceed the critical deposition rate as was proposed by Caussat et al. [33] from their modeling results (see

Section 2.6). Another way of progress could be to assist fluidization, by mechanical stirring or vibrating as detailed in Section 2.5.3.

According to Hsu et al. [144] and Kojima et al. [14] and [143], fines result from homogeneous nucleation of SiH_4 in the FB, leading to silicon nucleus formation and later to CVD growth into fine particles. Caussat et al. [91] emphasized the fact that fines are present only in the coldest upstream zones of the FBCVD reactor. Their formation could then proceed from low-temperature heterogeneous reactions, involving unconverted reactive species in the FB, thus leading to these oily/powdery products. Indeed, fines formation has been reported in the literature whenever SiH_4 conversion was not complete in the FB.

In order to prepare for industrialization of the process, Hsu et al. built a FBCVD reactor with an internal quartz liner so as to minimize metal contamination [144]. They also developed a seed generation device consisting in milling silicon granules with nitrogen impinging jets so as to produce silicon group B particles to be grown by FBCVD. Finally, their FB reactor was equipped with a particle withdrawal system through the distributor, in order to selectively take large particles out of the bed in a continuous or semicontinuous mode. The setup is schematically illustrated in Fig. 26. It consists in an externally water-cooled silicon tube 38 cm long and 2.2 cm i.d., in which particles are mildly fluidized so as to keep silane out of the tube and permit accumulation of large particles in the system.

Fig. 26. Particle withdrawal system developed by Hsu et al. Adapted from ref. [144].

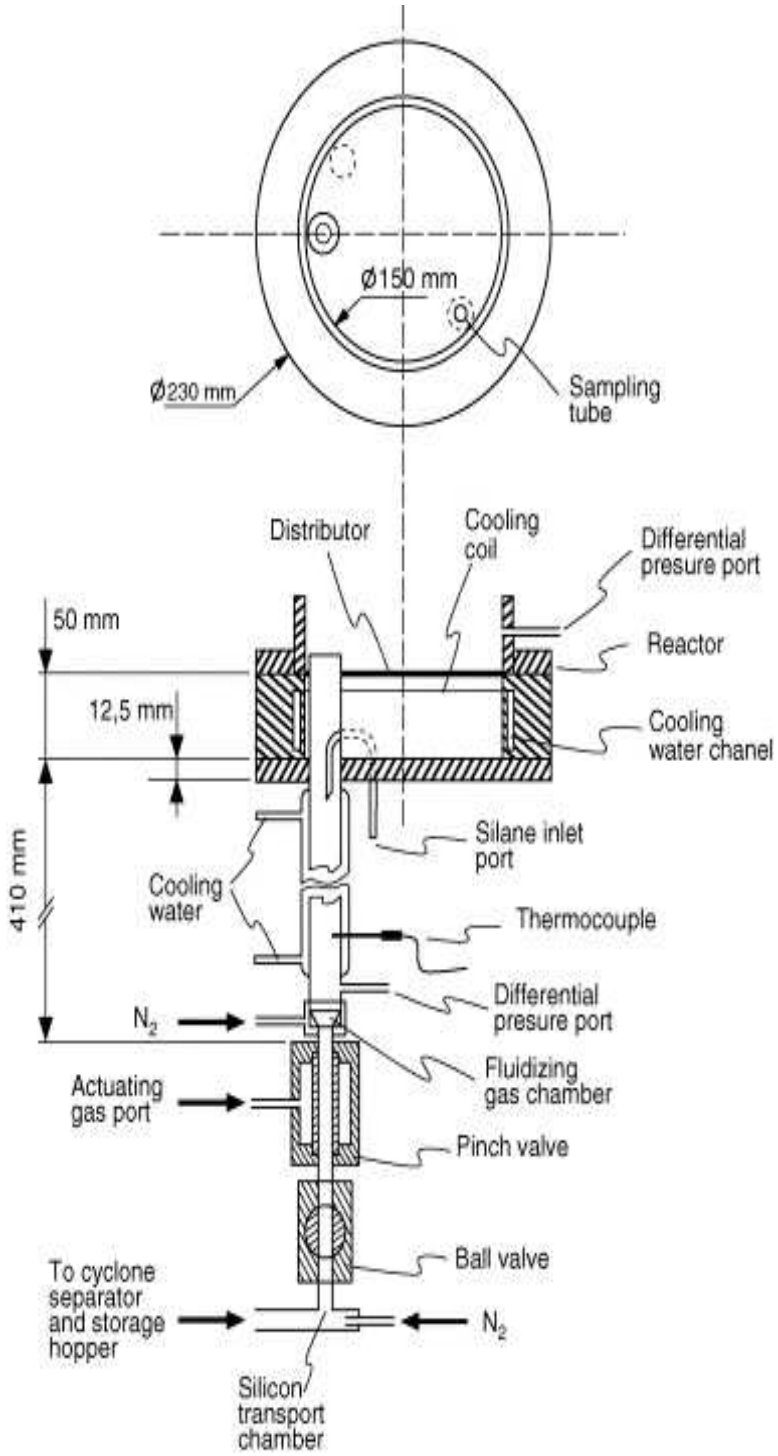

As can be seen in Fig. 27, and according to Kojima and Morisawa [142] and Caussat et al. [33], silicon deposits are composed of dense submicronic nodules. Their crystal state is polycrystalline. The fines are of lighter density. They are composed of hydrogenated amorphous silicon; their morphology is also nodular, but they are of smaller diameter than the deposit itself.

Fig. 27. SEM images of (a) a silicon deposit and (b) fines. Adapted from ref. [33].

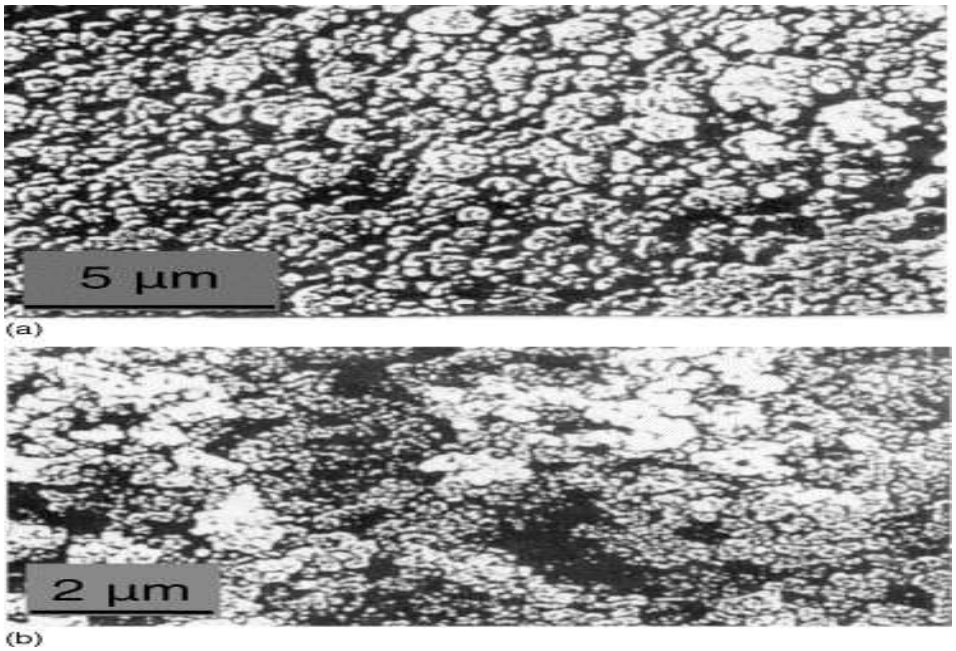

Over the last few years, a revival of interest has been shown in this FBCVD process. Indeed, this technology is currently under study to massively produce solar grade or even semiconductor grade polycrystalline granules [145] and [146]. It is worth noting that a key point for the emergence of photovoltaic cells in the next few years is a strong decrease in the cost of the raw material for the substrate, most often silicon.

3.4. Nuclear materials

"… *Fluidized-bed CVD was developed in the late fifties for a specific application: the coating of nuclear fuel particles for high temperature gas-cooled reactors* …" [147]. This statement, in one of the first comprehensive books on CVD, reveals that the development of materials for nuclear applications was the initial driving force for the development of FBCVD. Indeed, one of the first patents on FBCVD was submitted by the pioneer scientist of CVD Blocher, on the coating of nuclear fuel particles with mixture of pyrolytic carbon and SiC [148]. In this

context, FBCVD has been used to manufacture freestanding tungsten spheres and cylinders with a wall thickness of less than 5 μm, with the aim to produce metal foils as inertial confinement fusion targets [149]. The fluidization medium was H_2, which also allowed the reduction of WF_6 blown through the bed. Tungsten was thus deposited on the surface of molybdenum mandrels which were suspended in an appropriately selected 8 cm^3 fluidized bed consisting of ~350 μm, 12 g/cm^3 tungsten coated uranium carbide particles. After the end of deposition, wet leaching of Mo yielded pure W foils with the desired geometry. However, the main application of FBCVD for the processing of nuclear materials is essentially the deposition of multi-coatings composed of pyrolytic carbon and of SiC on radioactive particles for the primary containment of nuclear fission products. (e.g. [150] and [151]). Such multi-coatings should also present adequate microstructure and strength to withstand external load and to serve as a barrier of cooling gas contamination under reactor operation. Considerable progress was achieved in the eighties in this field, based on the need to obtain spherical fuel elements with high qualification yield ([15], [71], [152], [153] and [154] and references therein, in addition to an extensive patent literature). The replacement of SiC by other refractory carbides, such as ZrC [155] and later on NbC and TaC [156] was also proposed to improve the high temperature durability of the coated fuel particles, namely protection from the coolant gas both to prevent attack of the kernel and to limit fission product release. By using high-temperature halide chemistry, ZrC was deposited from methane and zirconium bromide $ZrBr_4$, while NbC and TaC were deposited by disproportionation of the corresponding chlorides formed from the chlorination of niobium and tantalum metal in a separate chamber and carried by argon stream to the FB. This accumulated know-how was considered later for the investigation of high temperature gas fuel nuclear reactors [157], [158] and [159]. All these works involve spouted bed CVD processes, despite the name FBCVD which was arbitrarily adopted in most of the above mentioned references. Appropriate denomination of the process was pointed only by Guilleray et al. [151] and by Ogawa et al. [155] who also provided information on the reactor used, namely 35 mm i.d. and 3 mm inlet nozzle at the base of a 60° cone. Other details, provided by the latter authors are the presence of a flat section between the inlet nozzle and the lower end of the cone to improve stabilization of the particle flow,[2] and introduction of the reactants and of the dilution gas through separate paths to decrease premature decomposition prior to entering the spouting cone, to regulate the gas-flow pattern below the nozzle and to control the particle flow pattern independently of the reactant concentration.

Fig. 28 shows a metallographic section of a high-temperature reactor fuel element with a so-called TRISO-type coating.[3] The 500 μm core is a uranium dioxide kernel. A 35 μm SiC layer (D) is sandwiched between two high-density pyrocarbon layers C (40 μm) and E (35 μm). The fuel element is separated from the coating by a buffer layer of porous carbon B (95 μm). This material has been processed in a SBCVD reactor in deposition conditions summarised in Table 2. Such processes typically operate at atmospheric pressure except for the previously mentioned deposition of NbC and TaC coatings, which were deposited at subatmospheric pressure [156].

Fig. 28. Metallographic equatorial section of a high temperature reactor fuel element, illustrating the different parts of the SBCVD coating. Adapted from ref. [15].

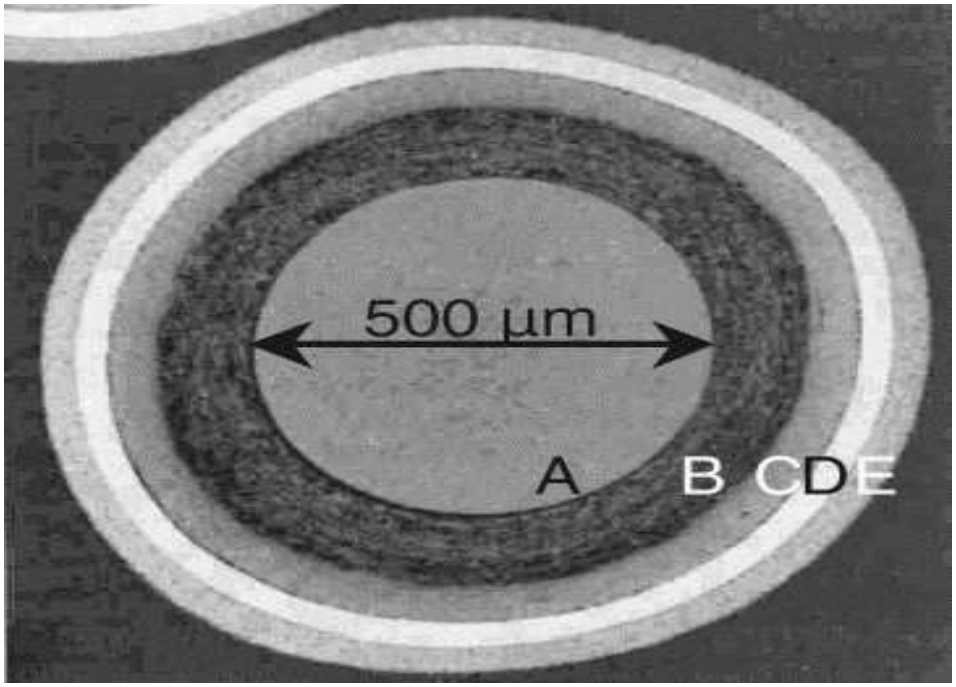

Table 2.

Processing temperature and composition of the gas phase for the deposition of the different phases in the coating of fuel kernel shown in Fig. 28

	Gas phase	Temperature (K)

	Gas phase	Temperature (K)
B	Ar,C_2H_2	1673
C, E	$Ar,C_2H_2/C_3H_6$	1573
D	H_2,CH_3SiCl_3	1873

The high deposition temperatures of the different layers allowed for a thermodynamic simulation of the corresponding processes [154]. Agreement between experimental and calculated results in terms of the nature of the phases deposited as a function of processing temperature and input gas composition was only found for the higher deposition temperatures. Satisfactory explanation of the obtained experimental results was made possible by considering a mass transfer rate-limiting model. However, the extreme environmental concerns of the use of such fuel elements, requires an analogous efficiency of the coating process. For example, Heit et al. reported that, to ensure sufficient retention of fission products – and especially the more volatile solids cesium and silver – in thorium high-temperature reactors, within a total of 1,000,000 coated particles after fuel element fabrication, not more than 60 individual particles are permitted to have broken SiC layers. Moreover, during operation in the reactor, not more than 200 additional particles are permitted to fail by cracking of the SiC layer [15]. While considering such severe constraints, stepwise increase in the coating batch size relatively to the previously mentioned dimensions was investigated by these authors for more economical manufacture. Beyond phase composition, coating microstructures is another important parameter, which has to be considered during the scale-up of the process. Heaney and Keeley first established relations between the microstructure of SiC coatings, and bed temperature and gas flow rates [71]. Then, they modified these coating parameters while scaling up the SiC process. A major phenomenon during the scale-up was found to be the strongly space dependent temperature of the bed and the existence of radial temperature profiles in the bed. Following these authors, changes in the values of other parameters, such as total gas flow and fluidized bed geometry (cone angle, etc.) are also necessary in the scale-up of such a spouted bed CVD process.

From the above elements, it appears that the FBCVD-based process for the processing of TRISO-type multi-coatings on UO_2 kernels is robust enough at least in terms of thermodynamic operating conditions. For example, it has been reported that the deposition technology of PyroC and SiC layers on 3 kg UO_2 kernels in 150 mm i.d. FBs has now been

mastered [158]. However, the global problem of simultaneously ensuring: (i) an appropriate microstructure of the coatings yielding optimum material performance, (ii) constant high product quality, (iii) economic operation and (iv) efficient scale-up of the process (with the aim of using 400 mm i.d. diameter FBs) still remains unsolved. To meet this objective, coupling of flow mechanisms in the bed, heat transfer and chemical reactions participating in the deposition should be modeled in order to dispose in fine of dimensioning tools allowing deposition conditions to be extrapolated to reactors of different sizes.

3.5. New materials

Emerging new applications of CVD on powders have appeared with the development of nanotechnologies. In particular, carbon nanotubes (CNTs) represent a fascinating new material that has attracted much attention in the past few years and intensive research has been performed to identify their remarkable properties and potential applications [5]. Multi- or single-walled CNT are now expected to bring significant breakthroughs in the technology of electronic and engineering materials. The large-scale synthesis of this material is currently the key to its commercial applications. Among the different techniques that have been applied for the production of CNTs [160], catalytic chemical vapor deposition (CCVD) appears to be the most promising due to its relatively low cost and potential high yield. Beside numerous reports concerning the preparation of CNTs on powders in fixed- or stacked-bed reactors, that will not be detailed herein, preliminary results with a FBCCVD reactor have appeared [161], [162], [163], [164], [165], [166], [167], [168] and [169]. The design of such a process is not at all trivial since the growth of CNTs is a catalytic process that is very sensitive to the operating conditions.

The synthesis of CNTs by CCVD methods involves the catalytic decomposition of a carbon-containing source on supported metal catalysts. Such a process is schematically illustrated in Fig. 29. It consists in passing a gaseous flow containing a given proportion of a hydrocarbon, over supported small transition metal particles of Fe, Co or Ni heated to the desired temperature (typically 823–1223 K) [5]. Numerous parameters of the catalytic process, such as temperature profile, gas composition, flow rates and of course catalyst nature and size play an important role on the features of the CNTs obtained. At a given temperature, depending mainly on the nature of both the catalytic metal and the carbon-containing gas, catalytic decomposition takes place on the surface of the metal particles, followed by mass-transport of the freshly produced carbon by surface and/or by volume diffusion until the carbon

concentration reaches the solubility limit and precipitation starts. According to the metal-support interaction, nanoparticles will remain (strong metal-support interaction—root growth) or not (weak metal-support interaction—tip growth) on the support.

Fig. 29. Schematic representation of CNT growth in a CCVD process.

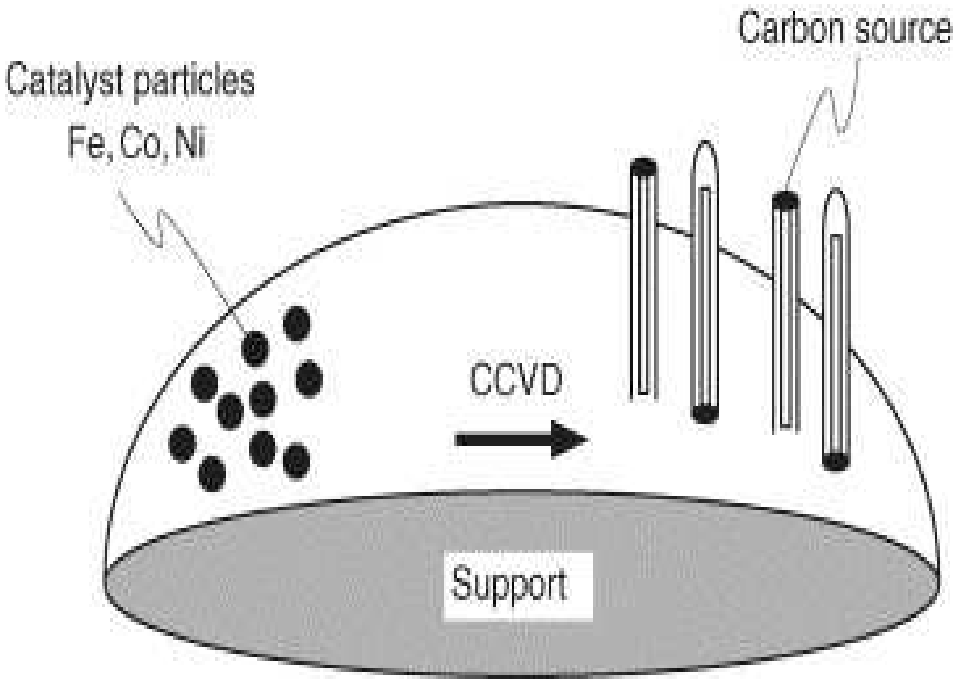

The main potential advantages of using a FBCCVD reactor for such a process are: (i) to ensure efficient mixing of the grains in the bed and efficient mass transfer through large exchange surfaces between the gaseous carbon source and the catalyst grains, (ii) to ensure a homogeneous temperature profile in the reaction zone and (iii) to consider the possibility of making continuous operations. The first two points are important for uniform growth of CNTs all over the catalyst grains and the latter for large-scale production. However, possible drawbacks can arise from the abrasive effect of the oxide supports used to prepare the catalysts which may lead to cutting the CNTs from the support or breaking them up. It is worth noting that such a phenomenon has never been observed during the FBCCVD synthesis of multi-walled CNTs on Fe/Al_2O_3 catalyst supports, since the CNT elutriation always remained very low [161]. Moreover, this method does not allow the production of aligned nanotubes that might be desired for specific applications. Finally, removal of the catalyst to obtain a pure material requires an additional step of purification.

From representative results obtained by different groups [161], [162] and [163], we emphasize the specific characteristics of the FBCCVD process. Concerning the advantages of using fluidized versus fixed bed systems, information provided by different laboratories is quite convergent. First of all, if the reaction is conducted under fixed- or packed-bed conditions, both lower carbon yields and lower selectivity towards CNTs are observed. Thus, in the case of multi-walled CNTs production on Fe/Al_2O_3 catalysts from ethylene [161], a yield of 60% was obtained for experiments performed in a fixed bed, to be compared with a yield of 90% in a fluidized bed. Additionally, the presence of unwanted carbon forms was evidenced by a combination of TEM observations and thermogravimetric analysis (TGA). The TEM micrographs of Fig. 30 illustrate CNT microstructures obtained in fixed-bed (a) and in fluidized bed (b) reactors [161]. It can be noticed that large amounts of undesired encapsulated metal particles are present in the former case while they are totally absent in the latter. In addition to these observations, TGA analyses have shown that selectivity towards CNT formation is close to 100% for fluidized bed experiments. On the contrary, in the material obtained in the fixed-bed reactor almost 17% of the available carbon is found in other-than-CNT forms. Similar results were obtained by Weizhong et al. [164]. Moreover, these authors noticed that CNT grown in a fluidised-bed reactor are obviously longer than those obtained in a packed-bed reactor. They also reported that the size of the composite ($CNT\text{-}Fe/Al_2O_3$) powder grains differs markedly from one reactor to the other. Starting with a Fe/Al_2O_3 catalyst powder presenting a 50 μm grain size, composite powders of 1–4 mm mean grain size are produced in the packed-bed reactor, whereas 45–50 μm mean grains size powders have been obtained using a fluidized-bed reactor.

Fig. 30. TEM micrographs of CNT produced (a) in a fixed-bed reactor and (b) in a FBCCVD reactor [161].

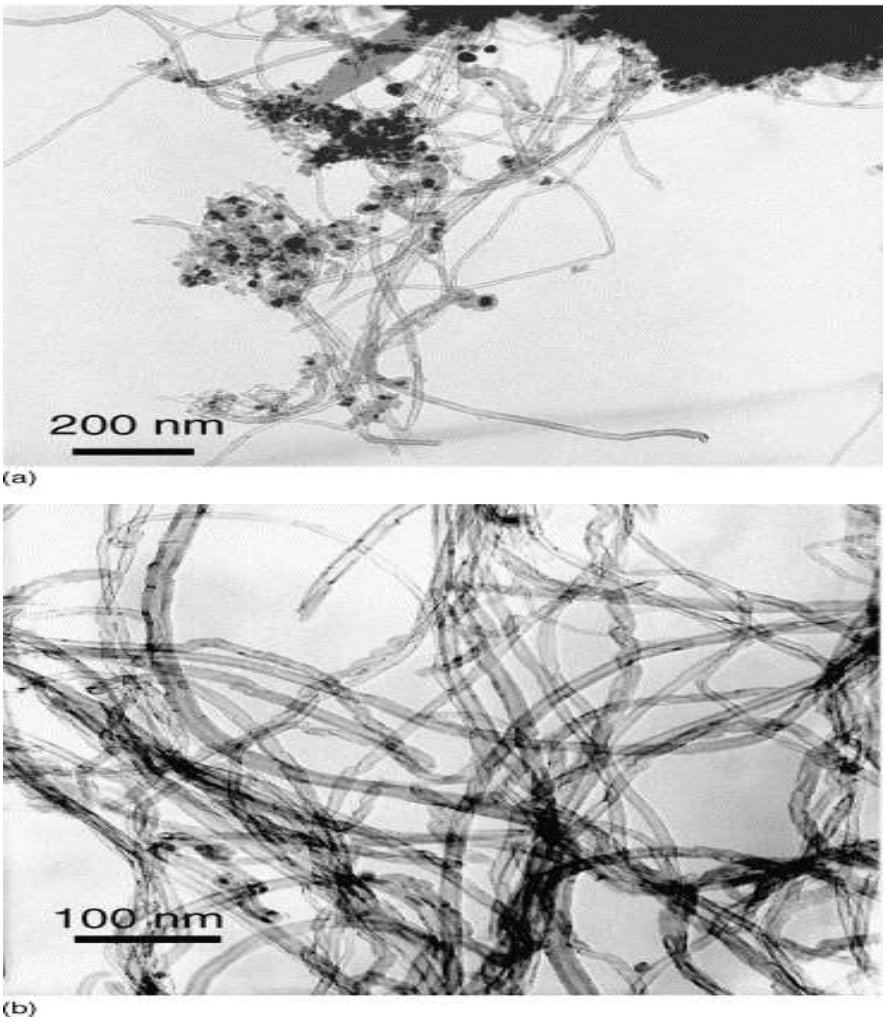

A very peculiar phenomenon observed in the FBCCVD process is linked to the impressive bed expansion that occurs during growth experiments. Corrias et al. reported that for an initial fixed-bed (catalyst powder) height of 3.5 cm, the final bed (composite powders CNT/catalyst) height can reach 1 m after a 2-h run [161]. The change of bed height with time is non-linear, which is certainly related with the growth mechanism of nanotubes. This spectacular expansion can be explained by the morphological differences observed between the initial catalytic powders and the final bed of composite powder particles. These differences are

clearly illustrated in the SEM micrographs of Fig. 31 [161]. In fact, CNTs form three-dimensional randomly oriented hanks, in which the initial catalytic alumina powders are embedded. The apparent density of this composite powder is very low, implying a high bed volume expansion. However, under the conditions tested, no decrease of the fluidization quality was detected, at least after 1 h of run. It is worth noting that, in pre-industrial equipments operating in continuous mode, the problem of bed height elevation and fluidization ratios evolution during runs will disappear. It is also worth mentioning that the bed expansions is associated with the use of very active catalyst for CNT growth; with catalyst of low activity or selectivity the changes in bed volume are expected to be less pronounced [167].

Fig. 31. SEM micrographs of the catalyst powder used for CNT growth (a) and of the composite powder obtained after CNT growth (b) [161].

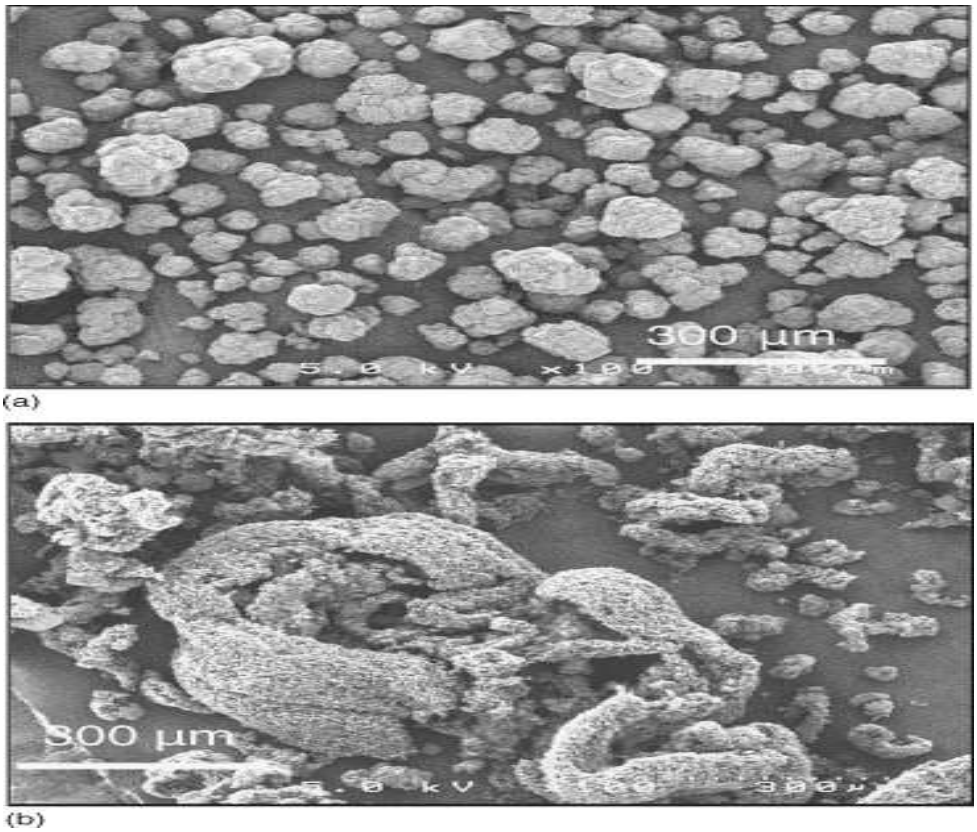

4. Other powders involving CVD processes

4.1. Coating parts in FBCVD reactors

It has already been mentioned that fluidized beds have found applications in thermal and thermochemical treatments as well as for the formation of wear and corrosion resistant protective coatings on metals. In the case of the thermochemical treatments (carburising, nitriding, carbonitriding and nitrocarburising), the gas mixture consists of reactive gases, such as methane and ammonia and inert gases, such as argon or nitrogen. These mixtures serve for the fluidization of an inert powder, mainly alumina and as a medium for the transition of, e.g. carbon and/or nitrogen into the surface of the material to be treated. The above conventional processes are presented in detail in ref. [170].

The combination of conventional fluidized bed technology with standard chemical vapor deposition has proven to be an effective method for the formation of wear as well as for corrosion resistant coatings on metals. The claimed economical and practical advantages of FBCVD over equivalent atmosphere processes are [171] and [172]:

- Reduction of the cycle time while still achieving the required microstructure and quality.

- Relatively low capital and operational costs.

- Immediate adjustment of the furnace atmosphere for the specific requirements.

- High and uniform heat transfer rate.

- Temperature uniformity resulting in a uniform coating.

A relatively broad spectrum of coatings has been obtained by the FBCVD process at high (above 1000 K) and low (below 1000 K) temperatures. Although the latter processes are of great technological interest as the distortion of the treated parts is kept to a minimum and the energy consumption is considerably reduced, the works presented up to now indicate that this technology is at the early stage of development.

4.1.1. Principles of the process

In the FBCVD process presented in this section, the parts to be coated are suspended within an FB furnace. The retort of the FB furnace is filled with a treating agent. As fluidizing gas, either inert or reactive gases or gas mixtures are used like Ar, N_2, Ar + H_2, Ar + $HCl_{(vapor)}$.

Generally, several options are available regarding both the treating agent and the fluidizing gases. The treating agent may consist of a filler or inert oxide, such as refractory powders of Al_2O_3, SiO_2, ZrO_2, TiO_2, etc., and a powder of a source master alloy or a metal, which serves as the donor of the element to be coated. The filler oxide also avoids the sintering of the metallic powder. An activator is used which reacts with the above powders producing vapor precursors of the coating forming element. As activators, either halides or alkali metal halides or alkaline earth metal halides or organometallic compounds can be used. The gas products of the chemical reaction between the donor and the activator react at the surface of the part to be coated followed by deposition and/or diffusion alloying. When carbon and/or nitrogen are provided from a source, carbide, nitride or carbonitride coatings can be formed. In the case of boriding, mixtures of Al_2O_3 and B_4C and of a halide salt or alkali metal halide as activator are used.

4.1.2. Types of coatings

The literature survey on the wear resistant cementing coatings has revealed a series of patents brought out by Arai et al. at the Toyota Central Research and Development Laboratory employing the FBCVD process for the formation of C, N, CN coatings of Ti-, V-, Cr-, Nb-, Ta-, Mn-, W- and Mo- on several metals, such as Fe, Ni, Co and their alloys [173], [174], [175], [176], [177], [178] and [179]. In another patent, a FB reactor has been applied for the formation of hard, wear resistant coatings on metals [180]. In this case, the liquid halides of the metal to be coated are evaporated in a separate reactor and subsequently mixed with the fluidizing gas. From a separate device, reactive gases selected for their ability to form nitride, carbide or carbonitride compounds with the metal halide are provided simultaneously to the FB reactor.

4.1.2.1. Ti-coatings

A significant amount of work has been performed especially for the high temperature deposition of Ti by FBCVD. Arai et al. have reported the formation of a TiC-coating of 7.5 μm on AISI W1 steel at 1223 K after 2 h treatment in a bed consisting of Al_2O_3 and FeTi as donor with NH_4Cl as activator [181]. Sanjurjo et al. deposited Ti, TiN and TiO_x on copper, Cu–Ni alloys, silica and steel [40] and [182]. The treating agent consisted of the elements to be coated. The fluidizing gas was mixed with a reactive one so that the coating precursors were generated in situ by the reaction of the particles in the bed. More specifically, a porous

free coating of Ti of 3–5 μm thickness on a Cu tube and a mirror like coating on silica tube were deposited, respectively, at 1023 K using a bed of Ti and HBr as activator. By injecting NH_3 in the same experimental setup, TiN-coatings of 3 and 1 μm were formed on a steel bar and a silica tube, respectively. The coatings on the steel bar were homogeneous and continuous, whereas on silica tube colored, mirror-like coatings were formed. Argon was the fluidizing gas in all cases.

Kinkel et al. showed that a uniform coating with a practically constant thickness of 16 μm was formed at a height of 300–700 mm above the bottom of the FB furnace on a C70 steel bar treated for 6 h at 1173 K with a FeTi donor and NH_4Cl activator [183]. This is illustrated in Fig. 32. Moreover, the authors revealed that the rate-controlling step in the formation of TiC-coatings on 100Cr6, C60 and S 6-5-2 steel grades is the diffusion of carbon into the coating or in the steel grade, as the coating thickness increases linearly with the square root of time (Fig. 33 [171]). In this work, a mixture of Al_2O_3 powder with a mean grain size of 175 μm and FeTi with 40 wt.% Ti and grain size distribution from 63 to 150 μm was used as treating agent and NH_4Cl was used as activator. The bed was fluidized by Ar. The carbon necessary for the formation of the coatings was provided by the steel substrates. A carbide free zone between the coating and the substrate may be formed in cases were the supply of carbon from the steel is limited (Fig. 34 [184]).

Fig. 32. Arrangement of the 14 mm × 14 mm steel bar in the Ø160 mm FB furnace (a) and coating thickness distribution across the height of the FB furnace (b). Adapted from ref. [183].

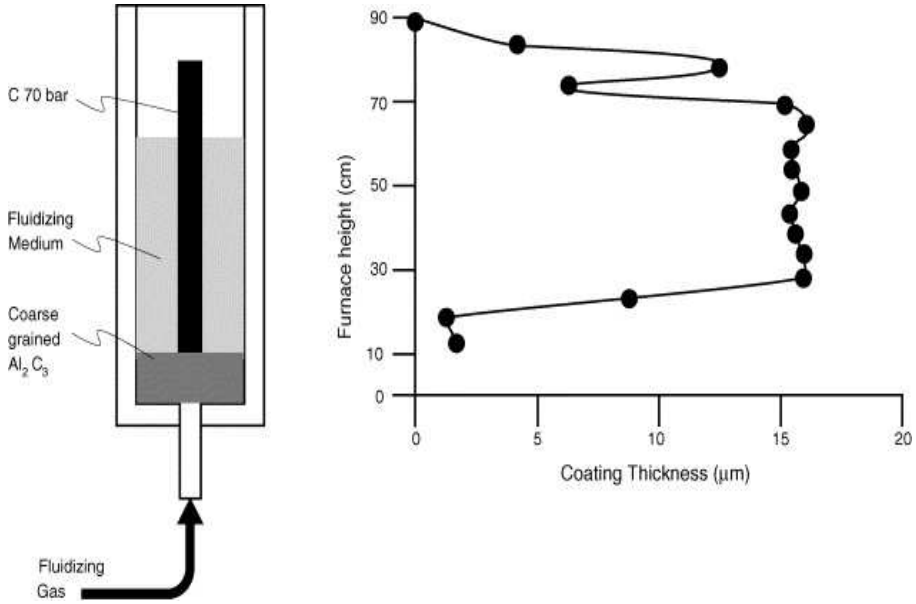

Fig. 33. Mean thickness of TiC coating vs. square root of treatment time at 1173 K. Adapted from ref. [171].

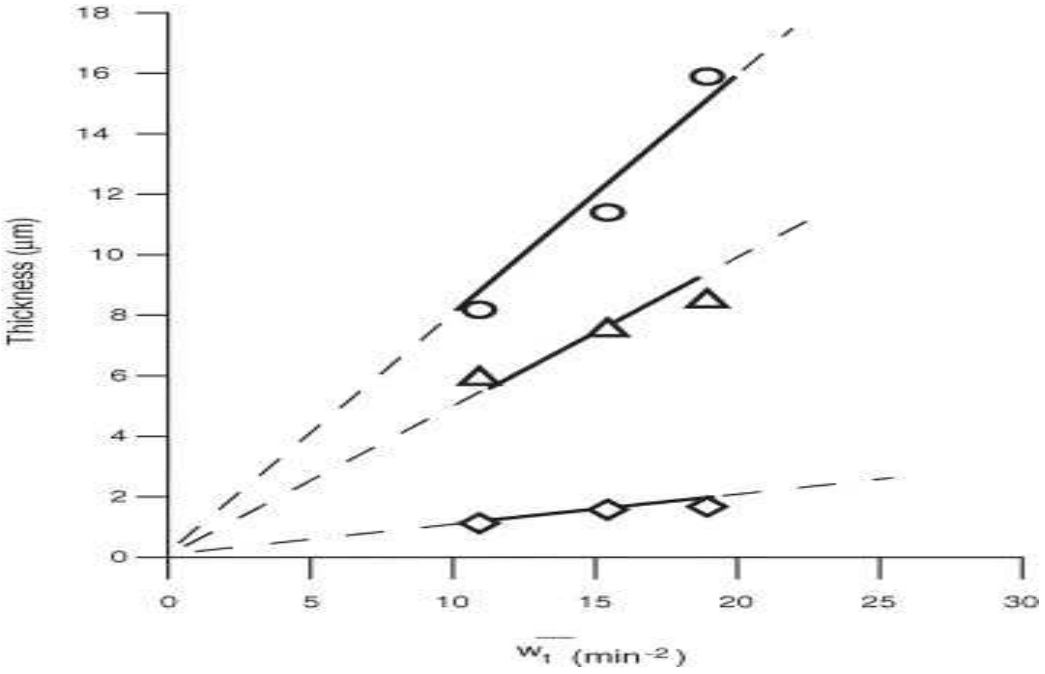

Fig. 34. Decarburisation zone at the TiC-substrate interface. Steel grade C60, treatment time 6 h at 1273 K, FeTi donor, NH_4Cl activator, coating thickness 15.1 μm [184].

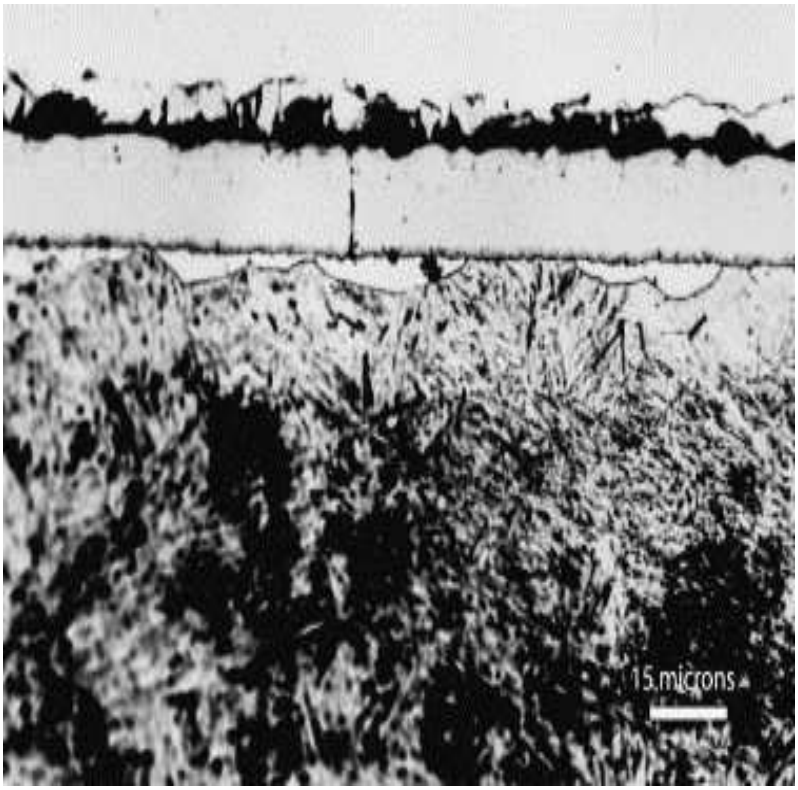

The Vickers microhardness of these coatings was in the range of 3000 HV. The surface roughness was found within the range of the CVD produced coatings with the values of R_a, R_z and R_{max} varying from 0.42 to 0.47, 1.9 to 4.88 and 2.0 to 8.2 μm, respectively [185]. In the SEM micrographs of Fig. 35, the initial stages of the formation (a) and after 1 h treatment (b) of TiC-coating formed on a 100CrMo7-3 steel grade are depicted. The coating is adherent to the surface as neither voids nor cracks are noticed at the interface.

Fig. 35. Scanning electron micrographs (a) initial stage of the formation (courtesy of S. Kinkel, G.N. Angelopoulos) (b) well developed TiC coating on a 100CrMo7-3 steel grade fractured cross-section after 1 h treatment at 1273 K [185].

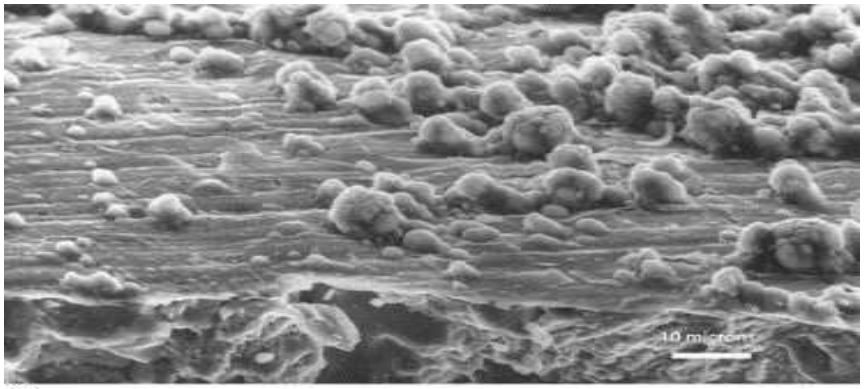

(a)

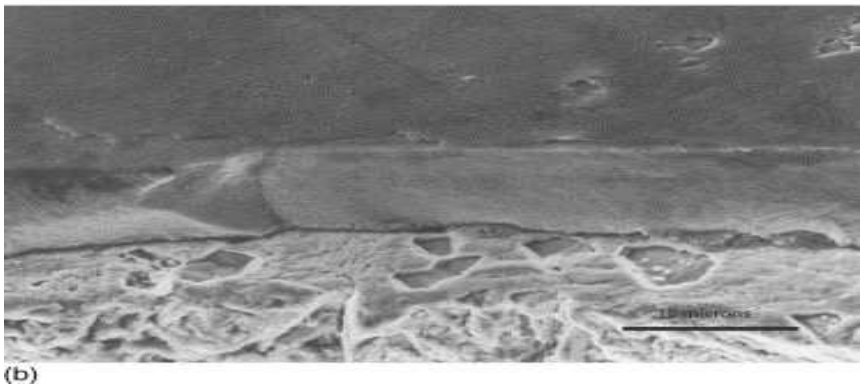
(b)

The modeling of the titanium carbide coating on carbon-containing steels by the FBCVD process without the presence of hydrocarbons in the gas phase has also been attempted [186]. The model, based on a simultaneous solution of the mass balance and diffusion equations of the system, provides solutions for variable carbon concentration in steel. The comparison of the numerical to the experimental results indicates that the model proposed predicts the rate of deposition of TiC-coatings to a satisfactory degree and can be applied on plain and alloyed carbon steels as well. In general, the above coating growth considerations hold true only if the treating agent can supply the amount of Ti required combining with the carbon supplied from the substrate. Until now, in most reports, the amounts of Ti-containing gaseous precursors are in excess in accordance to the above condition. Attempts at process optimization in terms of the consumable raw-materials have not been presented yet.

4.1.2.2. Cr-coatings

Conventionally, high-temperature FBCVD chromising processes are performed by feeding a halide activator in the FB furnace together with an inert carrier gas or with hydrogen that is also used for fluidization. The halide reacts with the chromium source powder of the treating agent mixture to form chromium halide gaseous precursor species. Following this principle,

chromising in fluidized beds was performed by Arai et al. using as, treating, agent a mixture of Al_2O_3 and Cr powders and, as activator, NH_4Cl [176], [178], [179] and [187]. A carbide layer was grown on carbon steels (AISI W1 and D2), consisting of M_7C_3 or $M_7C_3 + M_{23}C_6$, while on Armco iron an iron–chromium solid solution was formed. Treatment temperatures varied from 1073 to 1273 K and treating time up to 2 h. The authors claim that, in steels with a carbon content higher than 0.15%, chromium carbides are formed, their thickness increasing with the steel carbon content. In a low temperature process, a CrN layer of 8 μm was formed at 843 K after 50 h on pre-nitrated substrates. Kinkel et al. chromised 100Cr6 steel grade at 1173 K using, as treating agent, a mixture of Al_2O_3 and FeCr. The coating consisted of Cr, Fe and C and the XRD analysis showed the characteristic peaks of Cr_7C_3 phase [183]. Tsipas et al. reported on the formation of the Cr-containing coatings presented in Table 3 in the temperature range 1273–1373 K [188] and [189]. They used as treating agent, mixtures of Al_2O_3 powder with a mean grain size of 100 μm and compounds, such as Cr, Al, Fe, Yt, Hf, C, and $HfCl_4$, $CrCl_3$, NH_4Cl, $AlCl_3$ as donors and activators, respectively. Fig. 36 presents a typical morphology of a Cr–Y-coating obtained on H13 steel after 2 h treatment at 1373 K exclusively using Yt and $CrCl_3$.

Table 3.

Substrate materials and coating formed in FBCVD processes [189]

Substrate	**Coating**	**Thickness (μm)**	**Observations**
H13 steel	Cr(Hf) carbide	25–30	Very good adherence
100CrMo910	CrYt	150–200	–
H13 steel	CrYt	150–200	–
100CrMo910	CrAlYt	150–200	Very good adherence and uniformity
RENE 80	CrAl	150–200	–
INCONEL 718	CrHf	15–20	–
Ni–Al–Ti alloys	Cr/Hf	10–15	Non-uniform deposition
Ti–Al–V alloys	Cr(Hf traces)	20–25	Non-uniform deposition

Fig. 36. Surface morphology of Cr–Yt coating on H13 steel obtained at 1373 K after 2 h treatment. After ref. [189].

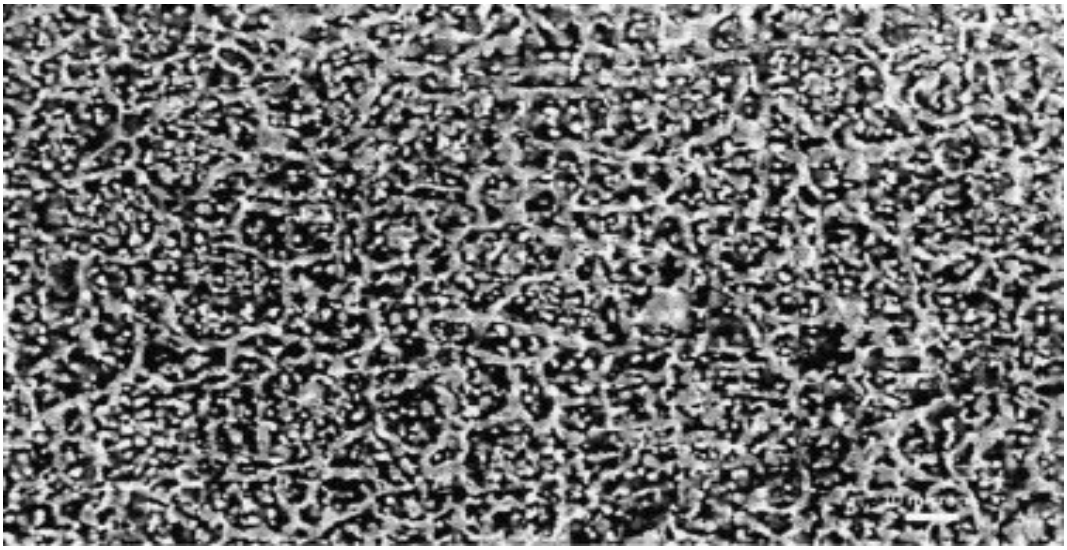

Christoglou et al. followed a two-step treatment for the deposition of an Al- and Cr-containing coating on nickel [190]. In Fig. 37, the multi-element coating is depicted. The inner white zone was formed at 853 K for 4 h with Al donor and HCl vapors as activator. Subsequently, without removing the sample from the furnace the temperature was increased to 1273 K and Cr powder was added. The treatment was continued for other 5 h. The resulting dense coating was comprised of a thin inner white AlNi zone, a poorly colored light grey Al phase of NiAl, an Al rich NiAl phase with a blue hue and an outer Cr rich grey phase. According to EDX microanalysis, the latter phase consisted of 25 at% Al, 12 at% Cr and 63 at% Ni.

Fig. 37. Cross-sectional optical micrograph of an Al–Cr coating obtained by a two-step process. At the first stage the samples were aluminized at 853 K, while at the second one chromising took place at 1273 K. HCl vapors were used to activate both processes [190].

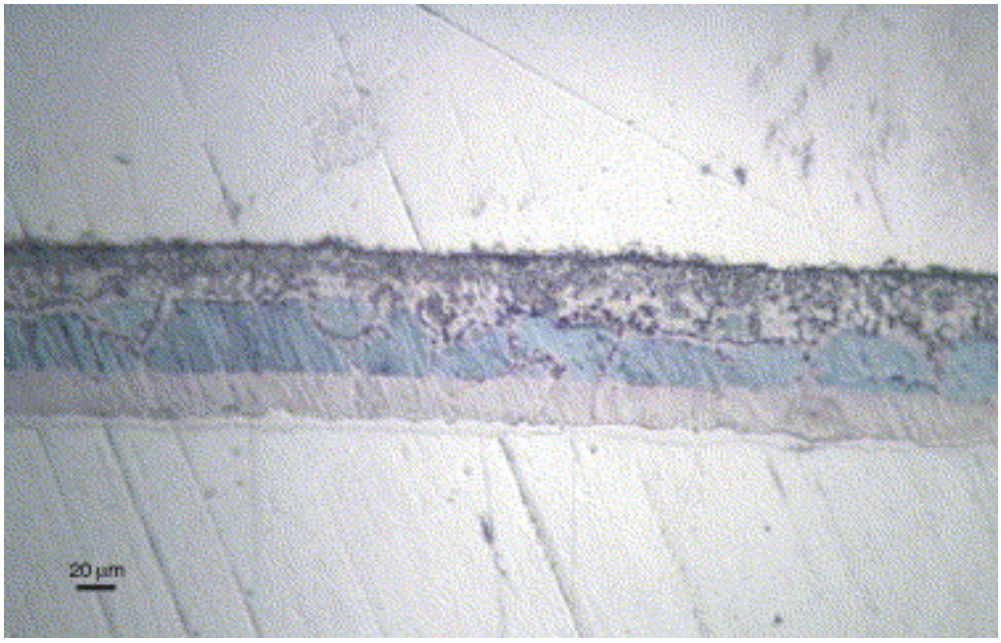

King et al. formed Cr(N,C)-coatings at 843 K on H13 tool steel also by a two-step process [191]. In the first step, the steel grade was nitrocarburised given a coat of nitrocarbide and subsequently chromium was transferred to the nitrocarbide surfaces from the gas phase by the reactions resulting from the reaction of HCl gas with the chromium powder donor. Two different experimental procedures were followed: under a H_2 atmosphere or not. The authors reported that addition of 30% H_2 to the fluidizing gas increased the rate of the coating formation. However, hydrogen induced a rapid loss of nitrogen from the surface. They also found that the iron nitride layer formed during the first step of the process; i.e. the formation of the nitrocarbide, strongly influenced the microstructure of the Cr(N,C)-coating and resulted in complicated surface microstructures. Moreover, the soft interlayers and brittle oxides formed below the surface are not likely to contribute to the adherence of the coating.

The application of the FBCVD process to form a carbide coating to enhance tool life was studied by Chen et al. [192]. They used a mixture of Al_2O_3 with powders of pure Cr as treating agent, pre-alloyed 71Cr–29Fe–0.03C, 66Cr–26Fe–7.7C as donors and NH_4Cl as

activator. The treatment of AISI M2, H13 and the of a modified D2 steel grade, was conducted in the temperature range 1223–1323 K for up to 4 h. The parabolic time-dependent results indicate that the system did not reach saturation even with 50 wt.% Cr donor addition. If the donor powder added was higher than 50 wt.%, poor fluidization behavior occurred, due to the approximately two-fold higher apparent density of the donor metals than of the alumina. The thickness of the chromium carbide coatings was not dependent on the steel grade but on the type of donor used. Pure chromium presented the thicker coatings and increasing the proportion of carbon in the donor decreased the thickness. The coatings formed mainly composed of $(Cr,Fe)_{23}C_6$ and of small amounts of $(Cr,Fe)_2N$ which was formed from the reaction between nitrogen from the NH_4Cl decomposition and Cr. The results also indicate that the rate-limiting step of coating growth is the diffusion of carbon through the substrate, i.e. the carbon available in the austenitic matrix at the temperature of the treatment process. The hardness of the coatings varied between HV1600 and HV1800 regardless of the type of steel substrate.

Lee and co-workers applied a Cr-coating by FBCVD on a Fe–Al-based alloy in order to study the influence of the surface modification on the resistance to environmental degradation [192] and [193]. They found that the Cr-coating was unable to stop the inward penetration of hydrogen during electrochemical tests. Instead, Cr promoted the permeation rate of hydrogen. However, the ductility of the Fe–Al alloy processed by the FBCVD process exhibited 4.7% elongation in comparison to 2.3% elongation of the uncoated one. The authors attribute this improvement to the existence of a Cr-Fe soft solid solution layer formed which helped to increase the ductility of the alloy.

On the other hand, according to Pérez et al. formation of a Cr-coating on AISI 304 stainless steel is not possible at 1173 K for 30 min under a reactive gas mixture containing 10% H_2 and 0.5 or 1% HCl [194] and [195]. This is probably due to the reaction of Fe with HCl and the formation of volatile $FeCl_2$, as weight loss of the samples was observed too. The authors suggest that higher treating temperatures and HCl(g) concentrations should be used to activate the deposition mechanism. In contrast, when IN-100 Ni-based alloy was used, even for short times, a Cr-coating was obtained. However in the case of IN-100 no diffusion took place. Therefore, a post-diffusion heat-treatment process is recommended for the required microstructure to be formed.

4.1.2.3. V-coatings

Vanadium hard coatings are the most widely used. The formation of vanadium carbide coatings on steels with the FBCVD process follows on the work of T. Arai on carbide coatings [176] and [177]. In the proposed process, the treating agent consists of 1–40 wt.% 100–200 mesh ferrovanadium containing 70 wt.% vanadium and of 80–100 mesh aluminium oxide. NH_4Cl was used as activator and Ar as fluidizing gas. In ref. [176], the authors claim the formation of a uniform VC-coating on a SKD 11 tool steel of 5–6 μm thickness at 1273 K for 2 h. The hardness of the coating was in the range of HV3000. In ref. [179], a nitrogen-containing gas was pumped into the furnace. In this case, on the surface of SK4 and SK11 tool steels, a uniform V(N,C)-coating was formed of 6–7 μm and 4–5 μm thickness, respectively, at 1273 K for 2 h.

Similar results were found in the work of Kinkel et al., where a uniform coating was formed at 1253 K on the surface of 100Cr6 tool steel (AISI L3), consisting, on the outside of $V(C,N)_{0.84}$ and inside of $VC_{0.84}$ [183]. The growth rate of the coating was proportional to the square root of the deposition time, suggesting that the rate-limiting step is the diffusion of carbon. Nakanishi et al. also reported the formation of a two-layer coating, the outer one consisting of $V_2(C,N)$ and the inner one of $V_8(C,N)_7$ [196]. Fig. 38 depicts the linear relation between the deposition time and the thickness of the vanadium carbide coating for various steel grades.

Fig. 38. Linear dependence of the VC-coating thickness on square root of treatment time for W1, D2 [196] and L3 [183] steel grades. Adapted from ref. [183].

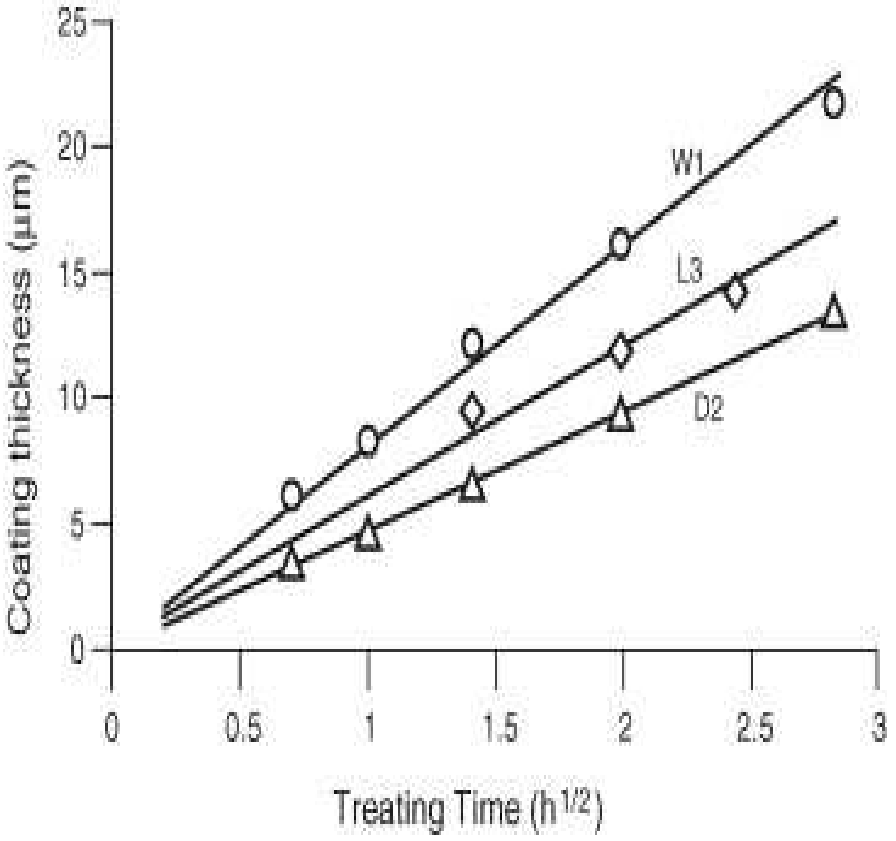

In Fig. 39, a typical cross-section of a VC-coating on 10Cr6 steel grade formed at 1253 K for 5.5 h is depicted [182]. The coating exhibits microhardness in the range of 2000 HV0.1, which is lower than the 3000 HV for the vanadium carbide coatings. The tribological properties of the coatings formed by the FBCVD process are similar to those deposited by salt bath or CVD techniques. Moreover, the FBCVD coatings exhibit better seizure resistance than the cemented carbide, excellent toughness and resistance to wear, corrosion, oxidation and peeling.

Fig. 39. Optical micrograph of a VC-coating on 10Cr6 steel grade formed at 1253 K for 5.5 h by the FBCVD process. After ref. [182].

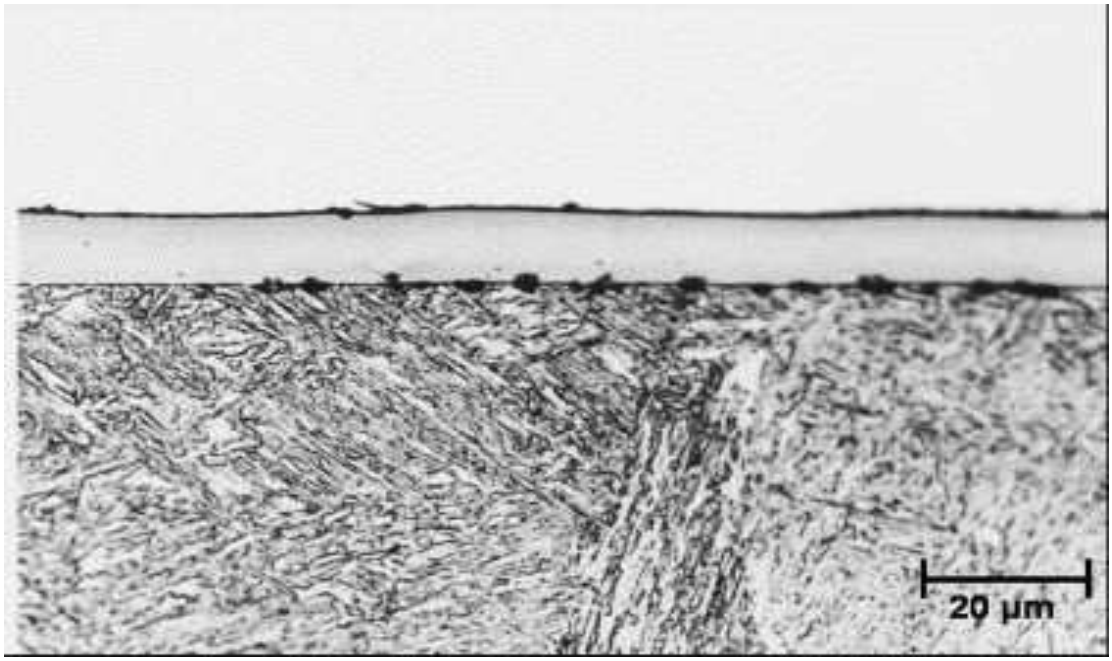

4.1.2.4. Boriding

Boriding by FBCVD is considered as simple, efficient and environmentally friendly [197]. Arai et al. performed the boriding process at 1223 K on a W1 0.9 wt.% C steel grade, using a treating agent consisting of Al_2O_3 and B_4C, and of KBF_4 or NH_4Cl as activators [187], [198] and [199]. The B_4C content was 40% and the activators 0.1, 0.5 and 1 wt.%. The thickness of the boride coating formed was uniform. The coating formed with NH_4Cl was thinner than with KBF_4. In both cases a single phase coating of Fe_2B was formed.

Graf von Matuschka et al. [200] and Rojan [201] used a boriding agent, specially developed by EKabor WB Germany. It is composed of spherical particles of 200–300 µm in diameter consisting of SiC and B_4C fine grains in a matrix of KBF_4. Their results indicate that the boriding effect decreases with increasing utilization time of the powder. According to the results of ref. [201], the growth rate of the coating is higher on a C15 plain carbon than on 42CrMo4 high alloyed steel, indicating that the alloying elements retard boron diffusion.

Recently, the group of Tsipas et al. has performed extensive developments on boride coatings on several materials by FBCVD [188], [202], [203] and [204]. In all cases, the treating agent used consisted of Al_2O_3 and B_4C, and either sodium or NH_4Cl or NH_4F as activator. The boride coating growth on Ni-, Cr-, Ti-substrates is presented in Fig. 40 according to the results of Tsipas and co-workers [204]. It is obvious that the boride process is not diffusion controlled. Actually, boriding is controlled by a two-step mechanism. In the first step, the boron containing treating agent reacts with the surface of the component, producing a thin compact boride layer. The second step is diffusion controlled. The overall mechanism depends on the type of substrate.

Fig. 40. Nickel, chromium and titanium boride coating growth at 1223 K. Adapted from ref. [204].

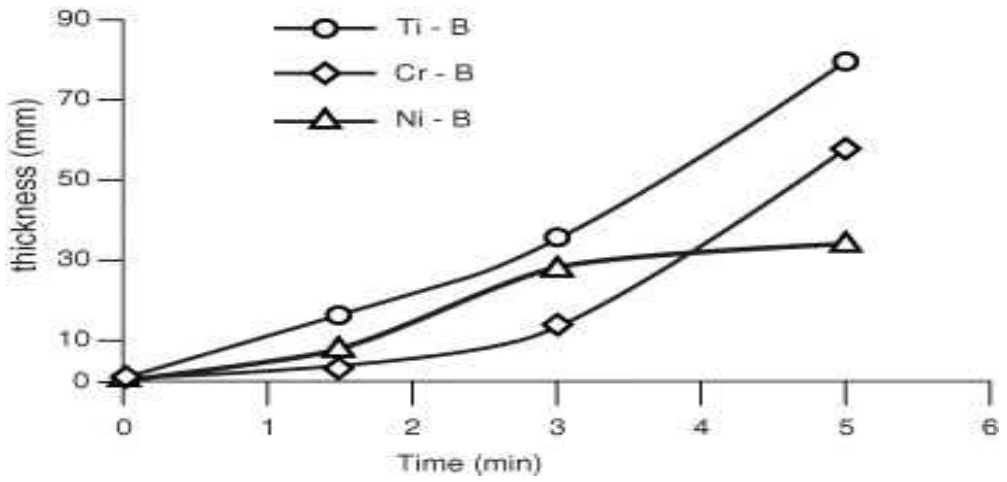

The wear resistance of Ni-boride coatings was evaluated by pin on disk test under dry wear conditions as the oxidation resistance of titanium boride coating by a cycling oxidation testing device. The results are presented in Fig. 41 and Fig. 42, respectively.

Fig. 41. Pin on disk dry wear resistance results for Ni-boride coating for different treatment time. Adapted from ref. [204].

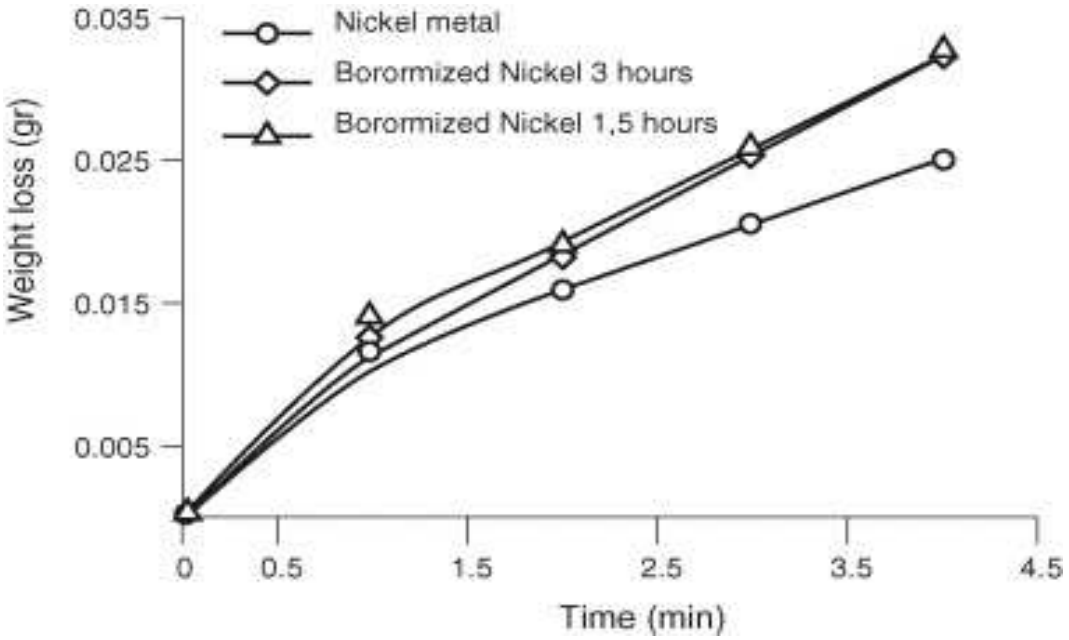

Fig. 42. Cyclic oxidation corrosion resistance test results for titanium boride coating. Adapted from ref. [204].

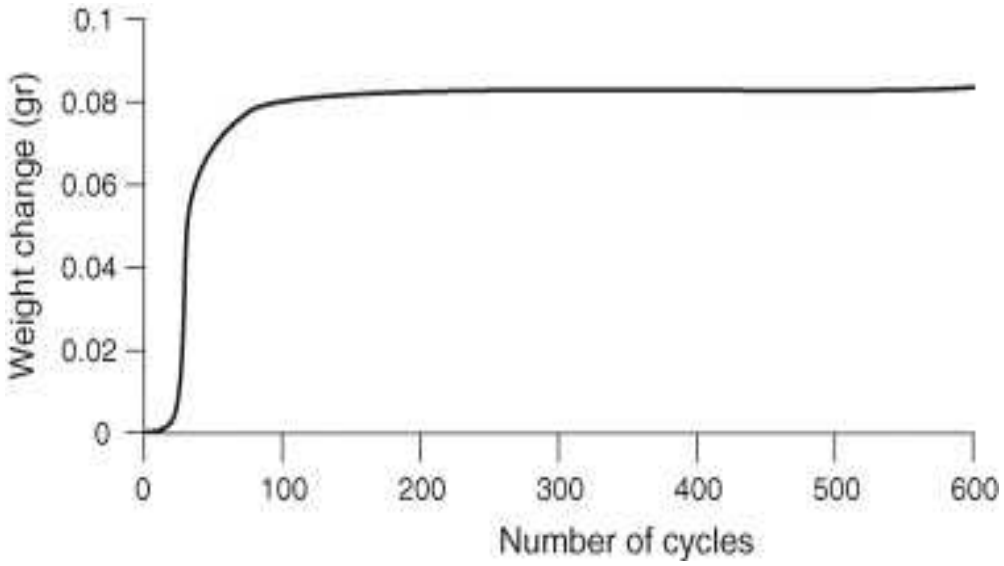

Optical micrographs of boride coatings on low carbon steel and on nickel are depicted in Fig. 43 adapted from Tsipas et al. [188], [202] and [203]. In ref. [203], a microstrain analysis was performed by means of the WINCRYSISE software. It is reported that, during the FBCVD process treatment of low carbon steels (Fig. 43a), the heterogeneous nucleation process of the

boride coating is limited leading to a relaxation of the formed layers and therefore crystals are grown free of any strain. In contrast, during pack cementation, residual stresses are setup due to the preferential precipitation of the coating phases in the early stages of crystallization.

Fig. 43. Boride coatings on different substrates by Tsipas et al. [188], [202] and [203]. Fe_2B coating on low-carbon steel substrate (a) and boride coating on nickel (b).

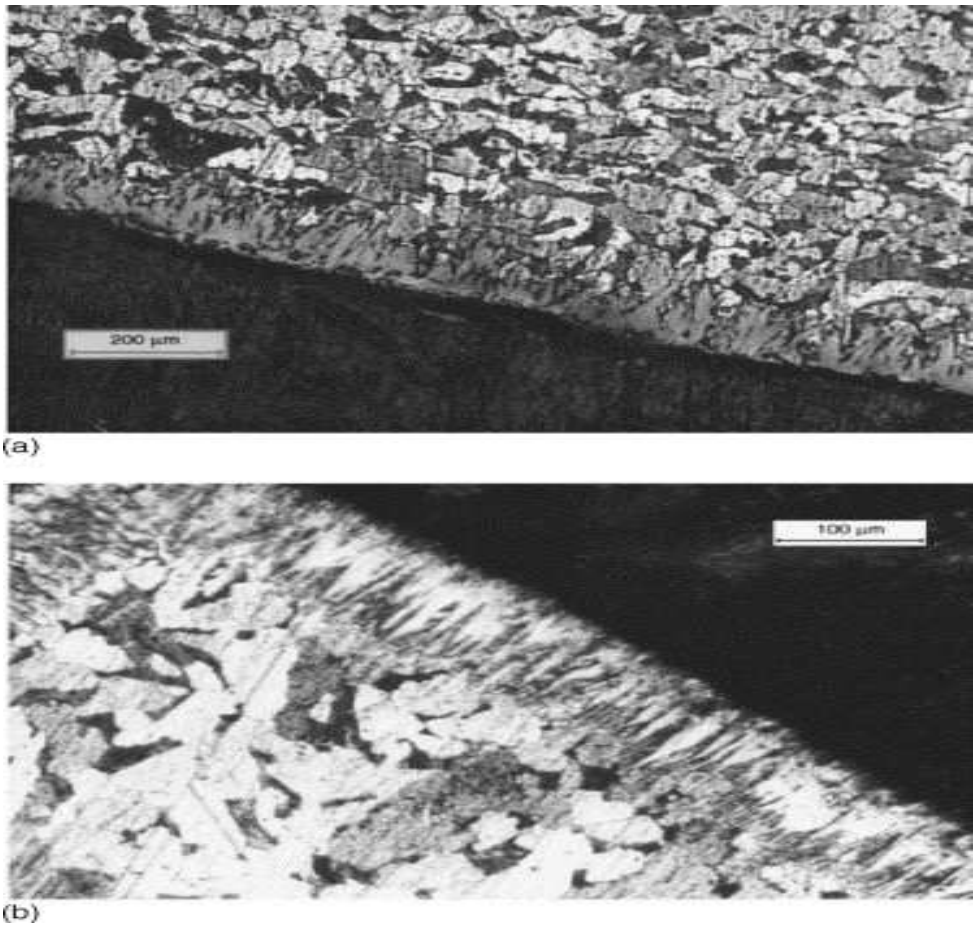

4.1.2.5. Si-coatings

Si-coatings can be successfully formed by low and high temperature FBCVD on copper and steel as well as on other materials, such as graphite fibres. According to Sanjurjo et al. at 873 K a thin (<1 μm) Si-coating and a non-porous, 3–4 μm homogeneous coating were formed on a Cu tube for 15 and 37 min treatment, respectively [182]. At 1023 K and 120 min

treatment, a Cu wire was totally siliconised. In all cases, the bed consisted of metallurgical grade silicon fluidized by Ar. For the coating process activation, vapors of HBr were mixed with the argon flow. According to the authors, the use of HBr vapors significantly lowers the temperature of formation of the bromosilane and subbromide intermediates ($SiBr_{x,x<4}$). By subhalide disproportionation, solid silicon is deposited on the substrate surface according to the reaction: $2SiBr_2 = SiBr_{4(g)} + Si_{(coating)}$. Therefore, although the estimated lifetime of the subhalides is very short, in the range of 100 ms, they are of great importance in coating formation, even though their partial pressures can be low. The above deposition mechanism is also supported by the fact that for temperatures of around 873 K, thin silicon layers are formed. At 1023 K or extended processing times, an interface phase of copper silicides is formed. Finally, the Si-coated Cu samples presented a clear increase in corrosion resistance. Similar results were obtained by the same authors using chloride-based chemistry [39]. In this case, the bed consisted of metallurgical grade silicon powder with a particle size of 250–500 μm mixed with 5 wt.% $CuCl_2$. For the process activation, HCl vapor was mixed with the Ar flow to obtain a partial pressure of 10–15 Torr. For temperatures in the range 623–773 K and relatively short deposition times (15 min), a homogeneous, dull orange-red coating was obtained. At temperatures greater than 773 K or longer deposition times (30 min), a dull grey copper silicate coating was produced. In some cases, metallic silicon was deposited. Deposition rates were 20 and 30 μm h^{-1} for low and high temperature processes, respectively. At temperatures above 873 K, a porous external dendritic layer as well as diffusion layer were observed.

Silicon-coatings were also deposited on AISI 304 stainless steel with a low temperature FBCVD process [205] and [206]. The authors used a bed consisting of Si powder (97.5% purity) fluidized by Ar. The required HCl and H_2 were added in the FBCVD reactor from the beginning of the process. It was observed that when the Fe-enriched phases Fe3Si and Fe_5Si_3 were formed, the coating adhered well to the substrate. On the contrary, the formation of FeSi and $FeSi_2$ Si-enriched phases, led to coating spallation. Fig. 44 depicts the formation of different silicides for various temperatures (a) and deposition times (b). The authors concluded that 723–773 K is the optimum temperature range to form adherent coatings. Coatings with good adhesion and homogeneity were also deposited on previously aluminized and heat-treated samples, indicating that inward Si diffusion is promoted by the presence of Al.

Fig. 44. Silicide formation on AISI304 stainless steel by Pérez et al. for different temperatures (a) and deposition times (b). Adapted from ref. [206].

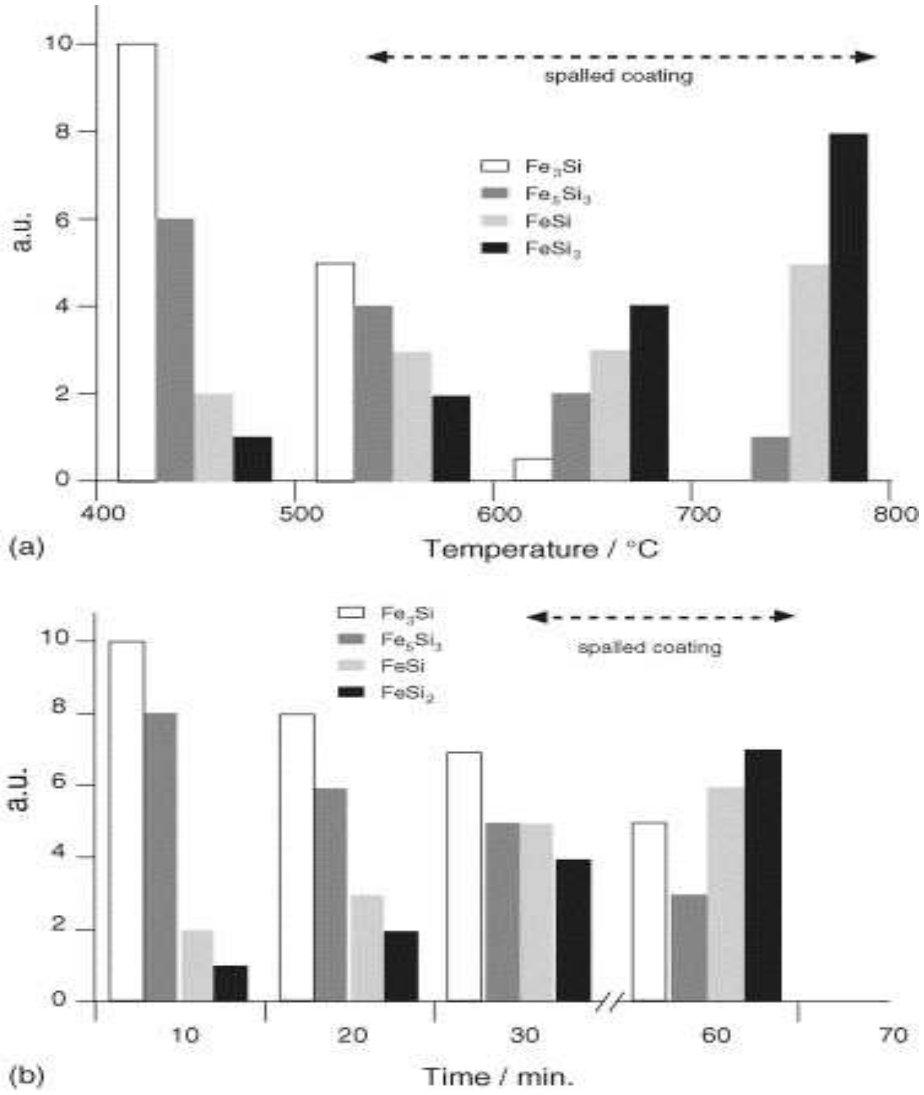

A 1243 K, high temperature siliconization of Armco iron was performed in ref. [183]. The bed consisted of Al_2O_3 and metallurgical grade FeSi and Si powders and was fluidized by a gas mixture of N_2 + 10% H_2. NH_4Cl was used as activator. A surface layer consisting of a solid solution of Si in α-Fe was produced. The Si-content of the layer was about 3.5 wt.%. This value did not change significantly for the coatings formed at 2, 4 and 6 h treatment indicating that, at this temperature, an equilibrium condition at the interface is maintained.

Moreover, since the coating thickness increased as a square root of time, it was concluded that the siliconizing rate is controlled by the inward diffusion of Si. The Vickers microhardness values obtained were in the range of 180 (HV0.025) as expected for Si-coatings on iron.

4.1.2.6. Al-coatings

The aluminization of iron, nickel, Fe-alloys, Ni-alloys and copper by high and low FBCVD processes has extensively been studied, due to the importance of these coatings against corrosion and hot corrosion and temperature applications.

In high-temperature applications, the melting point of aluminium restricts its use as a donor material. Therefore, FeAl or NiAl alloys have been used which are not readily available in powder form. Kinkel et al. aluminized Ni, Armco iron, and a nickel-based alloy at 1273 K using a bed consisting of alumina and FeAl, which was fluidized by Ar [183]. NH_4Cl was used as activator. The coating formed on Armco iron, consisted of two phases. The thickness of the outer FeNi phase varied from 36 to 25 μm and the one of inner Fe_3Al from 155 to 203 μm after 2 and 6 h treatment time, respectively. The deposition rate was 82 $\mu m/h^{1/2}$. The hardness of the outer phase is in the range of 450 HV; a corrosion test performed at 1173 K with a Na_2SO_4/V_2O_5 100:1 mixture for 24 h showed that the corrosion resistance increased over 16-fold after the coating process [207]. In the same study, it was shown that for nickel aluminization, the coating consisted of two phases: an external dark grey and an internal light grey phase as depicted in Fig. 45. The phases were identified by EPMA measurements as stoichiometric NiAl and solid solution of Al in Ni. On the contrary, on a NiCr23Fe substrate, a single NiAl phase coating was formed after 2 h at 1273 K. In the case of nickel, the hardness of the coating near the surface reached a value of 600 HV approximately and is generally brittle. Deposition rates were estimated at 30 $\mu m/h^{1/2}$ for nickel and 21 $\mu m/h^{1/2}$ for NiCr23Fe substrate at 1273 K. These results indicate that, as the coating growth was found analogous to the square root of time for both Ni and NiCr23Fe alloy, the rate-determining step is diffusion and not surface reaction. Moreover, the alloying elements for NiCr23Fe alloy retard the inward Al diffusion.

Fig. 45. Aluminide coatings on nickel for various treatment times at 1273 K and FeAl donor with 52 at% Al. The changes of the two different phases with time is illustrated. Adapted from ref. [207].

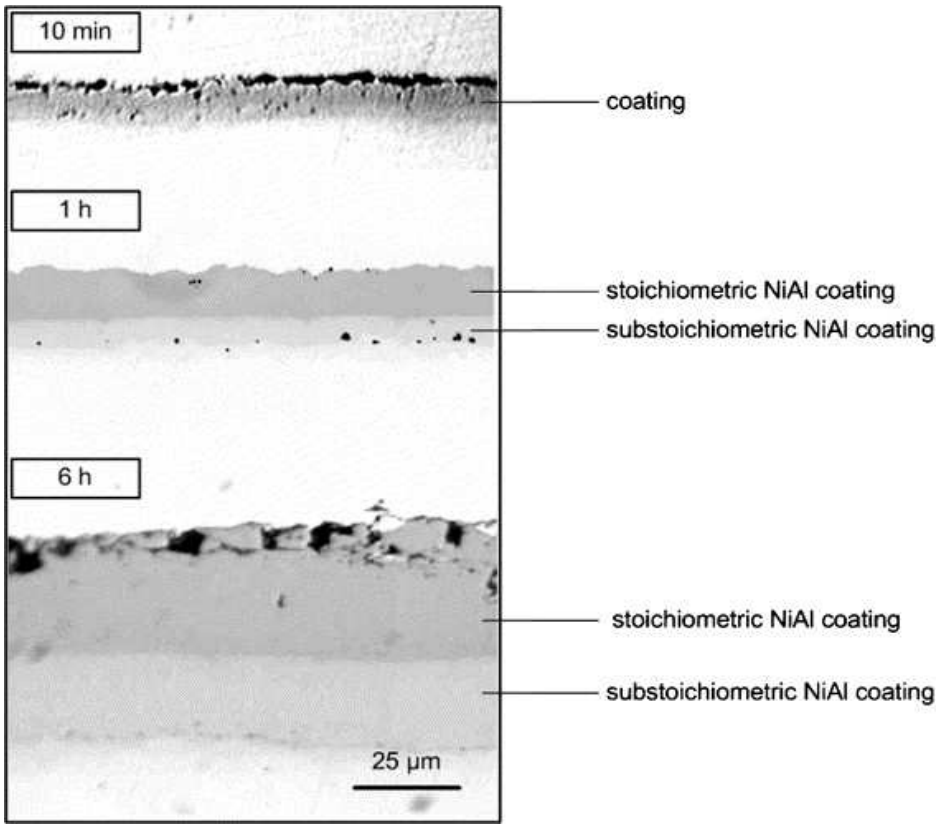

Based on the hypothesis that the surface of the sample is in thermodynamic equilibrium with the donor powder, Voudouris et al. [208] and Christoglou et al. [209] elaborated simplified process models for nickel and iron aluminization, respectively. The models were based on the diffusion equations and mass balances. With the help of these models, the coating growth rate, morphology and aluminium concentration profiles can be calculated with satisfactory agreement with experimental observed values. The comparison between the calculated and the measured by EPMA aluminium distributions for 4 and 6 h are presented in Fig. 46, indicating the good agreement between predicted and experimental values.

Fig. 46. Comparison between experimental and calculated values for aluminizing at 1273 K, FeAl donor 52 at% Al and NH_4Cl activator for 4 h (a) and for 6 h (b) treatments. Adapted from refs. [208] and [209].

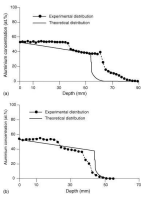

It is stated by Reynoldson that the ability to impart several metals as well as oxicarbonitrides at the surface of metal substrates at temperatures below 873 K by the FBCVD process, allows a totally new range of surface treatments to be applied in the metal working industry [210]. In this direction, the formation of aluminide coatings with low temperature FBCVD was extensively studied by the group of Pérez et al. [194], [195], [211], [212], [213] and [214] as well as in refs. [215] and [216]. The low-temperature processes have the advantage that aluminium powders can be used as donors as the temperatures are usually well below 893 K. In the case of Ni-aluminization, the rate-determining step is the exothermal reaction of Ni and Al to form NiAl. After the first 60 min of the process the rate-determining step becomes the inward diffusion of Al [215] and [216]. The micrograph of an Al-coating formed on an AISI 304 stainless steel is depicted in Fig. 47 together with the microanalysis results at different points and the Al, Cr, Fe, Ni distributions.

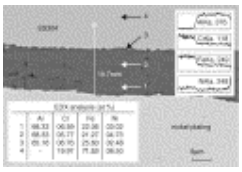 Display Full Size version of this image (44K)

Fig. 47. Back-scattered electron micrograph of an Al coating on AISI 304 stainless steel treated at 873 K for 1 h [215].

The above findings are in fair agreement with ref. [193]. However, in the case of 304 stainless steel aluminized at 798 K for 2 h 45 min in a bed consisting of Al powder and fluidized by a gas mixture of 89% Ar + 10% H_2 + 1% HCl, the formation of $FeAl_3$, Ni_2Al_3 and $AlFe4_3$ phases was attributed to the inward Al diffusion and the outward Fe and Ni diffusion. In this case, at the initial stages of deposition, Al_5Fe_2 intermetallic is formed together with an austenite to ferrite transformation due to Cr diffusion [210]. Beyond the increase of the coating thickness and assuming stress relief, the subsequent heat treatment in Ar atmospheres of aluminized AISI 304 stainless steel treated as above, significantly improved the corrosion

resistance due to the formation of sub-stoichiometric β-NiAl [210]. More specifically, the service life was extended for more than 200 h under continuous and 100 h under discontinuous oxidation conditions, respectively. In the first case, incomplete θ- to α-Al_2O_3 transformation, as in the latter one alumina scales and enrichment of Cr and Fe in the underlying scale has been observed to occur. However, outward aluminium diffusion may be able to re-heal the coating [212].

High temperature Knudsen cell mass spectrometry was used to study the reactions of $Al_{(s)}$ with $HCl_{(g)}$ and $HCl_{(g)} + H_{2(g)}$ in the temperature range of 400–900 K to perform the chemical modeling of aluminium coating on copper by FBCVD [217]. The measured pressures of $AlCl_3$ and AlCl by this device, were in a good agreement with the values predicted by thermochemical calculation in the temperature range 650–900 K. The authors conclude that AlCl gas is an important precursor for the coating formation. Under the determined most favorable conditions, a thin aluminium coating was formed on a copper wire treated for 30 min in a bed of Al at 1137 K fluidized by a 0.12% HCl, 7% H_2 gas mixture, the rest being Ar. At the initial stages of aluminium deposition, copper is expected to diffuse into the coating to form a solid solution first followed by the $CuAl_2$ phase. This is due to the fact that the diffusion of Cu in Al is 100 times faster than the diffusion of Al in Cu. If the temperature increases above 1198 K, the reaction between Cu and Al becomes very fast and may result in the production of Kirkendall effects and therefore porosity in the diffusion zone.

As a conclusion to this part, it is recalled that the combination of conventional fluidized bed technology with standard chemical vapor deposition has proven to be an effective method for the formation of wear as well as for corrosion resistant coatings on metallic pieces. The numerous advantages of this technique have led to broad spectrum of coatings containing Ti, Cr, V, B, Si and Al being obtained at temperatures between 700 and 1300 K. The presentation of the processing conditions and the materials obtained for each of these families revealed that such processes are technologically and economically promising, although much work is yet to be done to ensure industrial implementation.

4.2. Fabrication of powders by CVD

Historically, the first identified industrial processes for particles manufacture by CVD techniques correspond to carbonyl iron powder (CIP) and carbon black (CB) production. CIP was invented at BASF some 80 years ago and corresponds to the thermal decomposition of

iron pentacarbonyl [$Fe(CO)_5$]. Decomposition occurs in cavity decomposers and yields spherical, 1–10 μm diameter iron particles [218]. The decomposer is a pipe, externally heated by electricity or gas, into which iron pentacarbonyl vapors are admitted from the top. The [$Fe(CO)_5$] decomposes not on the wall, which is heated to $T > 300$ °C, but on iron particles circulating in the gas stream. Carbon and oxygen produced by the decomposition of carbon monoxide are incorporated in the iron. Addition of ammonia reduces the carbon and oxygen content but leads to incorporation of nitrogen in the iron particles. The cavity decomposer, invented by BASF in 1924, has not changed fundamentally. Various practices have been adopted to control the product, above all its particle size. Fine particles are obtained by admitting oil vapor into the decomposer, by diluting the carbonyl vapor with recycled carbon monoxide gas or by applying a temperature gradient from the top to the bottom of the decomposer. Fine particles result if the rate of flow of iron pentacarbonyl is high; larger ones, if the rate is low.

Carbon black are formed either by pyrolysis or by partial combustion of carbon-containing vapors (acetylene, natural gas, oil, …). The first processes were developed in the USA during the 19th century. Mixtures of gaseous or liquid hydrocarbons, which can be vaporized represent the raw materials preferable for the industrial production of carbon black. In general, the processes for CB production are divided into two groups: those employing partial combustion and those based on pure pyrolysis. This nomenclature is somewhat misleading insofar as the CB resulting from the partial combustion process is also formed by pyrolysis. The two types of processes differ in that air is used in the one to burn part of the feedstock, thus producing the energy required to carry out the pyrolysis, whereas in the other heat is externally generated and introduced into the process. Generally speaking, very narrow specifications (BET surface area, particle diameter, …) of CB can be achieved by adjusting the operating parameters. According to the carbon source and to the operating conditions, CB will have the following characteristics: C-content 80–99.5%, particles diameter 5–500 nm and specific surface area 10–1000 m^2/g.

In situ born unwanted parasitic powders during conventional silicon CVD from SiH_4 or chlorosilanes is also an important aspect of powder synthesis by CVD. This phenomenon has been extensively studied for several decades, because particle contamination is one of the major limitations for the efficient processing of semiconductors on wafers, especially during silicon epitaxy. For example, during fabrication of features smaller than 1 μm, as much as

75% of the yield loss, i.e. non-appropriate wafers, can be attributed to particle contamination [219]. Since feature sizes lower than 1 μm are significant in microelectronics, and because the intrinsic phenomena involved remain incompletely understood, the control of contamination due to in situ born submicron particles is an issue of major importance for future years [220].

Numerous experimental and modeling studies have been performed since the seventies, on particle contamination of silicon LPCVD processes from SiH_4 ([220] and references therein), $SiHCl_3$ [219] or mixtures of SiH_4 and oxygen [221]. The mechanisms most often recognized in particle formation first involve homogeneous chemical reactions leading to the formation of high-order silicon hydride species giving rise to solid particles through coagulation and deposition phenomena [220]. Various modeling approaches have been developed starting from the classical nucleation theory from supersaturated silicon vapor [222] to the complex general dynamic equation (GDE) approach, simultaneously considering non-isothermal gas reactive transport and particle nucleation, growth, condensation and coagulation. A difficulty in such studies is to identify and apply a convenient kinetic model for particle formation from the gas phase. Most authors use a detailed mechanism for homogeneous SiH_4 decomposition and hydride formation, and arbitrarily assume that compounds containing at least 10 silicon atoms are solid particles [219] and [220]. Another difficulty concerns the validation of models, since experimental data available are incomplete, occulting information on either aerosol particle size or concentration or composition [220].

Guidelines for minimizing particle contamination in CVD reactors have been deduced from simulation results. Pressure is recognized to have the most dramatic effect on particle formation, especially when higher than 80 Pa as illustrated in Fig. 48, adapted from ref. [221]. The presence of non-isothermal regions in the reactive chamber also seems to be a key factor in the contamination of CVD equipment [223] as do recirculation zones (vortices), where the gas residence time could be greater [219].

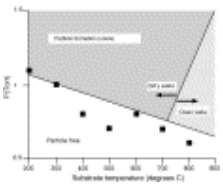
Display Full Size version of this image (27K)

Fig. 48. Pressure/temperature diagram of particle formation regime in the case of silicon oxide LPCVD from SiH_4/O_2. Adapted from ref. [221].

In order to control the synthesis of powders, various CVD processes have been specifically and successfully developed, including thermal, laser and plasma CVD [131]. These processing routes involving gaseous precursors are gaining popularity over wet chemistry or classical mechanical milling because they are in general cleaner, more energy-effective and environmentally sounder [224]. Indeed, the powders formed are of higher purity due to the use of gaseous reactants, which can be easily purified by distillation, while preparation of metallic, oxide and non-oxide powders is most often highly versatile by controlling the reacting atmosphere [225].

Homogeneous thermal CVD is certainly the most frequently met gas phase process for the synthesis of micrometric and more recently nanometric powders [226] and [227]. The principle of this technique is quite simple: gaseous precursors are directly injected into an empty cylindrical tube conveniently heated by electrical furnaces. Homogeneous nucleation leads to formation of seeds in the gas phase, which are then able to grow by classical heterogeneous CVD or coagulation mechanisms. Their final size will depend on their residence time in the reactive zone and on the local operating conditions prevailing in the reactor chamber, such as temperature, pressure, gas velocity or precursor mass fractions.

Homogeneous thermal CVD has most often been used to produce oxide powders, such as TiO_2, ZrO_2, SiO_2, Al_2O_3 or SiO_2–Al_2O_3 ([224] and [226] {Nakaso, 2003 #1086 [228]) Moravec, 1997 #2165}, other types of ceramic powders, such as SiC, Si_3N_4, AlN [225], [229] and [230], inorganic fullerene like nanoparticles (TiS_2, MoS_2) [231] and [232], semiconductor nanomaterials, such as GaN nanoparticles [233], copper nanoparticles [234] and composite particles [131] and [235]. It is worth noting that all these studies involve laboratory scale equipments, and consequently the productivity in terms of weight of synthesized particles per unit time is rarely mentioned. Moreover, when using liquid precursors, droplets are most often generated through a syringe pump; the scale-up of such a system to go towards high productivities is not easy.

As a characteristic example of homogeneous thermal CVD for powder synthesis, the equipment used by Nakaso et al. to produce titania nanoparticles is schematically presented in Fig. 49 [226]. The liquid precursors (titanium tetraisopropoxide TTIP or $TiCl_4$) are fed into an evaporator through an infusion pump. This liquid is evaporated into the nitrogen carrier gas and then introduced into a 13 mm diameter vertical reactor. When using $TiCl_4$, oxygen is added to the reactive gas. A four-zone electrical furnace allows convenient monitoring of the

thermal profile along the reactor axis. Temperature profiles ranging from 373 to 1073 K are organized. The produced nanoparticles are collected directly on a TEM grid by means of a corona discharge sampler. The chemical composition of nanoparticles at the exit of the reactor was investigated using FT-IR. Depending on the process parameters and on the materials processed, the major drawbacks of this technique can be the difficulty to control particle size distribution, and the formation of stable agglomerates. Fig. 50 presents TEM images of some TiO_2 nanoparticles prepared by these authors showing that both the precursor nature and the maximum temperature in the reactor play an important role in the final characteristics of the particles [226]. Whatever the particles processed, the exact mechanisms of action of each operating parameter are currently not well understood.

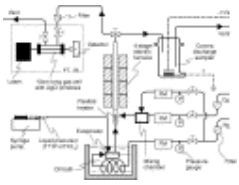
Display Full Size version of this image (47K)

Fig. 49. Experimental apparatus used for the generation of TiO_2 nanoparticles by thermal CVD. Adapted from ref. [226].

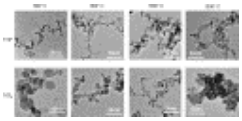
Display Full Size version of this image (88K)

Fig. 50. TEM images of TiO_2 nanoparticles from TTIP and $TiCl_4$ vapors under various reaction temperatures. After ref. [226].

In order to limit agglomeration and even to reduce average particle size, unipolar charges have been applied in the CVD chamber using a corona discharge ionizer [236]. Electrospray (ES) assisted CVD has also been developed for that purpose, consisting in unipolarly charging a spray of precursor droplets then evaporating them to form charged non-agglomerated nanoparticles [237] and [238]. Fig. 51 presents SEM images of titania nanoparticles generated using (a) ES-CVD and (b) conventional homogeneous CVD [237]. The nanoparticles generated are clearly in the form of aggregates in the conventional method whereas they are converted into isolated and non-agglomerated nanoparticles using ES-CVD.

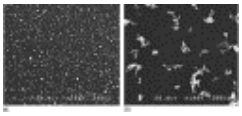 Display Full Size version of this image (68K)

Fig. 51. SEM images of titania nanoparticles generated by (a) ES-CVD and (b) conventional CVD. After ref. [237].

The mechanisms involved in the two routes: (a) homogeneous thermal CVD and (b) ES-CVD according to Nakaso et al. are schematically presented in Fig. 52 [237]. Unipolar ions are produced during evaporation of charged droplets in the ES, and on one hand these ions probably act as seed nuclei, increasing nucleation, and on the other hand, they are attached to the nanoparticles produced, thus lowering agglomeration through repulsive forces.

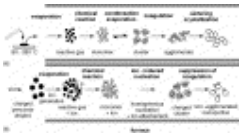 Display Full Size version of this image (69K)

Fig. 52. Particle formation mechanisms in (a) homogeneous thermal CVD and (b) ES-CVD. Adapted from ref. [237].

Moravec et al. [16] used an horizontal tube flow reactor, 2.7 cm in i.d. and 55 cm in length, to synthesize mixed alumina–silica particles, by simultaneous decomposition of aluminium tri sec butoxide (ATBO) and tetraethylorthosilicate (TEOS) in presence of air. The reaction temperature was of 773 K and the residence time in the reactor of 16.5 s. Samples of particles were collected on Millipore filters or deposited onto Cu grids. Particle production was in the range 10^6–8×10^6 cm^{-3}. It was higher from the mixture of precursors than from the sole ATBO but it was several times lower than from decomposition of pure TEOS. Depending on reactor temperature and precursor concentration, it was possible to synthesize: (i) alumina particles with intermixture of silica, (ii) alumina particles coated by a layer or nodules of silica and (iii) mixtures of particles of various compositions. Particles were partly crystalline and their diameter varied from several tens to several hundreds of nanometers. Numerous agglomerates of various shapes and sizes were present.

Porous alumina films made of homogeneously born nanoparticles have been synthesized by a hybrid process combining gas-to-particle conversion and heterogeneous CVD [239]. In this work, the formation of nanoparticles aggregates is desirable bcause deposition of these structures will lead to a highly porous microstructure. Alumina nanoparticles were formed at

atmospheric pressure in a vertical quartz reactor, 4.7 cm in i.d. and 1 m in length, surrounded by a three zone furnace. Within the quartz tube, nanoparticle deposition occured on planar substrates via thermophoresis[4] onto a vertically adjustable water-cooled stage maintained at 293 K. The precursor was aluminium acetylacetonate $Al(acac)_3$ under solid powder form. It was placed in an externally heated fixed bed sublimator. Ar and O_2 were the inlet gases. Reactor temperature was varied between 773 and 1273 K and some samples were annealed between 523 and 1173 K. Alumina films were only formed at temperature equal or greater than 973 K. They were composed of aggregates of primary particle size of about 18 nm. Below this temperature, nanoparticles were highly carbon contaminated. The deposition rate was of roughly 0.5 μm/min. It increased with temperature and decreased with processing time, due to an higher insulation with the water cooled stage. After annealing at 1173 K for 24 h, the specific surface area of the films increased dramatically from 60 to 185 m^2/g. The authors attributed this evolution to carbon contamination removal.

The homogeneous CVD process has also allowed the synthesis of CNTs by simultaneously introducing the gaseous catalyst precursor and the carbon source into the reactor. This homogenous route is also called “floating catalyst method”. The basic principle is to decompose a carbon source on nanometric metallic particles (generally Fe, Co or Ni) in order to obtain CNTs, the catalytic particles being formed directly in the reactor. The typical reactor used in this technique is a quartz tube placed in an oven where the gaseous feed, containing the metal precursor, the carbon source, hydrogen and carrier gases (N_2, Ar or He) are introduced. The first zone of the reactor is kept at a lower temperature and the second zone, where the formation of tubes occurs, is heated to 1073–1473 K. The metal precursor is generally a metallorganic compound: either a zero-valent carbonyl compound as $[Fe(CO)_5]$ [240] or a metallocene [241] and [242], that is decomposed in the first zone of the reactor to generate the nanometric metallic particles which can catalyse nanotubes growth. In the second part of the reactor, the carbon source is decomposed to atomic carbon, which then is responsible for the formation of nanotubes.

This technique is quite flexible and both single walled-nanotubes [243] and multi-walled nanotubes [244] have been produced depending on the carbon feedstock gas; it has also been exploited since some years in the production of vapor-grown carbon nanofibers [245]. Its main drawback is the difficulty to control the nucleation and growth of the metal nanoparticles and hence the CNTs formation is often accompanied by the production of

undesired by-products, such as amorphous carbon, carbon filaments or graphite covered particles. In order to finely tune this process and obtain selectively CNTs there are many parameters that have to be controlled, such as the choice of the carbon source, the reaction temperature that can affect the morphology and structure of the nanotubes, the metallorganic precursor to the carbon source ratio (for lower values SWNT production is obtained [242]), the reaction time and the composition of the inlet gaseous feed. Finally, it is worth noting that only small productions have been achieved and the scale-up towards industrial exploitation seems difficult because of the large number of parameters that have to be considered. Particularly, a better productivity will imply an increase in the quantity of metallorganic compound send in the reactor, and such an increase will produce big particles inactive for CNTs growth. An additional problem inherent to this process is the possibility of reactor plugging by deposition of metallic nanoparticles on the reactor walls followed by carbon deposition.

A significant breakthrough concerning this technique could be the HiPco™ process developed by Smalley et al., to produce SWNT [246]. This gas phase catalytic reaction uses carbon monoxide and an industrial gas to produce from [$Fe(CO)_5$] the SWNT material that is claimed to be relatively free of by-products.

Laser induced (LI) CVD was developed in the 1970s for the synthesis of ultrafine ceramic powders (Si, SiC, Si_3N_4). Owing to its advantages: clean, free of agglomerates, large output and continuous running operation; LICVD has become an attractive solution for producing nanosized materials. This method is based on the ability of gaseous reactive molecules to induce chemical reactions, such as thermo- or, laser dissociation for a specific laser wavelength [247]. Laser intensity, chamber pressure, temperature, inlet gas flow rate and composition are the main experimental parameters influencing the morphological characteristics of the particles. According to Wang et al. [247], the laser intensity has the greatest influence on the powder preparation process and the final particle size. Besling et al. [248] have produced an aerosol of nanosized ceramic particles homogeneously nucleated by laser radiation; these particles are deposited on a plane substrate by thermophoresis, and simultaneously densified by heterogeneous CVD in order to form layers of controlled porosity. Nanosized silicon [249] for optoelectronic applications and SiCN powders [248] are examples of materials prepared by this process.

Reactive thermal plasma enhanced CVD processes consist in injecting gaseous precursors into a plasma so as the species react with the plasma gas, or a quenching gas in the condensation region of the reactor. High cooling rates, due to the quenching gas or the fast expansion of plasma jet, allow homogeneous nucleation [250]. According to Costa et al. [251], this technique is interesting because the size, composition and crystallinity of the particles obtained can be controlled by the technological parameters of the discharge (pressure, radio frequency power and its modulation and gas composition). This technology is used for sintering applications, essentially of ceramics as well as for the reinforcement of alloys [250] and [251], for tribological applications in producing BN particles [251] or to form high surface SiN catalysis supports [252]. Liu et al. have produced Fe_2O_3 nanoparticles from ferrocene for gas sensors applications [253]. Nanosized Mo powders have been synthesized by the microwave plasma CVD method [254].

According to Zhu and Yan [229], expensive apparatus, presence of hard agglomerates as well as the occasional appearance of hollow particles are drawbacks for both LICVD and reactive thermal plasma enhanced CVD. Homogeneous thermal CVD offers unique advantages over them, especially lower cost equipment, easier control of process parameters and easier scale-up towards industrial conditions [229].

For each of these technologies, the reactor tube can be horizontal or vertical, this latter solution avoiding non-uniform effects of gravity on the particle flow [5]. Electrostatic filters are generally placed at the exit of the reactor to collect the particles formed. However, reaching high efficiencies in terms of nanoparticle collection still constitutes a main challenge.

Thus, production of powders by CVD technologies seems today to be conveniently mastered at the lab-scale. The range of materials studied is quite large, and includes pure silicon, numerous oxides and ceramics. However, it is worth mentioning that industrialization of the whole processes could be limited in the future by the following two common intrinsic drawbacks: (i) particles generally adhere to the reactor walls and can even plug them, their collection is then difficult and (ii) the main thermal transfer promoter being gaseous convection, thermal profiles in such dilute conditions are strong in the radial direction, inducing heterogeneities in particle characteristics; these thermal heterogeneities increase with the increase of reactor tube diameter.

5. Conclusions

Combination of CVD and powders is a relatively new and interdisciplinary field of research and technology. The present review has shown that, within this field, fluidized beds are a convenient medium to efficiently and economically produce or modify particulate materials by CVD. Indeed, in the most conventional cases, precursor conversion and deposit uniformity are excellent, design, build-up and scale-up are easy, and equipment costs quite low. Very high productivity can even be reached by operating in continuous mode. In addition, the efficient thermal and mass transfers prevailing in a fluidized bed allow selective processes to occur in particular cases.

When deposition takes place on powders in a FB, surface reactions often tend to be very intense, primarily due to the high surface-to-volume ratio of the substrate. In such cases, mass-transport often controls the process but the vigorous mixing of particles ensures uniform deposition.

One major consideration when coating or producing by CVD particulate-based materials is the ability of the latter to be fluidized. Although for some specific applications, such as production of catalytic materials, the powders belong to Geldart's class A or B categories, and can therefore be easily fluidized, most powders of interest in advanced materials usually fall into Geldart's class C category. These powders are very cohesive and difficult to handle, to fluidize and to process in a non-agglomerated form. High aspect ratios, usually met in nanomaterials, such as CNTs further aggravate handling and sometimes fluidization, and most fine powders are frequently handled, coated or modified in an agglomerated form. Thus, to efficiently design a FB-CVD process, the constraints linked to fluidization have to be taken into account. Spouted beds, circulating beds operating in turbulent and fast-transport regimes or vibro-fluidized beds are possible alternatives to classical fluidised-bed reactors.

Finally, the classical constraints associated with CVD processes like side deposition, clogging of the lines, homogeneous nucleation or precursor handling, will have to be carefully integrated for the rational design of the FB-CVD reactor but also of the final process. It is clear that such an integrated approach would have to be interdisciplinary and inputs from chemistry, chemical engineering and materials science would have to be considered simultaneously.

The potential of the CVD technology devoted to powders is high since it covers a wide range of operations, including: (i) surface treatment, (ii) manufacture of powders and (iii) coatings. As far as applications are concerned the FBCVD processes have been used for manufacturing coated nuclear fuel particles, catalytic materials, wear, oxidation and temperature resistant materials, materials for microelectronic or photovoltaic applications, powders and more recently nanomaterials, such as CNTs, or metallic or oxide nanoparticles. It is worth noting that when the material to coat is immersed in the FB, this allows production of different wear, oxidation and corrosion resistant coatings on metals. The coating formation mechanisms are probably similar to those occurring in conventional CVD and pack bed methods. Such processes present the advantages of being simple and relatively cheap. As the parts can be charged and withdrawn while the furnace is at the treating temperature, the process can be integrated into the heat treatment cycles.

Although it was the growth of the nuclear power industry in the 1960s that provided the drive for the development of fluidized-bed reactors to coat large volumes of powders, there are not yet any major industrial processes operating with such technology. The current applications of FB-CVD concern the manufacture of advanced engineering materials and it is worth mentioning that an extensive patent literature exists on the subject and that some SME's are already using this technology to manufacture custom powders. It can be reasonably expected that, in the near future nanotechnologies will contribute to intensifying the industrial development of powder treatment by FBCVD and the other CVD processes mentioned in this review.

Acknowledgements

We are indebted to Christian Bonzom of the National Institute of Applied Sciences (INSA), Toulouse, for the illustrations and to Peter Winterton of the Paul Sabatier University, Toulouse, for help with the English language.

References

C.K. Gupta and D. Sathiyamoorthy, Fluid Bed Technology in Materials Processing, CRC Press, Boca Raton, FL (1999).

I. Sanchez, G. Flamant, D. Gauthier, R. Flamand, J.M. Badie and G. Mazza, *Powder Technol.* 120 (2001), pp. 134–140.

K.P. de Jong, *Curr. Opin. Solid State Mater. Sci.* 4 (1999), pp. 55–62.

D. Kunii and O. Levenspiel, Fluidization Engineering, Butterworth-Heinemann, Newton, MA (1991).

M. Monthioux, P. Serp, E. Flahaut, C. Laurent, A. Peigney, M. Razafinimanana, W. Bacsa and J.-M. Broto In: B. Bhushan, Editor, *Nanotechnology Handbook*, Springer-Verlag, Heidelberg (2004), pp. 39–98.

P. Serp, P. Kalck and R. Feurer, *Chem. Rev.* 102 (2002), pp. 3085–3128.

A. Gleizes, A. Fernandes and J. Ghys-Dexpert, *Electrochem. Soc.* PV2003-08 (2003), pp. 565–571.

R.E. Toth, Patent US6372346 B1, 2002.

C. Vahlas, F. Juarez, R. Feurer, P. Serp and B. Caussat, *Adv. Mater. CVD* 8 (2002), pp. 127–144. Cited By in Scopus (0)

D. Geldart, Gas Fluidization Technology, John Wiley & Sons, Chichester, New York, Brisbane, Toronto, Singapore (1986).

L.-S. Fan, Gas–liquid–solid Fluidization Engineering, Butterworth Publishers, Stoneham, MA (1989).

In: J.F. Davidson, R. Clift and D. Harrison, Editors, *Fluidization*, Academic Press, London (1985).

D. Geldart, *Powder Technol.* 7 (1973), pp. 285–290.

T. Kojima, H. Hiroha, K. Iwata and T. Furusawa, *Int. Chem. Eng.* 32 (1992), pp. 739–748.

W. Heit, H. Huschka, W. Rind and G.G. Kaiser, *Nucl. Technol.* 69 (1985), pp. 44–54.

P. Moravec, J. Smolík and V.V. Levdansky, *Powder Technol.* 153 (2005), pp. 159–165.

B. Golman and K. Shinohara, *Trans. IChem. E* 77 (1999), pp. 39–46.

C. Li and B. Hua, *Thin Solid Films* 310 (1997), pp. 238–243.

A. Sherman, V. Arrietta, Patent WO9730797, 1997.

R. Hong and H. Li, *Prog. Nat. Sci.* 6 (1996), pp. 269–276.

A. Sherman and V. Arrietta In: T.S. Sudarshan, W. Reitz and J.J. Stiglich, Editors, *International Conference on Surface Modification Technologies, Minerals, Metals & Materials Society* (1996), pp. 291–299.

J.J. Stiglich, S. Raghunathan, A.J. Sherman and R.J. Dowding In: T.S. Sudarshan and M. Jeandin, Editors, *Surface Modification Technologies, vol. VIII*, Institute of Materials, Nice, France (1995), pp. 498–529.

S. Morooka, T. Okubo and K. Kusakabe, *Powder Technol.* 63 (1990), pp. 105–112.

O. Molerus, *Powder Technol.* 33 (1982), pp. 81–87.

W.R.A. Goossens, *Powder Technol.* 98 (1998), pp. 48–53.

R.J. Dry, M.R. Judd and T. Shingles, *Powder Technol.* 34 (1983), pp. 213–223.

M.F. Llop and N. Jand, *Chem. Eng. J.* 95 (2003), pp. 25–31.

J.R.R. Ruvalcaba, B. Caussat, M. Hemati and J.P. Couderc, *Can. J. Chem. Eng.* 77 (1999), pp. 35–44.

In: M.E. Fayed and L. Otten, Editors, *Handbook of Powder Science and Technology*, Chapman & Hall, New York, NY (1997).

S. Morooka, A. Kobata and K. Kusakabe, *AlChE Symp. Ser. No. 281* 87 (1991), pp. 32–37.

F. Juarez, A. Castillo, B. Pieraggi and C. Vahlas, *J. Phys. IV* 11 (2001), pp. 1117–1123.

B. Caussat, F. Juarez and C. Vahlas, *Powder Technol.* 165 (2002), pp. 63–70.

B. Caussat, M. Hemati and J.P. Couderc, *Chem. Eng. Sci.* 50 (1995), pp. 3615–3624.

N. Rohatgi, Silicon production in a fluidized reactor: final report, Jet Propulsion Laboratory, D.O.E., 1986, pp. 1012–1123.

F. Maury, L. Gueroudji and C. Vahlas, *Surf. Coat. Technol.* 86–87 (1996), pp. 316–324.

F. Maury, *J. Phys. IV* C5 (1995), pp. 449–463.

P. O'Brien, N.L. Pickett and D.J. Otway, *Chem. Vap. Deposition* 8 (2002), pp. 237–249.

M.J. Karches, *Verfahrenstechnik* 719 (2002), pp. 1–114.

A. Sanjurjo, B.J. Wood, K.H. Lau, G.T. Tong, D.K. Choi, M.C.H. McKube and H.K. Song, *Surf. Coat. Technol.* 49 (1991), pp. 103–109.

A. Sanjurjo, B.J. Wood, K.H. Lau, G.T. Tong, D.K. Choi, M.H. McKubre and H.K. Song, *Surf. Coat. Technol.* 49 (1991), pp. 110–115.

K.B. Mathur and P.E. Gishler, *AIChE J.* 1 (1955), pp. 157–164.

F. Juarez, Ph.D. Thesis, Accession number 1974, Institut National Polytechnique, Toulouse, France, 2002.

K.B. Mathur and N. Epstein, *Can. J. Chem. Eng.* 52 (1974), pp. 129–144. M. Olazar, *J. Chem. Technol. Biotechnol.* 76 (2001), pp. 469–476.

N.M. Rooney and D. Harrison, *Powder Technol.* 9 (1974), pp. 227–230. A. Nagarkatti and A. Chatterjee, *Can. J. Chem. Eng.* 52 (1974), pp. 185–195.

T. Kawaguchi, M. Sakamoto, T. Tanaka and Y. Tsuji, *Powder Technol.* 109 (2000), pp. 3–12.

K. Ijichi, Y. Uemura and Y. Hatate, *J. Chem. Eng. Jpn.* 33 (2000), pp. 526–528.

M. Olazar, R. Aguado and J. Bilbao, *AIChE J.* 46 (2000), pp. 1025–1033. K.G. Marnasidou, S.S. Voutetakis, G.J. Tjatjopoulos and I.A. Vasalos, Chemical reaction engineering for the 21st Century, *15th International Symposium on Chemical Reaction Engineering* Newport Beach, CA (1998), pp. 274–275.

F.J. Weinberg, T.G. Bartleet, F.B. Carleton and P. Rimbotti, *Combust. Flame* 72 (1988), pp. 235–239.

| M. Olazar, J.M. Arandes, G. Zabala, A.T. Aguayo and J. Bilbao, *Ind. Eng. Chem. Res.* 36 (1997), pp. 1637–1643.

M. Morstein, M. Karches, C. Bayer, D. Casanova and P.R.V. Rohr, *Chem. Vap. Deposition* 6 (2000), pp. 16–20.

M. Karches, C. Bayer and P.R.v. Rohr, *Surf. Coat. Technol.* 116–119 (1999), pp. 879–885.

H.S. Shin and D.G. Goodwin, *Mater. Lett.* 19 (1994), pp. 119–122.

M. Matsukata, H. Oh-hashi, T. Kojima, Y. Mitsuyoshi and K. Ueyama, *Chem. Eng. Sci.* 47 (1992), pp. 2963–2968.

M. Horio, R. Hanaoka and M. Tsukada, *Proc. Jpn. Symp. Plasma Chem.* 1 (1988), pp. 213–218.

F. Juarez, D. Monceau, D. Tetard, B. Pieraggi and C. Vahlas, *Surf. Coat. Technol.* 163–164 (2003), pp. 44–49.

N. Epstein and P.P. Chandnani, *Chem. Eng. Sci.* 42 (1987), pp. 2977–2981.

C. Xu and J. Zhu, *Chem. Eng. Sci.* 60 (2005), pp. 6529–6541.

S. Alavi and B. Caussat, *Powder Technol.* 157 (2005), pp. 114–120.

L.F. Hakim, J. Blackson, S.M. George and A.W. Weimer, *Chem. Vap. Deposition* 11 (2005), pp. 420–425.

Y. Mawatari, T. Koide, Y. Tatemoto, S. Uchida and K. Noda, *Powder Technol.* 123 (2002), pp. 69–74.

J.R. Wank, S.M. George and A.W. Weimer, *Powder Technol.* 121 (2001), pp. 195–204.

Y. Takao, M. Awano, Y. Kuwahara and Y. Murase, *Kona* 14 (1996), pp. 168–175.

J. Kim, G.Y. Han and C.H. Chung, *Thin Solid Films* 409 (2002), pp. 58–65.

I. Kimura, K. Ichiya, M. Ishii and N. Hotta, *J. Mater. Sci. Lett.* 8 (1989), pp. 303–304.

G. Rios, H. Gibert and J.P. Couderc, *Chem. Eng. J.* 13 (1977), pp. 101–109.

I. Kimura, N. Hotta, K. Ichiya and N. Saito, *Nippon Seramikkusu Kyokai Gakujutsu Ronbunshi* 97 (1989), pp. 1525–1529.

I. Kimura, N. Hotta, J.-I. Niwano and M. Tanaka, *Powder Technol.* 68 (1991), pp. 153–158.

J.A. Heaney and J.T. Keeley, *AIP Conf. Proc.* 301 (1994), pp. 1485–1493.

K. Shinohara, B. Golman, K. Watanabe and S. Chiba, *J. Chem. Eng. Jpn.* 30 (1997), pp. 514–519.

B. Golman, S. Ishino and K. Shinohara, *J. Chem. Eng. Jpn.* 30 (1997), pp. 1138–1140.

M.J. Rhodes, M. Sollaart and X.S. Wang, *Powder Technol.* 99 (1998), pp. 194–200.

S.H. Park and S.D. Kim, *Polym. Bull.* 41 (1998), pp. 479–486.

M. Karches, M. Morstein and R. von Rohr, *Surf. Coat. Technol.* 169–170 (2003), pp. 544–548.

F. Bretagnol, M. Tatoulian, E. Francke, F. Arefi-Khonsari and J. Amouroux, *Proceedings of 16th International Symposium on Plasma Chemistry* Taormina, Italy (2003), p. 526.

S. Guo, J. Zhao, W.V. Ooij and S. Datta, *Proceedings of 16th International Symposium on Plasma Chemistry* Taormina, Italy (2003), p. 533.

M. Theobald, P. Baclet, O. Legaie and J. Durand, *J. Vacuum Sci. Technol. A* 19 (2001), pp. 118–123.

M. Theobald, O. Legaie, P. Baclet and A. Nikroo, *Fusion Sci. Technol.* 41 (2002), pp. 238–241.

M. Theobald, J. Durand, P. Baclet and O. Legaie, *J. Vacuum Sci. Technol. A* 18 (2000), pp. 278–284.

K. Kato and C.Y. Wen, *Chem. Eng. Sci.* 24 (1969), pp. 1351–1369.

D. Kunii and O. Levenspiel, *Ind. Eng. Chem. Fundam.* 7 (1968), pp. 446–452.

B.A. Partridge and P.N. Rowe, *Trans. Inst. Chem. Eng.* 44 (1966), pp. T335–T349.

B. Caussat, M. Hemati and J.P. Couderc, *Powder Technol.* 101 (1999), pp. 43–55.

B. Caussat, M. Hémati and J.P. Couderc, *Chem. Eng. J.* 58 (1994), pp. 223–237.

T. Furusawa, T. Kojima and H. Hiroha, *Chem. Eng. Sci.* 43 (1988), pp. 2037–2042.

S.K. Iya, R.N. Flagella and F.S. Di Paolo, *J. Electrochem. Soc.* 129 (1982), pp. 1531–1535.

S. Lai, M.P. Dudukovic and A. Ramachandran, *Chem. Eng. Sci.* 41 (1986), pp. 633–641.

K.Y. Li, S.H. Peng and T.C. Ho, *AIChE Symp. Ser.* 85 (1989), pp. 77–82.

B. Caussat, M. Hemati and J.P. Couderc, *Chem. Eng. Sci.* 50 (1995), pp. 3625–3635.

C. Guenther, T. O'Brien and M. Syamlal, *Fourth International Conference on Multiphase Flow* New Orleans, LA (2001), pp. 1–12.

J.R. Grace and F. Taghipour, *Powder Technol.* 139 (2004), pp. 99–110.

H. Arastoopour, *Powder Technol.* 119 (2001), pp. 59–67.

L.R. Pozzo, J.R. Brandi, L.J. Giombi, A.M. Baltanás and E.A. Cassano, *Chem. Eng. Sci.* 60 (2005), pp. 2785–2794.

In: G. Ertl, H. Knözingzr and J. Weitkamp, Editors, *Preparation of Solid Catalysts*, X. Mu, U. Bartmann, G.M., G.W. Busser, U. Weckenmann, R. Fischer, M. Muhler, Appl. Catal. A 248 (2003) 85–95.

T.A. Kainulainen, M.K. Niemelä and A.O.I. Krause, *Catal. Lett.* 53 (1998), pp. 97–101.

P. Serp, L. Château, R. Feurer, A. Kiennemann and P. Kalck, *J. Mol. Catal.* 136 (1998), pp. 269–278.

T. Miyao, I. Shishikura, M. Matsuoka and M. Nagai, *Chem. Lett.* (1996), pp. 561–562.

K. Tomishige, K. Asakura and Y. Iwasawa, *J. Catal.* 157 (1995), pp. 472–481.

K. Tomishige, K. Asakura and Y. Iwasawa, *Chem. Lett.* (1994), pp. 235–238.

K. Tomishige, K. Asakura and Y. Iwasawa, *J. Catal.* 149 (1994), pp. 70–80.

K. Tomishige, K. Asakura and Y. Iwasawa, *Catal. Lett.* 20 (1993), pp. 15–22.

K. Tomishige, K. Asakura and Y. Iwasawa, *J. Chem. Soc., Chem. Commun.* (1993), pp. 184–185.

In: B. Cornils, W.H. Herrmann, R. Schlögl and C.-H.C.-H. Wong, Editors, *Catalysis from A to Z*, Wiley, Weinheim, Germany (2000).

K.P. Reddy and T.L. Brown, *J. Am. Chem. Soc.* 117 (1995), pp. 2845–2854.

A. Zecchina, E.E. Platero and C.O. Arean, *Inorg. Chem.* 27 (1988), pp. 102–106.

H.T. Gomes, P. Serp, P. Kalck, J.L. Figueiredo and J.L. Faria, *Top. Catal.* 33 (2005), pp. 59–68.

P. Serp, R. Feurer, R. Morancho and P. Kalck, *J. Catal.* 157 (1995), pp. 294–300. J.R.R. Ruvalcaba, B. Caussat, M. Hemati and J.P. Couderc, *Chem. Eng. J.* 73 (1999), pp. 61–66.

J.L. Figueiredo, M.F.R. Pereira, M.M.A. Freitas and J.J.M. Orfao, *Carbon* 37 (1999), pp. 1379–1389.

A.E. Aksoylu, J.L. Faria, M.F. Pereira, J.L. Figueiredo, P. Serp, J.C. Hierso, R. Feurer, Y. Kihn and P. Kalck, *Appl. Catal. A* 243 (2003), pp. 357–365.

P. Serp, R. Feurer, Y. Kihn, P. Kalck, J.L. Faria and J.L. Figueiredo, *J. Mater. Chem.* 11 (2001), pp. 1980–1981.

P. Serp, J.C. Hierso, R. Feurer, Y. Kihn, P. Kalck, J.L. Faria, A.E. Aksoylu, A.M. Pacheco and J.L. Figueiredo, *Carbon* 37 (1999), pp. 527–530.

P. Serp, unpublished.

P. Serp, R. Feurer, R. Morancho and P. Kalck, *J. Mol. Catal. A: Chem.* 101 (1995), pp. L107–L110.

P. Serp, J.-C. Hierso and P. Kalck, *Top. Organomet. Chem.* 9 (2005), pp. 147–171.

C. Vahlas, N.M. Hwang, F. Maury and L. Gueroudji, *Chem. Vap. Deposition* 4 (1998), pp. 96–99.

C. Vahlas, F. Maury and L. Gueroudji, *Chem. Vap. Deposition* 4 (1998), pp. 69–76.

N.M. Hwang and D.Y. Yoon, *J. Mater. Sci. Lett.* 13 (1994), pp. 1437–1439.

N.M. Hwang and D.Y. Yoon, *J. Cryst. Growth* 143 (1994), pp. 103–109.

J.-C. Hierso, R. Feurer and P. Kalck, *Chem. Mater.* 12 (2000), pp. 390–399.

G.H. Dierssen, D. Rowenhorst, T. Gabor, D.E. Broberg, Patent EP133343, 1985.

J. Miyake, H. Koyama, S. Oishi, T. Kanazawa, Patent JP60258481 A2, 1985.

D.P. Stinton and W.J. Lackey, *Ceram. Eng. Sci. Proc.* 6 (1985), pp. 707–713.

J. Endo, T. Arai, H. Takeda, Patent EP0252480 A2, 1988.

Q.H. Powell, T.T. Kodas and B.M. Anderson, *Chem. Vap. Deposition* 2 (1996), pp. 179–181.

C.C. Chen and S.W. Chen, *J. Mater. Sci.* 32 (1997), pp. 4429–4435.

N. Eustathopoulos, M.G. Nicholas and B. Drevet, Wettability at High Temperatures, Pergamon (1999).

T. Hanabusa, S. Uemiya and T. Kojima, *Chem. Eng. Sci.* 54 (1999), pp. 3335–3340.

K. Tsugeki, T. Yoshikawa, H. Maeda, K. Kusakabe and S. Morooka, *J. Am. Ceram. Soc.* 76 (1993), pp. 3061–3065.

K. Tsugeki, T. Kato, Y. Koyanagy, K. Kusakabe and S. Morooka, *J. Mater. Sci.* 28 (1993), pp. 3168–3172.

M.M. Michorius, M.H. Haafkens, Patent EP0443659, 1995.

M.C. Lafont, F.J.L., C. Vahlas, Scripta Mater. 51 (2004) 699–703.

K.B. Mathur and N. Epstein, Spouted Beds, Academic Press, Inc., London (1974).

F. Juarez, M.-C. Lafont, F. Senocq and C. Vahlas, *Electrochem. Soc.* PV 2003-08 (2003), pp. 538–548.

B.E. Williams, J.J.J. Stiglich, R.B. Kaplan, in: A. Crowson, E. Chen (Eds.), Tungsten and Tungsten Alloys—Recent Advances, The Metallurgical Society, Warrendale, PA, 1991, pp. 95–101.

T. Itagaki, *Nippon Kinzoku Gakkaishi* 59 (1995), pp. 1157–1164.

R.E. Toth, I. Smid, A. Sherman, P. Ettmayer, G. Klader and G. Korb, *Adv. Powder Metall. Part. Mater.* 8 (2001), pp. 113–126.

A. Biswas, D. Baker, A. Sherman and G.D.W. Smith, *Adv. Powder Metall. Part. Mater.* 6 (2002), pp. 97–109.

T. Kojima and O. Morisawa, *Asian Conference on Fluidized Bed and Three Phases Reactors* (1988), pp. 270–277.

T. Kojima and O. Morisawa, *J. Phys. IV* 1 (1991), pp. 475–482.

G. Hsu, N. Rohatgi and J. Houseman, *AIChE J.* 33 (1987), pp. 784–791.

Y.H. Kim, Y.K. Park, Patent US6541377, 2003.

SGSilicon, Sumitomo to market poly-Si in Far East, Photovoltaics Bull. (2003) 1.

H.O. Pierson, Handbook of Chemical Vapor Deposition (CVD). Principles, Technology and Applications, Noyes Publications, Westwood NJ, USA (1992).

J.M. Blocher, Jr., Patent US3249509, 1966.

D.W. Carroll and W.J. McCreary, *J. Vac. Sci. Technol.* 20 (1982), pp. 1087–1090.

R.J. Akins and J. Bokros, *Carbon* 12 (1974), pp. 439–452.

J. Guilleray, R.L.R. Lefevre, M.S.T. Price and J.-P. Thomas In: H.E.H.J.M. Blocher Jr. and L.H. Hall, Editors, *Fifth International Conference on Chemical Vapor Deposition* Slough, England (1975), pp. 727–748. Cited By in Scopus (0)

J.M. Blocher Jr., *Thin Solid Films* 77 (1981), pp. 51–63.

E. Gyarmati, A.-W. Mehner and E. Wallura In: J. Bloem, G. Vespui and L.R. Wolff, Editors, *Proceedings of the Fourth European Conference on Chemical Vapor Deposition* Eindhoven, Netherlands (1983), pp. 313–320.

K. Minato and K. Fukuda, *J. Nucl. Mater.* 149 (1987), pp. 233–246.

T. Ogawa, K. Ikawa and K. Iwamoto, *J. Nucl. Mater.* 97 (1981), pp. 104–112.

J.W. Adams, R.E. Barletta, P.E. Vanier, M.B. Dowell and J.W. Lennartz, *AIP Conf. Proc.* 301 (1994), pp. 245–251.

B.G. Kim, Y. Choi, J.W. Lee, Y.W. Lee, D.S. Sohn and G.M. Kim, *J. Nucl. Mater.* 281 (1999), pp. 163–170.

C. Tang, Y. Tang, J. Zhu, X. Qiu, J. Li and S. Xu, *J. Nucl. Sci. Technol.* 37 (2000), pp. 802–806.

K. Sawa, S. Suzuki and S. Shiozawa, *Nucl. Eng. Des.* 208 (2001), pp. 305–313.

C. Journet and P. Bernier, *Appl. Phys. A* 67 (1998), pp. 1–9.

M. Corrias, B. Caussat, A. Ayral, J. Durand, Y. Kihn, P. Kalck and P. Serp, *Chem. Eng. Sci.* 58 (2003), pp. 4475–4482.

M. Pérez-Cabero, I. Rodriguez-Ramos and A. Guerrero-Ruíz, *J. Catal.* 215 (2003), pp. 305–316.

P. Mauron, C. Emmenegger, P. Sudan, P. Wenger, S. Rentsch and A. Züttel, *Diamond Relat. Mater.* 12 (2003), pp. 780–785.

Q. Weizhong, W. Fei, W. Zhanwen, L. Tang, Y. Hao, L. Guohua, X. Lan and D. Xiangyi, *AIChE J.* 49 (2003), pp. 619–625.

S.M. Bachilo, L. Balzano, J.E. Herrera, F. Pompeo, D.E. Resasco and R.B. Weisman, *J. Am. Chem. Soc.* 125 (2003), pp. 11186–11187.

P. Serp, R. Feurer, C. Vahlas, P. Kalck, Patent WO2003002456, 2003.

Y. Wang, W. Fei, G. Luo, H. Yu and G. Gu, *Chem. Phys. Lett.* 364 (2002), pp. 568–572.

D. Venegoni, P. Serp, R. Feurer, Y. Kihn, C. Vahlas and P. Kalck, *Carbon* 40 (2002), pp. 1799–1807.

M. Gessien Nijkamp, Ph.D. Thesis, Universiteit Utrecht, The Netherlands, 2002.

R.W. Reynoldson, Heat Treatment in Fluidized Bed Furnaces, ASM International, Materials Park, OH (1993).

S. Kinkel, G.N. Angelopoulos and W. Dahl, *Surf. Coat. Technol.* 64 (1994), pp. 119–125.

R.W. Reynoldson, *Surf. Coat. Technol.* 71 (1995), pp. 102–107.

T. Arai, J. Endo, Patent EP161684, 1985.

T. Arai, J. Endo, Patent EP166216, 1985.

T. Arai, J. Endo, H. Takeda, Patent EP238666, 1986.

T. Arai, J. Endo, H. Takeda, Patent EP252480, 1987.

T. Arai, J. Endo, H. Takeda, Patent EP268248, 1987.

T. Arai, K. Nakanishi, H. Takeda, H. Tachikawa, Patent EP471276, 1991.

T. Arai, H. Takeda, H. Kawaura, Patent EP303191, 1988.

J.E. Jupka, R. Staffin, S.S. Bhatia, British Patent 2171420A, 1986.

T. Arai, J. Endo and H. Takeda, *Nippon Netsu Shori Gijutsu Kyokai Koen Taikai Koen Gaijoshu* 25 (1987), pp. 47–48.

A. Sanjurjo, M.C.H. McKubre and G.D. Craig, *Surf. Coat. Technol.* 39/40 (1989), pp. 691–700.

S. Kinkel, G.N. Angelopoulos, D.C. Papamantellos and W. Dahl, *Steel Res.* 66 (1995), pp. 318–324.

S. Kinkel, N. Voudouris and G.N. Angelopoulos, Characterisation of Ti-bearing coatings on steels by a fluidised bed CVD process, *Fourth International Symposium on Adverse Composites, COMP'95* Corfu, Greece (1995), pp. 303–310.

S. Kinkel, Oberflächenbehandlung von Stählen im Wirbelbett nach dem CVB-Verfahren, RWTH Aachen, 1996.

N. Voudouris and G.N. Angelopoulos, *Surf. Coat. Technol.* 115 (1999), pp. 38–44.

T. Arai, J. Endo and H. Takeda, *Fifth International Conference on Heat Treatment of Materials, vol. 3* Budapest, Hungary (1986), pp. 1335–1341.

D.N. Tsipas, K.G. Anthymidis and Y. Flitris, *J. Mater. Proc. Technol.* 134 (2003), pp. 145–152.

D.N. Tsipas and Y. Flitris, *J. Mater. Sci.* 35 (2000), pp. 5493–5496. C. Christoglou and G.N. Angelopoulos, *J. Phys. IV France* 11 (2001), pp. 1125–1130.

P.C. King, R.W. Reynoldson, A. Brownrigg and J.M. Long, *Surf. Coat. Technol.* 179 (2004), pp. 18–26.

F.-S. Chen, P.-Y. Lee and M.-C. Yeh, *Mater. Chem. Phys.* 53 (1998), pp. 19–27.

P.-Y. Lee, L.-H. Chiu, C.-F. Yang, W.-D. Chen, W. Kai and J.P. Chu, *Mater. Sci. Eng. A* A239–240 (1997), pp. 736–740.

F.J. Pérez, M.P. Hierro, F. Pedraza, C. Gomez and M.C. Carpintero, *Surf. Coat. Technol.* 120–121 (1999), pp. 151–157.

F.J. Pérez, M.P. Hierro, F. Pedraza, C. Gomez, M.C. Carpintero and J.A. Trilleros, *Surf. Coat. Technol.* 122 (1999), pp. 281–289.

K. Nakanishi, H. Takeda, H. Tachikawa and T. Arai, *Heat Surf.* (1992), pp. 507–510.

K.G. Anthymidis, E. Stergioudis and D.N. Tsipas, *Mater. Lett.* 51 (2001), pp. 156–160.

T. Arai, *Third International Conference on Surface Modification Technology* (1990), pp. 587–598.

T. Arai, J. Endo and H. Takeda, *Ind. Heating* 54 (1987), pp. 18–19.

A. Graf von Matuschka, N. Trausner and J. Ziese, *HTM* 43 (1988), pp. 21–25.

P. Rojan, *HTM* 43 (1988), pp. 56–60.

K.G. Anthymidis, P. Zinoviadis, D. Roussos and D.N. Tsipas, *Mater. Res. Bull.* 37 (2002), pp. 515–522.

K.G. Anthymidis, N. Maragoudakis, G. Stergioudis, O. Haidar and D.N. Tsipas, *Mater. Lett.* 57 (2003), pp. 2399–2403.

K.G. Anthymidis, G. Stergioudis and D.N. Tsipas, *Sci. Technol. Adv. Mater.* 3 (2002), pp. 303–311.

F.J. Pérez, M.P. Hierro, C. Carpintero, F. Pedraza and C. Gomez, *Surf. Coat. Technol.* 140 (2001), pp. 93–98.

F.J. Pérez, M.P. Hierro, M.C. Carpintero, C. Gómez and F. Pedraza, *Surf. Coat. Technol.* 160 (2002), pp. 87–92.

N. Voudouris and G.N. Angelopoulos, *High Temp. Mater. Process.* 2 (1998), pp. 165–175.

N. Voudouris, C. Christoglou and G.N. Angelopoulos, *Surf. Coat. Technol.* 141 (2001), pp. 275–282.

C. Christoglou, N. Voudouris and G.N. Angelopoulos, *Surf. Coat. Technol.* 155 (2002), pp. 51–58.

R.W. Reynoldson, *Heat Treat. Met.* 28 (2001), pp. 15–20.

F.J. Pérez, F. Pedraza, M.P. Hierro and P.Y. Hou, *Surf. Coat. Technol.* 133–134 (2000), pp. 338–343.

F.J. Pérez, M.P. Hierro, F. Pedraza, M.C. Carpintero, C. Gomez and R. Tarin, *Surf. Coat. Technol.* 145 (2001), pp. 1–7.

F.J. Pérez, F. Pedraza, M.P. Hierro, J. Balmain and G. Bonnet, *Surf. Coat. Technol.* 153 (2002), pp. 49–58.

F. Pedraza, C. Gómez, M.C. Carpintero, M.P. Hierro and F.J. Pérez, *Surf. Coat. Technol.* 190 (2005), pp. 223–230.

C. Christoglou, C. Bulancea and G.N. Angelopoulos, *Steel Res.* 75 (2004), pp. 353–358.

C. Christoglou, Ph.D. Thesis, University of Patras, Greece, 2004.

K.H. Lau, A. Sanjurjo and B.J. Wood, *Surf. Coat. Technol.* 54/55 (1992), pp. 234–240.

Ullman's Encyclopedia of Industrial Chemistry, Wiley-VCH, Weinheim (2006).

S. Kommu, B. Khomami and P. Bismas, *Chem. Eng. Sci.* 59 (2004), pp. 359–371.

A.A. Onischuk, A.I. Levykin, V.P. Strunin, K.K. Sabelfeld and V.N. Panfilov, *J. Aerosol Sci.* 31 (2000), pp. 1263–1281.

S.M. Suh, M.R. Zachariah and S.L. Girshick, *J. Aerosol Sci.* 33 (2002), pp. 943–959.

C.S. Herrick and D.W. Woodruff, *J. Electrochem. Soc.* 131 (1984), pp. 2417–2422.

H. Gris, B. Caussat and J.P. S Couderc, *Proceedings of first European Congress on Chemical Engineering ECCE1, vol. 3* Firenza, Italy (1997), pp. 2161–2164.

S.-Y. Lu, H.-C. Lin and C.-H. Lin, *J. Cryst. Growth* 200 (1999), pp. 527–542.

S. Kavecky, B. Janekova, J. Madejova and P. Sajgalik, *J. Eur. Ceram. Soc.* 20 (2000), pp. 1939–1946.

K. Nakaso, K. Okuyama, M. Shimada and S.E. Pratsinis, *Chem. Eng. Sci.* 58 (2003), pp. 3327–3335.

P. Holister, J.-W. Weener, C. Roman Vas, T. Harper, Nanoparticles Technology White papers no. 3, Cientifica, 2003.

P. Moravec, J. Smolik and V.V. Levdansky, *J. Aerosol Sci.* 31 (2000), pp. S927–S928.

W.Z. Zhu and M. Yan, *Mater. Chem. Phys.* 55 (1998), pp. 68–73.

K. Kubo, K. Itatani, F.S. Howell, A. Kishioka and M. Kinoshita, *J. Eur. Ceram. Soc.* 15 (1995), pp. 661–666.

A. Margolin, R. Popovitz-Biro, A. Albu-Yaron, L. Rapoport and R. Tenne, *Chem. Phys. Lett.* 411 (2005), pp. 162–166.

R. Tenne, Y. Feldman, A. Zak, R. Rosentsveig, Patent WO0234959, 2006.

Y. Azuma, M. Shimada and K. Okuyama, *Chem. Vap. Deposition* 10 (2004), pp. 11–13.

A.G. Nasibulin, L.I. Shurygina and E.I. Kauppinen, *Colloid J.* 67 (2005), pp. 1–20.

P. Moravec, J. Smolik and V.V. Levdansky, *J. Aerosol Sci.* 30 (1999), pp. S353–S354.

M. Adachi, T. Tsukui and K. Okuyama, *Jpn. J. Appl. Phys.* 42 (2003), pp. L77–L79.

K. Nakaso, B. Han, K.H. Ahn, M. Choi and K. Okuyama, *J. Aerosol Sci.* 34 (2003), pp. 869–881.

K. H. Ahn, M. Choi, Korea Patent 10-2001-0009951, 2001.

Q.T. Nguyen, J.N. Kidder Jr. and S.H. Ehrman, *Thin Solid Films* 410 (2002), pp. 42–52.

R. Marangoni, P. Serp, R. Feurer, Y. Kihn, P. Kalck and C. Vahlas, *Carbon* 39 (2001), pp. 443–449.

Y.Y. Fan, H.M. Cheng, Y.L. Wei, G. Su and S.H. Shen, *Carbon* 38 (2000), pp. 789–795.

R. Sen, A. Govindaraj and C.N.R. Rao, *Chem. Phys. Lett.* 267 (1997), pp. 276–280.

O.A. Nerushev, M. Svenningsson, L.K.L. Falk and F. Rohmund, *J. Mater. Chem.* 11 (2001), pp. 1122–1132.

F. Rohmund, L.K.L. Falk and F.E.B. Campbell, *Chem. Phys. Lett.* 328 (2000), pp. 369–373.

G.G. Tibbetts, C.A. Bernardo, D.W. Gorkiewicz and R.L. Alig, *Carbon* 32 (1994), pp. 569–576.

R.E. Smalley, J.H. Hafner, D.T. Colbert, K. Smith, Patent US19980601010903, 1998.

W.X. Wang, S.H. Liu, Y. Zhang, Y.B. Mei and K.X. Chen, *Physica B* 225 (1996), pp. 137–141.

W.F.A. Besling, P.J.J.M. van der Put and J. Schoonman, *J. Aerosol Sci.* 26 (1995), pp. S907–S908.

S. Tamir and S. Berger, *Thin Solid Films* 276 (1996), pp. 108–111.

P. Fauchais, A. Vardelle and A. Denoirjean, *Surf. Coat. Technol.* 97 (1997), pp. 66–78.

J. Costa, E. Bertran and J.L. Andujar, *Diamond Relat. Mater.* 5 (1996), pp. 544–547.

G. Viera, J.L. Andujar, S.N. Sharma and E. Bertran, *Surf. Coat. Technol.* 100–101 (1998), pp. 55–58.

Y. Liu, W. Zhu, O.K. Tan and Y. Shen, *Mater. Sci. Eng. B* 47 (1997), pp. 171–176.

B. Liu, H. Gu and Q. Chen, *Mater. Chem. Phys.* 59 (1999), pp. 204–209.

Corresponding author. Tel.: +33 562 885 670; fax: +33 562 885 600.

[1] Elutriation is the process in which fine particles are carried out of a fluidized bed due to the fluid flow rate passing through the bed. Typically, fine particles are elutriated out of a bed when the superficial velocity through the bed exceeds the terminal velocity of the fines in the bed. However, elutriation can also occur at slower velocities.

[2] Different gas inlet designs have been proposed to improve the stability of the bed. See for details ref. [127], pp. 112–116, and references therein.

[3] The TRISO fuel particles contain a small kernel of nuclear fuel encapsulated by alternating layers of C and a barrier layer of SiC. The SiC shell provides the primary barrier for

radioactive elements in the kernel and metallic fission products. The performance of this barrier under adverse conditions is key to containment.

Thermophoresis corresponds to mass diffusive transfer due to thermal gradients resulting in particle migration from hot to cold regions.

Original text : Elsevier.com